Republic of Iraq
Ministry of Higher Education
and Scientific Research
University of Babylon
College of Science for Women
Department of Chemistry

Synthesis of ZnO Nanoparticles *via* Thermal Decomposition of Zinc Schiff Base Complexes and Their Usage Photocatytic Degradation of Alizarin Yellow G Dye

AThesis

Submitted to the Council of the College of Science for Women, University of Babylon in Partial Fulfillment of the Requirements for the Degree of Master of Science in chemistry

By

Hadeer Mohammed Subhi

B.S.C Babylon Univresity 2018

Supervised By

Asst. Prof . Dr. Hazim Yahya Al- jubury **Asst. Prof . Dr. Ali Taleb Bader**

2022 A.D **1444 A.H**

بِسْمِ اللهِ الرَّحْمنِ الرَّحِيمِ

وَعِنْدَهُ مَفَاتِحُ الْغَيْبِ لَا يَعْلَمُهَا إِلَّا هُوَ وَيَعْلَمُ مَا فِي الْبَرِّ وَالْبَحْرِ وَمَا تَسْقُطُ مِنْ وَرَقَةٍ إِلَّا يَعْلَمُهَا وَلَا حَبَّةٍ فِي ظُلُمَاتِ الْأَرْضِ وَلَا رَطْبٍ وَلَا يَابِسٍ إِلَّا فِي كِتَابٍ مُبِينٍ

(صدق الله العلي العظيم)

الأنعام (٥٩)

Supervisor's Certification

We, certify thesis entitle

" Synthesis of ZnO Nanoparticles *via* Thermal Decomposition of Zinc Schiff Base Complexes and Their Usage Photocatytic Degradation of Alizarin Yellow G Dye"

Was prepared under our supervision at the University of Babylon / College of Science for Women as a partial Requirements for the degree of Master in Chemistry

Signature: **Signature:**

Name: Assist. Prof Dr. Hazim Yahya **Name:** Assist. Prof. Dr. Ali Taleb Bader

Address: College of science for women /Department of Chemistry

Date: ٥ / ١ / 2022

Recommendation of Head of Chemistry Department

According to the available recommendation , I forward this thesis for Discussion

Signature of Chemistry Department

Name: Dr.Hazim Yahya Mohammed

Scientific Degree : Assistant Professor

Address : Head of Chemistry Department

University of Babylon / College of Science for Women

Date: ٥ / ١ / 2022

Certification of the Examining Committee

We certify that we have read this thesis entitled **"Synthesis of ZnO Nanoparticles *via* Thermal Decomposition of Zinc Schiff Base Complexes and Their Usage Photocatytic Degradation of Alizarin Yellow G Dye"** . And as examining committee examined the Master student **"Hadeer Mohammed Subhi "** in its content, we find that it is adequate to award her degree of Master in Chemistry with degree (Excellence).

Committee Chairman:
Signature:

Name: Dr. Abbas Jasim Atiyah
Scientific order: Prof.
Address: Babylon University / College of Science / Chemistry Department
Date: 17/11 **2022**

Committee Member
Signature:

Name: Dr. Basim Ibrahim AL-Abdaly
Scientific order: Prof.
Address: Baghdade University/
College of Science/ Chemistry Department
Date: 17/10/ **2022**

Committee Member
Signature:

Name: Dr. Ayad F. Alkaim
Scientific order: Prof.
Address: Babylon University /
College of Science for Women/ Chemistry Department
Date: 17/11 **2022**

Committee Member (Supervisor)
Signature:

Name: Dr. Hazim Yahya Al- jubury
Scientific order: Asst. Prof .
Address: Babylon University /
College of Science for Women / Chemistry Department
Date: 17/10/ **2022**

Committee Member (Supervisor)
Signature:

Name: Dr. Ali Taleb Bader
Scientific order: Asst. Prof .
Address: Babylon University /
College of Science for Women/ Chemistry Department
Date: 17/10 / **2022**

Date of examination
Deanship authentication of science for women
Approved for the college committee of graduate studies
Committee Member
Signature:

Name: Dr. Abeer Fauzi Murad
Scientific order: Prof.
Address: Babylon University /
College of science for women
Date: 17/10/ **2022**

University of Babylon
College of Science for Girls

Dedications

I dedicate this thesis to the one who taught me tenderness, and to the one who proudly bears his name, and I ask Allah to extend his life so that he may see fruits that have come to be harvested after the long awaited **"My Dear Father".**

To my angel in life, to the meaning of love, tenderness and dedication to the smile of life and the secret of existence, and to whom that her supplication was the secret of my success, my dearest beloved **"My Beloved Mother".**

To those who have great merit in encouraging and motivating me, and from whom I learned perseverance and diligence, and to those with whom I am greater and upon whom I depend, and to those with whom I gain strength and boundless love, and to those with whom I knew the meaning of life **"My Sister Hala and My Brothers Haider and Hussein".**

To those who showed brotherhood and were distinguished by loyalty and giving and to whom I accompanied them in the happy and sad paths of life, and to those who were with me on the path of success and goodness, thank you to everyone who helped me and I ask Allah to help me and help you.

Hadeer
2022

Acknowledgements

Praise be to Allah, the lord of the worlds, and peace and blessings be upon the prophet Muhammad, the faithful, the good, the pure, and the companions who are hospitable and follow them with kindness to the day of religion.

I would like to extend my sincere thanks and gratitude to my supervisors, the esteemed Assist. Prof Dr. Hazim and, Assist. Prof Dr. Ali Taleb Bader, for their continuous and continuous scientific efforts and guidance, administrative facilities and follow-up throughout the research period, asking the almighty god to pay their mistake and preserve them in the service of science.

I also extend my sincere thanks to the presidency of the university of Babylon - the deanship of the college of science for Women and the presidency of the department of chemistry for giving me the opportunity to complete my scientific career.

My thanks and gratitude to Dr. Ayad alkaim and Dr. Sadiq abdul hussain karim

Finally, I extend my sincere thanks and appreciation to all of the professors and students of my colleagues and fellow graduate students (masters) and students (initial stages) who extended a helping hand and help me. Wishing them continued success and success...god bless them.

Hadeer

2022

Summary

This work consists of three parts:

Part One:

The two ligands L_1(benzylimino)methyl)phenol) and L_2(2-((benzylimino)methyl)benzene-1,4-diol) were synthesized by the condensation of benzylamine with aromatic aldehyde: 2-hydroxy benzaldehyde and 2- hydroxy-3-methoxy benzaldehyde respectively . The ligands were characterized by using different techniques such as: melting point, FT-IR, UV-Vis, ^{1}H-NMR, ^{13}C-NMR, (TGA).

The synthesis complexes of these ligands with which metal were synthesized by the reaction of zinc acetate with the ligands ($L_1$and L_2) as the molar ratio (1:1) and (1:2) (metal: Ligand). These complexes have been characterized and studied by physicochemical and analytical properties such as FT-IR and UV-Vis spectra, molar conductivity and TGA analysis.

Part Two:

Zinc oxide (ZnO) nanostructures had been prepared using thermal decomposition method for metal complexes by calcinated at 700 ^{o}C for 4 hours.Zinc oxide (ZnO) nanostructures were characterized of by X-ray diffraction (XRD), FT-IR, (SEM), (TEM), EDX and UV -Vis Diffuse Reflectance and BET techniques. Crystallite size and average crystallite size of the prepared Zinc oxide (ZnO) nanostructures were calculated employing Scherer equation. The resultant data from these techniques mentioned above were agreed quite well with the suggested molecular formula of the complexes and have been suggested the geometry of their structures where all complexes the (C_1 to C_4) were taken the tetrahedral geometry .

Part Three:

The photocatalytic activity of the prepared Zinc oxide (ZnO) nanostructures was examined using AYG dye as the test dye in aqueous solution under UV irradiation.

The studied factors studied such as were the initial AYG dye concentration, amount of catalyst, initial pH of the solution, light intensity, hydrogen peroxide and the temperature of the dye solution.

The effect of the initial concentration of the dye solution was studied and the results showed that the rate of reaction decrease with increase the concentration of dye and the reaction is a pseudo first-order reaction. The optimal dosage of the catalyst was found to be (0.13 g/100 mL) for the prepared Zinc oxide (ZnO) nanostructures.

Investigation of the effect of initial pH of the dye revealed that the optimum pH of the solution is (8.75). The increasing in the light intensity caused to increase the rate of photo catalytic degradation.

Effect of temperature was investigated also employing Arrhenius equation, and the results showed that the increase in temperature is accompanied with an increase in the rate of the reaction. indicating that the photocatalytic degradation of (AYG) is an endothermic reaction.

The activation energy of the reaction was calculated, and it was found to be (32.52) $kJ.mol^{-1}$.

Entropy and enthalpy values were calculated employing Eyring equation. Entropy values were found to be ($^{-}$0.166) $kJ.mol^{-1}$, these results showed that the randomness was decreased. Enthalpy values were found to be (52.52) $kJ.mol^{-1}$ the positive value indicating that the photocatalytic degradation of dye is an endothermic reaction.

Gibb’s free energy was calculated for each type of the photo catalysts used in this study, and the values were found to be (81.98) $kJ.mol^{-1}$, These results show that the reaction is non-spontaneous.

Table of Contents

Contents	Pages
Summary	**I-III**
Table of Contents	**IV-VIII**
List of Tables	**IX-X**
List of Figures	**X-XIII**
List of scheme	**XIV**
List of Abbreviations	**XIV-XVI**

Table of Contents

Chapter One: Introduction

Item	Title	P. No.
1.1	Nano science and Nanotechnology	**1**
1.1.1	Properties of Nano structured materials	**1-2**
1.1.2	Techniques of Nanomaterial Synthesis	**2-3**
1.1.3	Synthesis Methods of Nanostructures	**3-4**
1.1.4	Nanomaterial's Classification	**4-6**
1.1.5	Application of Nano materials	**7**
1.2	Zinc Oxide (ZnO)	**7-8**
1.2.1	The Crystal structure of ZnO	**8-9**
1.2.2	Optical properties of ZnO	**10**
1.2.3	Application of ZnO Nanostructures	**10**
1.2.3.1	Medical application	**10**
1.2.3.2	The textile industry	**11**
1.2.3.3	Electronics application	**11**
1.2.3.4	Catalysts	**11-12**
1.2.3.5	Chemicals and biosensor applications	**12**
1.3	Types of Heterogeneous Photocatalysis	**12**

1.3.1	Noble Metal-Based Photocatalysis	**12-13**
1.3.2	Semiconductor-Based Photocatalysis	**13-15**
1.3.3	Principles of Heterogeneous Photocatalysis	**15-17**
1.4	Advance Oxidation Processes (AOP_S)	**17-18**
1.5	Coordination chemistry	**18-19**
1.5.1	Chelate and Chelating Effect	**19-21**
1.6	Schiff bases	**21-22**
1.6.1	Classification of Schiff bases	**22-23**
1.7	Dyes	**23-25**
1.7.1	Alizarin Yellow G Dye (AYG)	**26**
1.7.1.1	Product Information of AYG Dye	**27**
1.8	A Review of Studies	**28-32**
1.9	The aims of Present Work	**33**

Chapter Two: Experimental Part

Item	Title	P. No.
2.1	Chemical Reagents	**34-35**
2.2	Instrumentation	**35**
2.2.1	Decomposition and Melting Points	**35**
2.2.2	U.V-Visible spectrophotometer(Uv-vis)	**35**
2.2.3	Fourier Transform Infra-Red spectrophotometer(FTIR)	**35**
2.2.4	Nuclear Magnetic Resonance(^{1}H-NMR and ^{13}C-NMR) spectroscopy	**35-36**
2.2.5	Molar Conductivity Measurements	**36**
2.2.6	Scanning electron microscopy (SEM)	**36**
2.2.7	X-rays diffraction(XRD)	**36**
2.2.8	Thermal Gravimetric Analysis(TGA)	**36**
2.2.9	Transmission Electron Microscopy(TEM)	**36**

2.2.10	Energy Dispersive X- ray Analysis (EDX – Elemental)	**37**
2.2.11	UV-visible spectrophotometer with Lisper diffuse reflectance accessory	**37**
2.2.12	Bruner–Emmett–Teller(BET)	**37**
2.3	Synthesis of ligands their Complexes and ZnO nanoparticle	**37**
2.3.1	Synthesis of Ligands (L1 and L2)	**37-38**
2.3.2	Synthesis of Zn(II) Schiff complexes	**38**
2.3.3	Synthesis of ZnO Nanoparticles	**39**
2.4	Photocatalytic Reactor Set up	**40**
2.5	Parameters effecting on photocatalytic pegradation process	**40**
2.6	Thermodynamic Parameters	**41**
2.6.1	Determination the activation energy	**41**
2.6.2	Determination enthalpy of activation and entropy of activation	**41**
2.6.3	Determination of Gibbs free energy	**41**
2.7	photocatalytic degradation	**42**
2.7.1	Photocatalytic Degradation of AYG Dye	**42**
2.7.2	Effect of the Initial Concentration substrate on photocatalytic degradation process using constant mass of coupled of ZnO Nano particles	**42**
2.7.3	Effect of pH on the Photocatalytic Degradation Process Using ZnO Nano Particles	**42**
2.7.4	Effect of Temperature on the Photocatalytic Degradation Process Using ZnO Nano Particles	**43**
2.7.5	Effect of intensity on the photocatalytic degradation process using ZnO Nano particles	**43**

2.7.6	Effect of hydrogen peroxide on the photocatalytic degradation process using ZnO Nano particles	**43**

Chapter Three: Results and Discussion

Item	Title	P. No.
3.1	FT-IR Spectra	**44**
3.1.1	FT-IR Spectra of Salicylaldehyde	**44**
3.1. 2	FT-IR Spectra of Benzyl Amine	**44**
3.1.3	FT-IRSpectra of Schiff Base Ligand 2-(Benzylimino)Methyl)Phenol (L1) And Their Complexes	**44-45**
3.1.4	FT-IRSpectra of 2,5-Dihydroxy Benzaldehyde	**45**
3.1.5	FT-IR Spectra of Schiff Base ligand 2-((benzylimino)methyl)Phenol (L_2) and their Complexes	**46**
3.1.6	FT-IR spectra for C_1 to C_4 comlexes	**47-48**
3.2	^{1}H-NMR Spectra	**49**
3.2. 1	^{1}H-NMR Spectra of (L_1)	**49**
3.2.2	^{1}H-NMR Spectra of (L_2)	**50**
3.2.3	^{13}C-NMR spectra of L_1	**51**
3.2.4	^{13}C-NMR Spectra of L_2	**52**
3.3	Electronic spectra and molar conductance	**53**
3.3.1	Electronic spectra of Schiff base ligands (L_1 ,L_2), (C_1.C_4) complexes and molar conductivity	**53-55**
3.4	Thermal Gravimetric Analysis(TGA)	**56**
3.4.1	TGA of the Ligands and some their Metal Ion Complexes	**56-60**
3.5	Characterization of the Synthesis Znic oxide Nanoparticles	**61**

3.5.1	FTIR for the Zinc Oxide Nanoparticles	**61**
3.5.2	X-rays Diffraction (XRD) Analysis for the Zinc Oxide Nanoparticles	**62-65**
3.5.3	Scanning Electron Microscopy (SEM) for Synthesized ZnO	**65-67**
3.5.4	EDX analysis of ZnO nanoparticles	**68-70**
3.5.5	Transmittance Electron Microscopy (TEM)	**70-72**
3.5.6	UV -Vis Diffuse Reflectance for ZnO Nps	**73-76**
3.5.7	Surface area analyzer	**76-77**
3.6	Degradation of AYG dye by photo catalysis	**78**
3.6.1	Preliminary experiments	**78-79**
3.6.2	Effect of different process on the photo-catalytic-degradation for AYG dye	**79**
3.6.2.1	Effect of the mass of ZnO nanoparticles on photo catalytic degradation of the AYG dye	**79-83**
3.6.2.2	Effect of AYG dye initial concentration on the photocatalytic degradation process	**84-87**
3.6.2.3	The effect of light intensity on photo degradation of AYG dye using ZnO nanoparticles	**87-90**
3.6.2.4	Effect of pH on photocatalytic degradation of AYG dye	**90-93**
3.6.2.5	Effect of Hydrogen Peroxide	**94-97**
3.6.2.6	Temperature effect of on photo-catalytic-degradation for AYG dye	**97-101**
3.7	Conclusions	**102-103**
3.8	Future work	**104**

List of Table

Chapter One :Introduction

Item	Title	P. No.
1.1	Methods for nanostructures synthesis	**4**
1.2	Application of nanomaterial in different fields	**7**
1.3	Energy band gap and wavelength sensitivity of different semiconductors.	**15**

Chapter Two : Experimental Part

Item	Title	P. No.
2.1	lists all commonly used laboratory chemicals and reagents .These ingredients were utilized without any additional purification	**34-35**
2.2	Complex Symbol, Complex Formula, Metal Salt, Weight (G)Metal Salt, Weight (G) Ligands	**38**

Chapter Three :Results and Discussion

Item	Title	P. No.
3.1	FTIR peaks for ligands(L_1 and L_2) and their complexes	**48**
3.2	λ_{max} nm(ט cm^{-1}), Assignment, Suggested geometry Malar conductivity Ohm^{-1} .cm^2. $mole^{-1}$ for the ligands and complexs	**54**
3.3	Thermal Decomposition Data L_1,L_2, and their Znic (II) Complexes:	**57**
3.4	The Crystallite Size (D) of ZnO nanoparticles from difference complexes	**63**
3.5	EDX of zinc oxide nanoparticles from differences complexes	**68**
3.6	The band gap energy for different complexes	**74**
3.7	The change in A_t/A_0 with irradiation time on different masses of ZnO nanoparticle's	**81**

3.8	change of A_t/A_0 through irradiation-time on different-concentration for AYG dye	**85**
3.9	The change of A_t/A_0 through irradiation-time on different light intensity.	**88**
3.10	change for At/A_0 through irradiation-time on different pH Value .	**91**
3.11	change for A_t/A_0 through irradiation-time on different initial H_2O_2 solution Value .	**95**
3.12	Change of At/A0 through irradiation-time of different-temperature.	**98**
3.13	The thermodynamic parameters of the photocatalytic degradation of dye	**101**

List of Figure

Chapter One : Introduction

Item	Title	P. No.
1.1	Two approaches of the nanoparticles synthesis	**3**
1.2	Nanomaterials with different morphologies	**6**
1.3	(a) Wurtzite crystal structure and (b) zinc blende crystal structure of ZnO	**9**
1.4	Energy level diagram for n and p-type semiconductors	**14**
1.5	A schematic diagram illustrating the principle of photo catalysis	**16**
1.6	Classification of Advanced Oxidation Process	**18**
1.7	Classification of dyes based on ionic charge with corresponding properties, chemical types and some of the reported toxicity impacts (in blue), and based on chemical structure with corresponding chromospheres	**25**
1.8	Alizarin Yellow G Dye (AYG)	**27**

Chapter Two : Experimental Part

Item	Title	P. No.
2.1	optical photo for main parts of the photocatalytic degradation system	**40**

Chapter Three : Results and Discussion

Item	Title	P. No.
3.1	FT-IR Spectra for Benzyl Amine, Salicylaldehyde and ligand One	**45**
3.2	FT-IR Spectra for Benzyl Amine,2,5-dihyroxybenzaldehyde and ligand two	**46**
3.3	FT-IR Spectra for C_1 to C_4 complexes	**48**
3.4	^{1}H-NMR Spectra for L_1	**49**
3.5	^{1}H-NMR Spectra for L_2	**50**
3.6	^{13}C-NMR Spectra of L_1	**51**
3.7	^{13}C-NMR Spectra of L_2	**52**
3.8	Uv –visible Ligand one and it's complexes	**55**
3.9	Uv –visible Ligand two and it's complexes	**55**
3.10	TGA thermogram of L 1	**58**
3.11	TGA thermogram of C_1	**58**
3.12	TGA thermogram of C_2	**59**
3.13	TGA thermogram of L_2	**59**
3.14	TGA thermogram of C_3	**60**
3.15	TGA thermogram of C_4	**60**
3.16	FTIR spectra for ZnO from C_1 to C_4 Complexes	**61**
3.17	X-ray Diffraction Pattern of the Zinc Oxide Nanoparticles Synthesized from C_1 Complex	**63**
3.18	X-ray Diffraction Pattern of the Zinc Oxide Nanoparticles Synthesized from C_2 Complex	**64**
3.19	X-ray Diffraction Pattern of the Zinc Oxide Nanoparticles synthesized from C_3 Complex	**64**
3.20	X-ray Diffraction Pattern of the Zinc Oxide Nanoparticles Synthesized from C_4 Complex	**65**
3.21	SEM and Histogram of the Zinc Oxide Nanoparticles Synthesized from C_1 Complex	**66**

3.22	SEM of the Zinc Oxide Nanoparticles Synthesized from C_2 Complex	**66**
3.23	SEM of the Zinc Oxide Nanoparticles Synthesized from C3 Complex	**67**
3.24	SEM of the Zinc Oxide Nanoparticles Synthesized from C 4 Complex	**67**
3.25	EDX for Zinc oxide nanoparticles from C_1	**68**
3.26	EDX for Zinc oxide nanoparticles from C_2	**69**
3.27	EDX for Zinc oxide nanoparticles from C_3	**69**
3.28	EDX for Zinc Oxide Nanoparticles from C_4	**70**
3.29	Transmittance Electron Microscopy for ZnO NPs from C_1	**71**
3.30	Transmittance Electron Microscopy for ZnO NPs from C_2	**71**
3.31	Transmittance Electron Microscopy for ZnO NPs from C_3	**72**
3.32	Transmittance Electron Microscopy for ZnO NPs from C_4	**72**
3.33	Diffuse reflectance of Synthesized ZnO nanoparticles from difference complexes	**74**
3.34	Band gap energy of ZnO Nps from C_1 complex	**75**
3.35	Band gap energy of ZnO Nps from C_2 complex	**75**
3.36	Band gap energy of ZnO Nps from C3 complex	**76**
3.37	Nitrogen ads option-desorption isotherms for ZnO from C_1complex	**77**
3.38	Pore size distribution of ZnO nanoparticles from C_1 complex	**77**
3.39	The variation of PDE% of AYG dye with type of process	**79**
3.40	Variation in (At / A0) with irradiation time at 10 ppm of the prepared dye	**82**
3.41	Chang in Ln (A0 / At) through irradiation-time at different of the mass of ZnO nanoparticles using UV radiation.	**82**
3.42	Effect of dye concentration on photo degradation rate constants	**83**
3.43	Photocatalytic degradation efficiency using 10ppm of AYG against mass of ZnO nanoparticles.	**83**
3.44	Variation in (A_t / A_0)with irradiation time at different concentrations of dye	**85**

3.45	Linear variation of lnC_0 /C_t versus time for the photocatalytic degradation of AYG dye at different initial concentrations	**86**
3.46	Photocatalytic degradation efficiency using 0.13 g / 100 ml ZnO Nano particles against different concentration of AYG dye	**87**
3.47	Variation in (A_t / A_0) with irradiation time at different light intensity.	**89**
3.48	Chang in Ln (A_0 / A_t) through irradiation-time at different intensity of light.	**89**
3.49	Photocatalytic degradation efficiency using 0.13g / 100 ml ZnO nanoparticles and 10 ppm of AYG dye for different light intensity	**90**
3.50	Variation in (At / A0) with irradiation time at different initial pH solution.	**92**
3.51	Chang in Ln (A0 / At) through irradiation-time at different pH using UV radiation, initial AYG dye.	**92**
3.52	Effect of pH on photo degradation rate constants	**93**
3.53	Photocatalytic degradation efficiency using 0.13g / 100 ml ZnO nanoparticle and 10 ppm of AYG dye for different initial pH.	**93**
3.54	Chang in Ln (A_0 / A_t) through irradiation-time at different-H_2O_2 using UV radiation, initial AYG dye.	**96**
3.55	Effect of H_2O_2 on photo degradation rate constants	**96**
3.56	Photocatalytic degradation efficiency using 0.13g / 100 ml ZnO nanoparticles and 10 ppm of AYG dye for different H_2O_2 concentrations	**97**
3.57	Variation in (At / A0) with irradiation time at different Temp	**99**
3.58	Chang in Ln (A0 / At) through irradiation-time at different-temperature using UV radiation, 10 ppm of AYG dye and (0.13g / 100 ml) ZnO nanoparticle's.	**99**
3.59	Arrhenius plot of AYG dye.	**100**
3.60	Eyring equation plot ln(k/T) against 1000/T for AYG dye	**100**

List of Scheme

Chapter One :Introduction

Item	Title	P.No
1.1	formation of schiff base	22

Chapter Two: Expeirmental Part

Item	Title	P. No.
2.1	Synthesis of Ligands ($L_1$and L_2)	38
2.2	synthesis of ZnO nanoparticles	39

Directory of Abbreviations

Abbreviations	Description
AYG	Alizarin Yellow G
Å	Angstrom
Atm	Atmosphere
Abs	Absorbance
BET	Brauner Emmet Teller
B.D.H	British Drug Houses
β	Full width at half- maximum intensity of the diffraction peaks
CB	Conduction band
˚C	Centigrade
C_o	Initial Concentration
Comm.	Commercial
CVD	Chemical Vapor Deposition
C.D.H	Central Drug House
C.T	Charge Transfer
C 1	$[Zn(L_1)(H_2O)_2].2CH_3CO_2H$
C 2	$[Zn(L_1)_2].2CH_3CO_2H.2H_2O$
C 3	$[Zn(L_2)(H_2O)_2].2CH_3CO_2H$

C_4	$[Zn(L_2)_2].2CH_3CO_2H.\ 2H_2O$
^{13}CNMR	Carbon 13- Nuclear Magnetic Resonance
DMSO	Dimethyl Sulfoxide
Eq	Equation
SEM	Scanning Electron Microscopy
FTIR	Fourier Transform Infrared Spectroscopy
G	Gram
GCC	Gulf consolidated contractors
JCPDS	Joint committee on powder diffraction standards
h^+ VB	Positive hole valance band
^{1}HNMR	Proton-Nuclear Magnetic Resonance
Log	Logarithm
L_1	2-(benzylimino)methyl)phenol
L_2	2-(benzylimino)methyl)benzene-1,4-diol
Min	Minute
mL	Milliliter
mW	Milliwatt
M.P	Melting Point
NMs	Nanomaterial
NPs	Nanoparticles
Oct	Octahedral
Pre.	Prepard
PVS	physical vapor synthesis
Ph	Potential of hydrogen
R	Universal gas constant
TGA	Thermal gravimetric analysis
UV–vis	Ultraviolet–visible
VB	Valance band
W	Weight
XRD	X-ray diffraction

ZnO NPs	Zinc Oxide Nanoparticles
Hν	The photon energy
λ	Wavelength
λ_{max}	Maximum wavelength
K	Adsorption rate constant
K_L	Langmuir constant
ΔH	Change of enthalpy
ΔS	Change of entropy
ΔG	Gibbs free energy
PDE	Photo Degrade Efficient
AOPs	Advance Oxidation Processes
RF	Radio Frequency

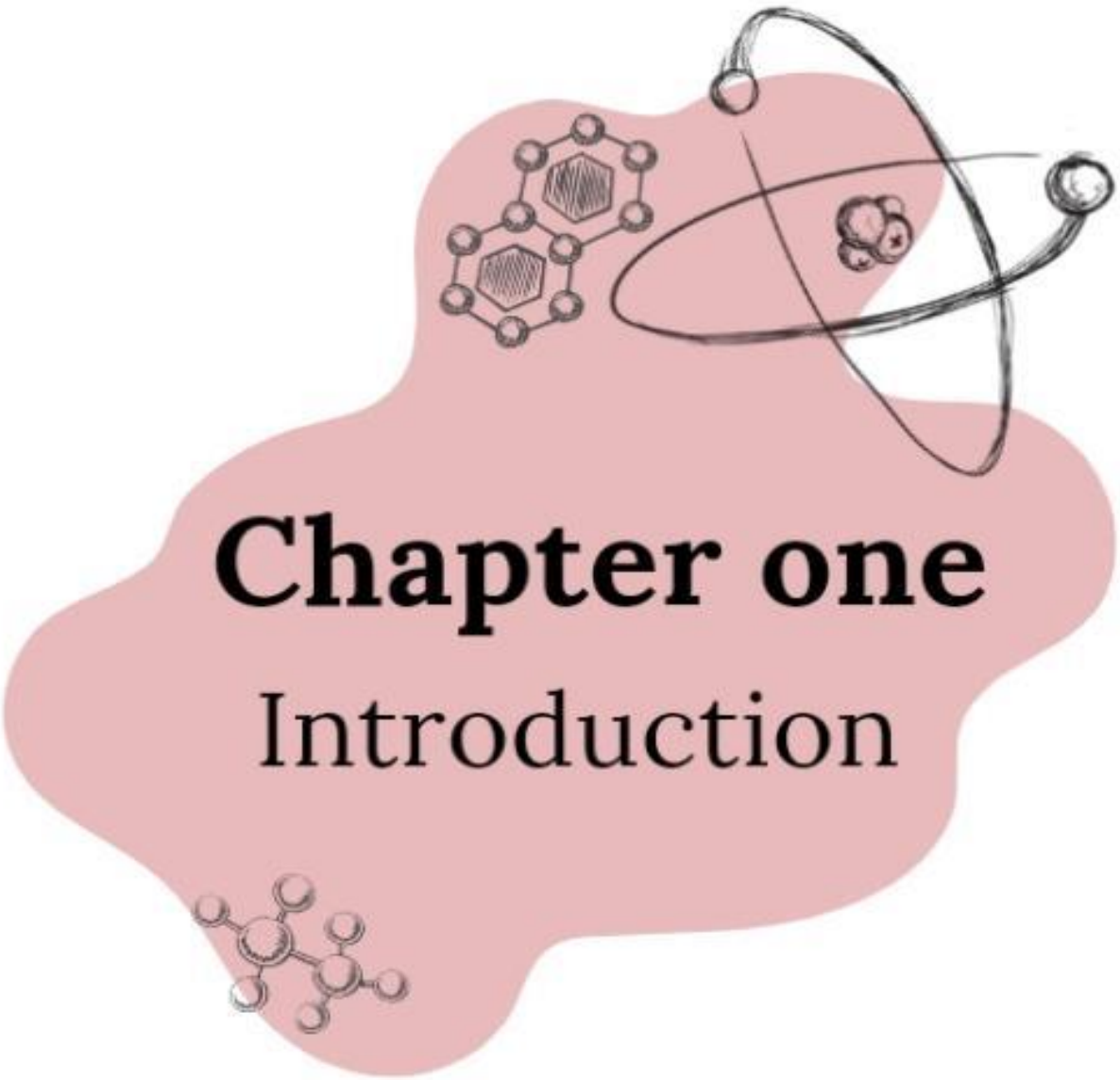

Chapter one

Introduction

1.1 - Nano science and Nanotechnology :

The Nano word originates from the Latin term meaning dwarf, the perfect range provided by nanotechnology refers to a part per thousand million of a specific unit so the nanometer is one thousand millionth of a meter (1nanometers = 10^{-9} meters). The science of nanotechnology as a science deals specifically with the mechanisms that happen at the molecular level and the size of the nanoscale, it is the science of material with a length of 10^{-9} to 10^{-7} meters [1].

Nanoscience study phenomena and processes of materials at the atomic, molecular and macromolecular scales because the properties differ greatly between these scales and main scales, or it is the science of materials and devices that have changed greatly due to their nanoscale size, structures, components, and characteristics (physical, chemical, and biological). While nanotechnology refers to the design, preparation, diagnosis and applications of structures, devices and techniques for controlling the shape and size of nanoscale components [2, 3].

Nanotechnology has been widely used in many fields such as applied science, engineering and medicine for many decades[3].

1.1.1 -Properties of Nano structured materials :

With the whole expansion in several areas of applications, nanostructured have demonstrated an active field research and an economic technical sector. Nano structured has obtained fame in technological developments owing to their adjustable physical and chemical properties like melting point, electrical and thermal conductivity, catalytic activity, light absorption and scattering resulting in improved performance over wholesale counterparts[4]. Depending on the Environmental Protection Agency, “nanomaterial can exhibit unique properties dissimilar than the equivalent chemical compound in a larger

dimensions" a bridge between the huge materials and tiny structures (atomic or molecular)[5] .

The bulky materials have fixed physical properties, nevertheless of size, on the other hand the nano scale properties depend on the size. The basic properties of materials can be controlled by creating nanometer scale structures, like melting degree, magnetic properties, charging capacity also the color, although the chemical structure does not change .

Taking advantage of this possibility will produce a new products and high performance technologies that could not have been provided earlier. Nanostructures have extremely wide surface area to volume ratios, which makes their ideal and utilize in many fields[6] .

1.1.2- Techniques of Nanomaterial Synthesis :

Two fundamental approaches are used in the synthesis of nanoparticles as shown in Figure. (1.1), which can be of natural or synthetic origin and show unique properties in the nanoscale.

The first approach is a "top-down" method that involves dividing solids into small parts by an external force[7] .

To supply the energy needed to form nanoparticles there are numerous technologies (physical, chemical, and thermal) are applied, this approach has the disadvantage of being costly to implement and perfect surfaces and edges cannot be obtained due to the cavities and roughness that occur in nanoparticles formation according to this route[8] .

Another approach, called as "bottom-up", is depending on adding and joining (gas, liquid) atoms or molecules. This approach has the advantage of obtaining excellent nanoparticle synthesis results and does not create waste (that needs to be removed) and the sizes of nanoparticles can be controlled and obtaining nanoparticles at a smaller size[9].

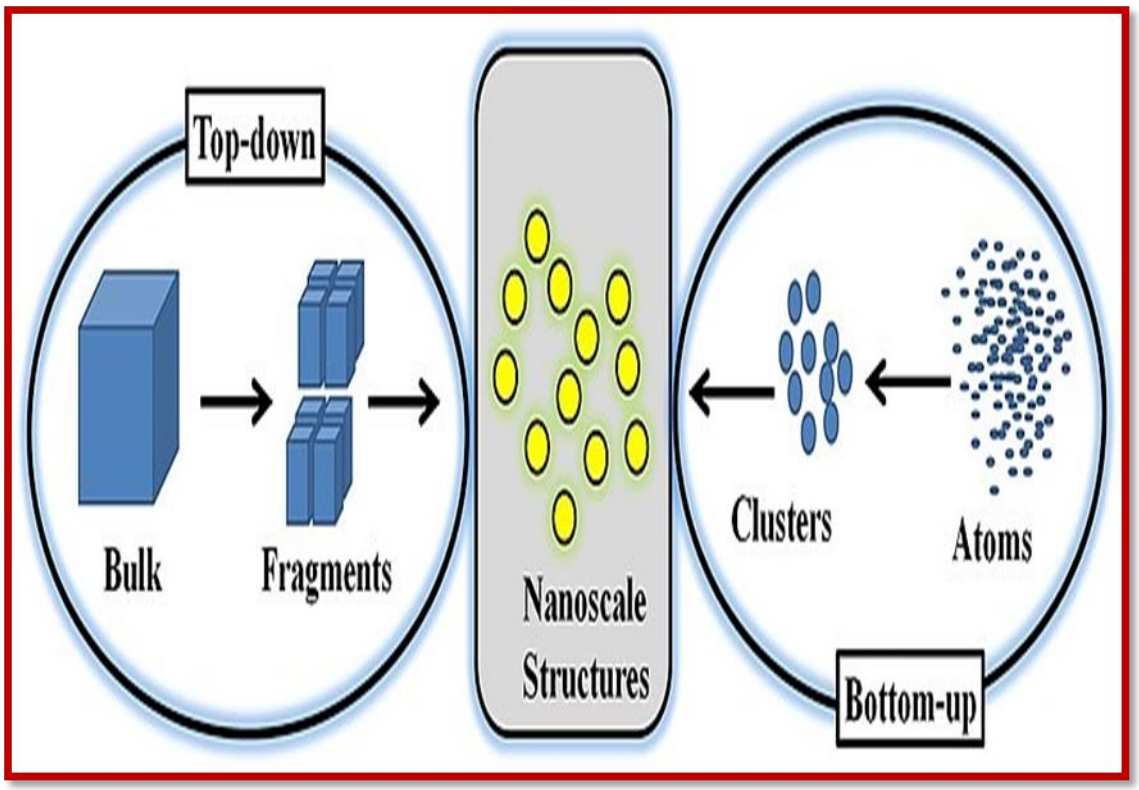

Fig. (1.1): Two approaches of the nanoparticles synthesis

1.1.3- Synthesis Methods of Nanostructures:

The nanostructures can be manufactured in various forms using different synthesis processes, that nanostructures are less than three dimensions can be prepared in the range of 1–100 nm. Nanostructures are made by using various techniques, these nanoparticles can be prepared in liquid dispersion and dry particles .

Nano scale structures are made by constructing from atoms or by reducing the magnitude from micro particles to nanoparticles which are shown in Table(1.1) [10, 11].

Table(1.1): Methods for nanostructures synthesis

No	Bottom-up method	Top-down method
1	Sol-gel	Mechanical milling
2	Chemical vapor deposition (CVD)	Nanolithography
3	Laser Pyrolysis	Laser ablation
4	Wet synthesis	Sputtering
5	Spinning	Thermal decomposition
6	Plasma arcing	Spark Discharge
7	Molecular Self-Assembly	Ultrasound
8	Molecular beam epitaxial (MBE)	Microwave

1.1.4 - Nanomaterial's Classification :

The first idea for classification of Nanomaterial has been sorted by Gleiter et al. [12],they classified nanomaterial based on their chemical composition as well as crystalline forms, but the Gleiter classification was not perfectly completed because it did not depend on the dimensions of the nanostructures and the nanoparticles [13].

Pokropivny and Skorokhod introduced in 2007 [14] a new nanomaterials classification plan that included newly advanced composites like Zero dimensional, One dimensional, Two dimensional and Three dimensional, nanomaterials as seen in Figure.(1.2).

This categorization depends on the transfer of the electron along the dimensions in nanomaterials .

Materials with nanostructures were classified by Richard W. Siegel [10] into four categories, depending on the dimensions as defined by zero dimensional nanomaterials, electrons are entrapped in a space without dimensions, while on one dimension nanomaterials contain the electrons can passage along the axis (X). As well as two dimensional nanomaterial has electronic movement along the (X–Y) axis while the electrons of three

dimensional nanomaterial has move along (X, Y, Z) axis respectively[14]. The Classification of nanomaterials depending on their dimensional can be catarized as follows [15]:-

1- Zero Dimensional Nanostructures(0D) :

All dimensions of materials are measured inside the scale of nano (there are no dimensions outside the nanoscale 100 nm) or Zero-dimension. Quantum dots are the most widespread example of quantum dots nanomaterials with 0-D.

2- One Dimensional Nanostructures(1D) :

One-dimensional materials include nanotubes, nanowires and nanofiberes. They are materials that have one dimension outside the nanoscale. This leads to needle like-shaped nanomaterial.

3- Two Dimensional Nanostructures(2D):

Materials where in 2D are not limited to the scale of nano, two dimension nanomaterial offer plate-like forms. Those include nanolayers and nanofilms.

4- Three Dimensional Nanostructures(3D):

Bulk nanomaterials do not contain any nanoscale in dimension. These materials have three random dimensions over 100 nanometers. The material contains a nanocrystalline structure or contains the existence of advantages on the nanoscale with respect to the crystalline nanostructures, huge nanomaterials can contain several configuration of crystals in nano size, at most it bein diverse directions, in terms of existence of advantage on the nanoscale, was material in three dimensional may have dispersions of nanoparticles, nanotubes, and nanowires bundles add to the multi nano layers .

Different nanopharticales, nanomaterales,are bassed in Figure(1.2)

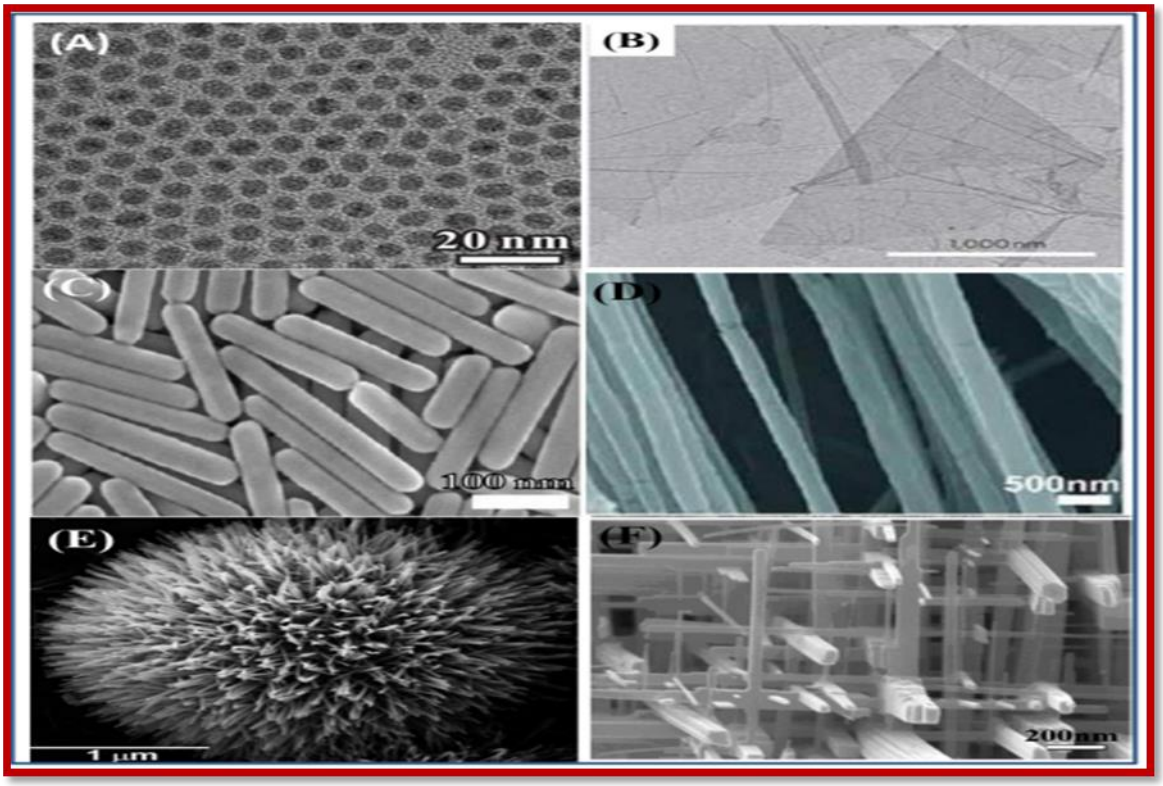

Fig. (1.2) : Nanomaterials with different morphologies:

(A) nonporous Pd nps (0D)[16],

(B) Graphenenanosheets (2D)[17],

(C) Ag nanorods (1D) [18],

(D) polyethylene oxide nanofibers (1D)[19],

(E) urchin-like ZnO nanowires (3D), reproduced from[19],

(F) WO3 nanowire network (3D)[20].

1.1.5- Application of Nano materials:

Nanomaterials are used in the broad of environment and can be is outlined in Table (1.2).

Table (1.2): Application of nanomaterial in different fields[21].

No	Applied field	Application
1.	Nano medicines Nano drugs	Drug delivery, Medical devices and Tissue engineering
2.	Nano scale chemicals compounds and Cosmetics	Paints and coatings
3.	Food Sciences	Processing, nutracetical food and nanocapsules
4.	Environment and Energy	Water and air purification filters, fuel cells and photovoltaic cell
5.	Military and Energy	Biosensors, weapons and sensory enhancement
6.	Electronics	Semiconductors chips, memory storage, photonica and optoelectronics
7.	Scientific Tools	Atomic force, microscopic and scanning tunneling microscope

1.2 -Zinc Oxide (ZnO):

Zinc oxide is known as II–VI semiconductor and , individuallyugn. ZnO has a unique chemical sensing , optical, semiconducting, piezoelectric, and electric conductivity properties .

In the near of ultraviolet range the ZnO characterized by 3.3 eV as a large band gap directly ,and have a natural n-type electrical conductivity, ZnO have 60 meV excitonic binding energy at RT. ZnO with These characteristics enabling to have amazing applications in different fields [22, 23] .

Zinc Oxide has very strong ionic bonding between Zn and O, In spite of the fact that Zinc Oxide shows light covalent character. ZnO-nps have

two region UVB and UVA that represent high optical absorption , high photochemical activities, and high Catalytic Peoformance [24].

Examine as of late, have strongly centered around the prepare of nanosized ZnO particles under different conditions and methods, due to the properties can be changed or adjusted of metal oxide particles depending on route of the preparation method [25] .

ZnO can be prepare through different techniques by controlling the parameters of preparation . The clearly utilizing of different methods can make diverse morphologies furthermore unique sizes of ZnO particles. Accordingly, the physical and chemical parameters for example the temperature, pH, precursors, and the solvent type were very considered.

A grouping of ZnO nanostructures with various development morphologies, for example, nanorings, nanosphere, nanoneedles , nanowires, nanotubes and nanorods have been successfully prepared [26]. The subject which is much fascinating is the getting of ZnO nano particles by a novel technique is hydrothermal method, have some advantages for example relatively low temperature, the utilization of low cost ,simple setup, big deposition area, and environment friendly, that make it different compared with others [27].

1.2.1- The Crystal structure of ZnO:

A large portion of group 12–16 binary compounds crystallize in the frame the wurtzite phase, it known likewise to crystallize in rocksalt and the cubic zinc blende structures, as shown in Figure.(1.3). The blende phase of zinc oxide can be stable just growth on cubic structures [28], but the another phase rocksalt is need a high-pressure metastable and it forming at ~10 GPa with very high temperature, and cannot be stabilized . The calculations theoretical show another phase of ZnO a fourth phase is cubic cesium chloride, might be possible at a great degree high temperatures, in any case, but that not yet observed experimentally [29].

In normal ambient conditions the wurtzite symmetry is thermodynamically supported over the zinc blende .

In both cases, every cation is surrounded by four anion arranged in four corners of a normal tetrahedron with the cation at the middle. Similarly, four cations surround each anion. ZnO bond possesses good ionic character which is reflected in its band gap [30].

In hexagonal wurtzite structure, the crystal can be depicted as alternating planes that are made out of tetrahedral coordinate Zn^{2+} and O^{2-} ion and stacked along c- Axis [29] .

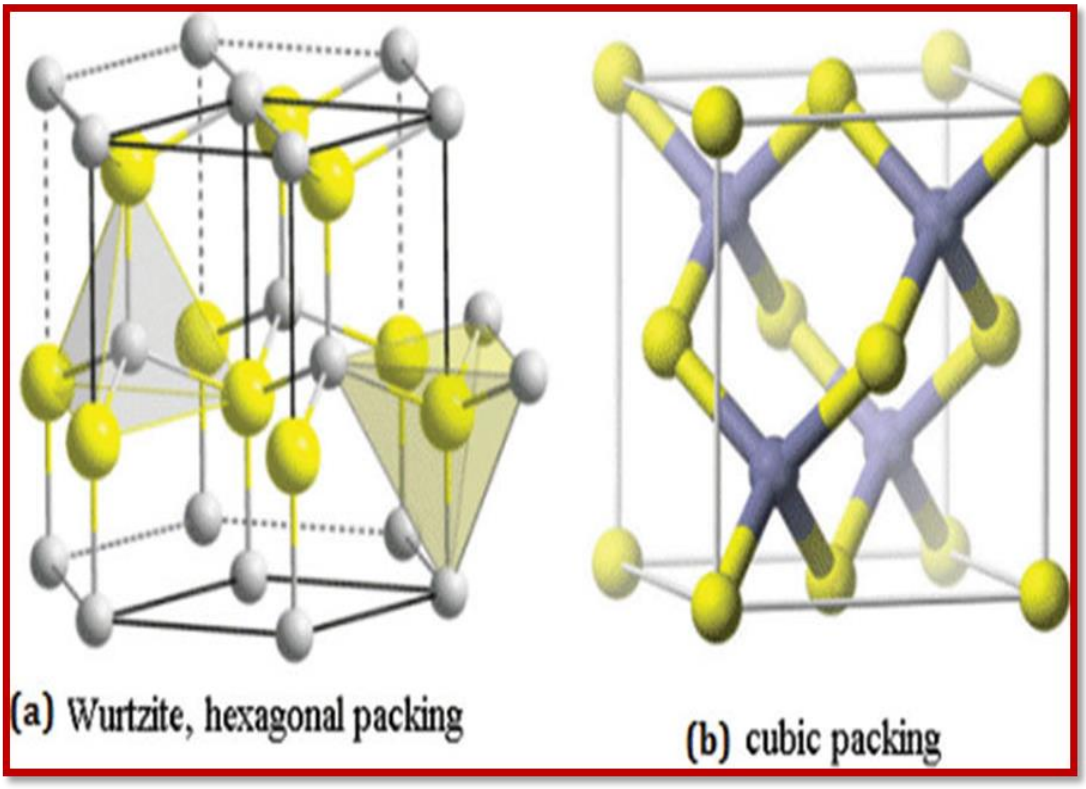

Fig. (1.3): (a) Wurtzite crystal structure and (b) cubic packing crystal structure of ZnO[31]

1.2.2- Optical Properties of ZnO :

Intrinsic and extrinsic impacts both contribute to the optical properties of a semiconductor. The moves of the electrons in C.B and holes in V.B are treated as intrinsic optical transitions, in which the excitonic effects due to the Coulomic interaction are also included [32]. Extrinsic properties are related to the electronic states made in the band gap by dopants/impurities or complexes and point defects, which influence both emission and optical absorption processes neat zinc oxide is white and transparent[33].

Advantages contribute with a great band gap involve lower electronic noise, high-power operation, voltages higher breakdown, high temperature, and ability to sustain a big electric fields. The band gap of zinc oxide can furthermore be adjusted from ~3–4 eV via its all combination with magnesium oxide or cadmium oxide [34].

1.2.3- Application of ZnO Nanostructures :

Due to its versatility and multifunctionality zinc oxide creates attention in the research field related to its applications. A large number of synthesis techniques also been developed by which ZnO can be grown in different nanoscale forms and thus different nanostructures can be fabricated with different shapes ranging from nanowires to nanobelts and even nanosprings .

1.2.3.1-Medical Application:

Zinc oxide with about 0.5% iron(III) oxide, this mixture is called calamine and is used in calamine lotion. Zincite and hemi-morphite when they are mixed with eugenol, the mixture is called zinc oxide eugenol[35]. Active ZnO inhibits the growth of bacteria such as(*Propionibacterium acnes*) which results in less of the sebum wich is an oily substance secreted by the sebaceous glands in mammalian skin being split into the free fatty acids which in turn act to inflame the follicle wall [36].

1.2.3.2- The Textile Industry :

Numerous researchers have been dealing with water repellent ,self-cleaning, and Ultraviolet-blocking textiles.

The textile applications, not only zinc oxide biologically compatible, as well as the covering nanostructured Zinc Oxide are more air-permeable and efficient as UV-blockers compared with their bulk counterparts [37].

1.2.3.3-Electronics Applications :

Zinc Oxide is well known of 3.37 eV as a large direct band gap at RT. Therefore, light emitting diodes (leds) and laser diodes is a most common potential applications [38] .

1.2.3.4-Catalysts:

Zinc oxide is used to catalyze dehydrogenation (organic reactions). Active zinc oxide is derived from zinc hydroxide or carbonate are used in these applications.

Due to its high photosensitivity , zinc oxide has attracted much attention with respect to the degradation of various pollutants [39], stability and wide band gap [40].

Surface area of zinc oxide, which depend on the synthesis method, are important factors for determining its photocatalytic activity.

In a photocatalytic system, photo-induced molecular transformation or reaction takes place at the surface of the catalyst.

A basic mechanism of photocatalytic reaction on the generation of electron–hole pair and its destination is as follows: when a photocatalyst is illuminated by the light stronger than its band gap energy, electron migrates from valance band (VB) to conduction band (CB) and holes are formed in valance band; these holes can generate hydroxyl radicals which are highly oxidizing in nature.

Hole can react with dye molecule and abstract electron from dye molecule and process of degradation start[41].

1.2.3.5- Chemicals and Biosensor Applications:

Nanostructures of zinc oxide exhibit interesting properties including high catalytic efficiency and strong adsorption ability , moreover to its unique optical, piezoelectric ,semi-conducting and magnetic properties.

Due to its high isoelectric point (9.5) ,fast electron transfer and biocompatibility , interest has recently been focused onto the application of ZnO in biosensing [42].

1.3 - Types of Heterogeneous Photocatalysis:

1.3.1 Noble Metal-Based Photocatalysis:

In the history of heterogeneous photocatalysis, a lot of noble metals oxides transmaition , Pt, Pd, Ru, Ir and Rh, and some metal oxides, such as Ti, Zn, Ce and Cr, have been used as photocatalysts [43].

A good photocatalyst should be photoactive, able to harnest visible and/or near UV light energy, biologically and chemically inert, stable towards photocorrosion, low in cost and toxicity[44].

It is well known that metals oxides are generally more active catalysts than noble metal in majority of applications. However, noble metals are less resistant to poisoning than metal oxides, and can be a potential hazard to the environment.

Moreover, due to absence of band gap and the continuum of electronic states in the noble metal structures, the photogenerated electron-hole pairs can be readily recombined, which leads to deactivation of the active sites and a reduction in photocatalytic efficiency.

Hence, metal oxides are more suitable to be used in various applications as photocatalysts.In fact, according to Matatove-Metal and Sheintuch

[45], there are some criteria for catalysts to be used in industrial applications, such as high activity, resistance to poisoning and stability over time at elevated temperatures, mechanical stability and resistance to attrition, non-selectivity, physical and chemical stability under various conditions.

1.3.2 Semiconductor-Based Photocatalysis:

Semiconductors are materials usually solid chemical elementsw or compounds that have an electrical conductivity between conductors and insulator[46].

The important character to make the ZnO,TiO_2 and some semiconductors is good sensitivity for light in processes of redox is electronic structure of this semiconductors .Semiconductor materials are materials in which both of valance band (V.B) and conduction band (C.B) are isolated by energy gap (E_g)[47]. Two kind of semiconductors, it's called n and p-type [48]. The energy at which the probability of an energy level being involved by an electron is exactly 1/2 at 0K is Fermi level. Fermi level for the semiconductor movements in the band gap region[49]. The Fermi level For n-type doping shifts toward C.B edge, and the doping of p-type shifts toward the V.B edge[50, 51] as shown in Figure. (1.4)

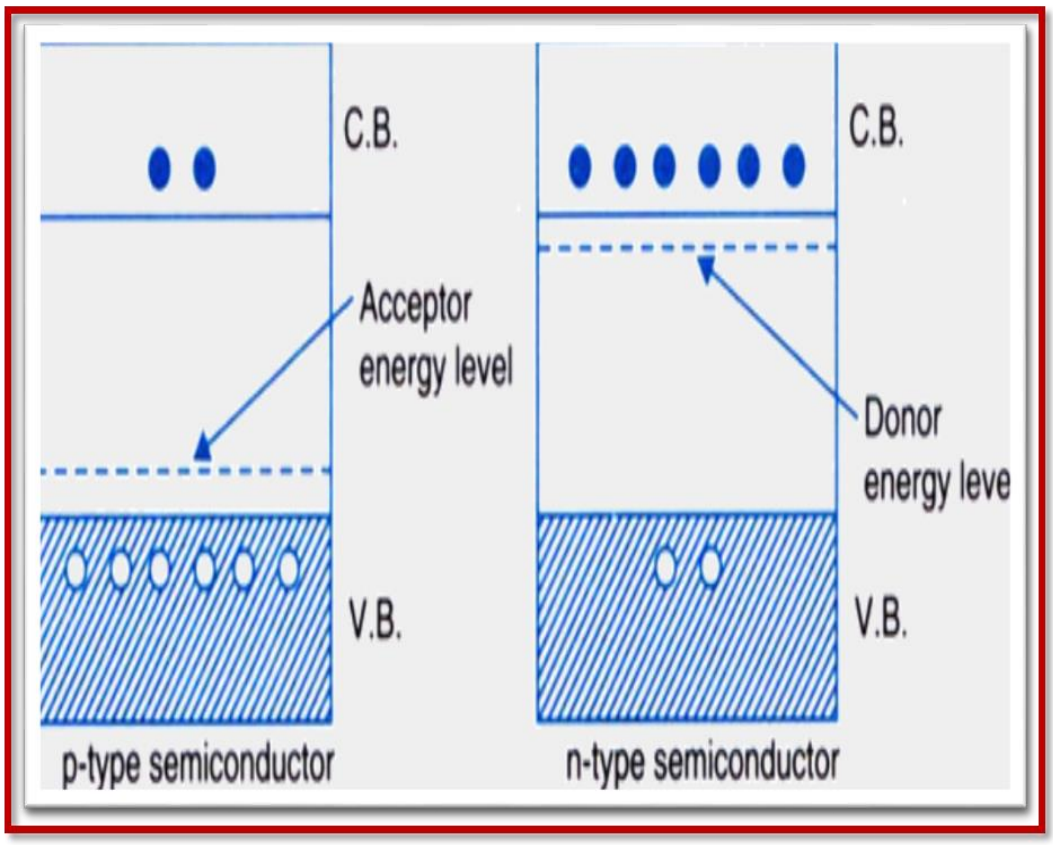

Fig. (1.4): Energy level diagram for n and p-type semiconductors [52].

The band theory is necessary to understand semiconductor properties . In this theory at 0 K, a perfect crystal of a semiconductor material has a group of very close and filled electronic states, this is called valance band (V.B).

Another group of close and empty electronic state is called conduction band (C.B), and E_g between them is called energy gap[53]. Table (1.3) summarizes the most common semiconductor used in photocatalysis , their band gap and respective wavelength sensitivity [54].

Table (1.3): Energy band gap and wavelength sensitivity of different semiconductors.

No.	Semiconductor	Eg (eV)	λ (nm)
1.	CdS	2.4	517
2.	Fe_2O_3	2.3	539
3.	$SrTiO_3$	3.2	388
4.	TiO_2 (rutile)	3.0	413
5.	TiO_2 (anatase)	3.2	388
6.	WO_3	2.8	443
7.	ZnO	3.2	378

A doped semiconductor has a big difference in the concentration of the two types of charge carriers. When the semiconductor is exicted, holes and electrons are generated by light absorption. The sensitivity of a semiconductor to the energy photon is indicated by the energy of band gap.

An important effect is the recombination on the semiconductor. Direct recombination may occur when the electron returns from C.B edge to V.B edge. Indirect recombination occurs with an inter mediate energy level .This method of recombination can be particularly effective because the intimidated energy level can capture the hole and electron [55].

1.3.3- Principles of Heterogeneous Photocatalysis:

Homogeneous catalysis refers to catalysts that exist in the same phase (gas or liquid) as the reactants and are thus difficult to be separated, while heterogeneous catalysis refers to catalysts that do not exist in the same phase as the reactants and are therefore easily to be separated[56] Typically, heterogeneous catalysis involves the use of solid catalysts placed in a liquid reaction mixture[57].

The mechanism of photocatalysis using zinc oxide as a catalyst is illustrated in Figure.(1.5). When the suspended solution is irradiated by incident photons with energies equal or larger than the band gap of zinc oxide(3.37 eV) the electrons in the a low energy valence band (VB) of the semiconductor photo catalyst are excited into the a high energy conduction band (CB), leaving an equal number of the corresponding holes in the valance band [58] (Eq. (1.1)

$ZnO + hv \longrightarrow ZnO(^{-}e + ^{+}h)$…… (1.1)

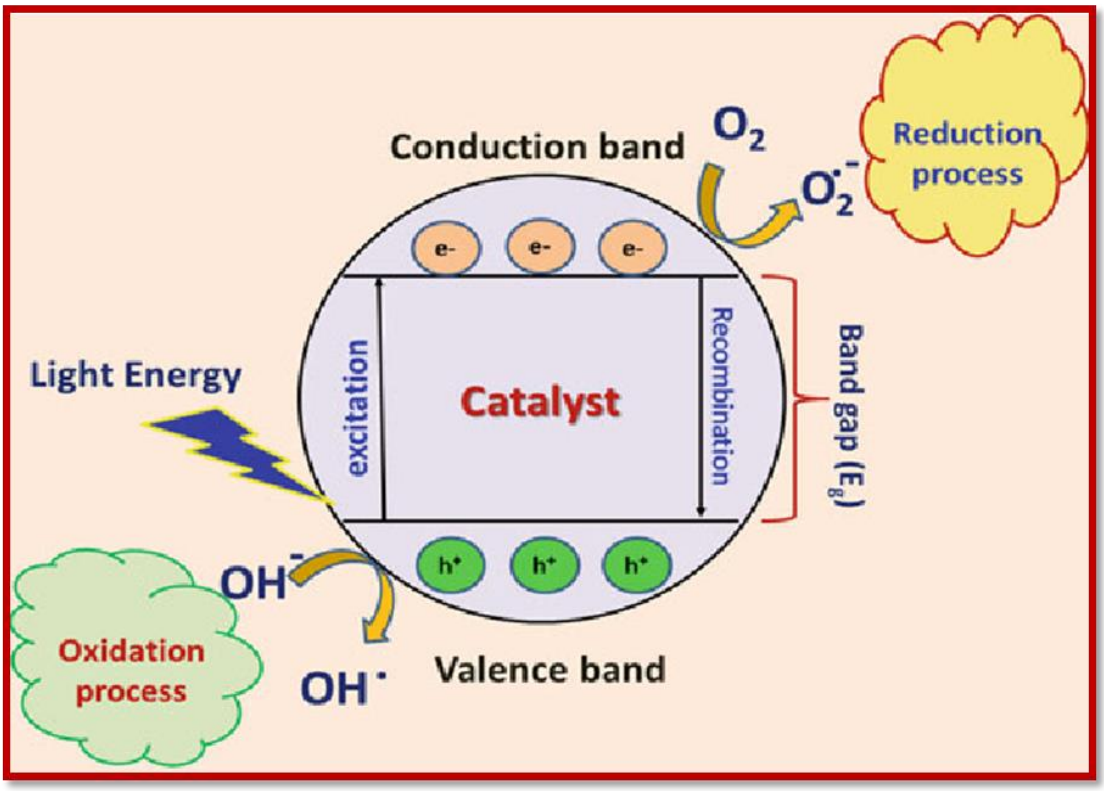

Fig. (1.5): A schematic diagram illustrating the principle of photo catalysis[59]

The holes in the valance band can be oxidize the pollutants

^{+}h + dye $\longrightarrow$ dye$^{\cdot}$ +degradation of the dye ……...….(1.2)

Or generate high reactive hydroxyl radicals (OH·) by decomposition of water

$^{+}h + H_2O \longrightarrow H^{+} + OH^{\cdot}$ ……(1.3)

Or reaction with hydroxyl ions (-OH) in water, are involved in an oxidation reaction .

$^{+}h + {}^{-}OH \longrightarrow {}^{\cdot}OH$ ……...(1.4)

On the other hand, the photo electrons that are formed in the conduction band on the catalyst surface, and participate in a reduction reaction,This proass can reduce adsorbed oxygen into superoxide anions.[60] [61]

$^{-}e + O_2 \longrightarrow {}^{\cdot -}O_2$ ……(1.5)

Or peroxides

$2e^{-} + O_2 + 2H^{+} \longrightarrow H_2O_2$ ……(1.6)

As a result formation hydroxyl radicals (OH·)

$^{-}e + H_2O_2 \longrightarrow {}^{-}OH + {}^{\cdot}OH$ ……..…..(1.7)

[62]

The hydroxyl radical is a highly powerful, non-selective oxidant (E° = +3.06 V) which gives a partial or complete decomposition of many organic compounds

[63]

$^{\cdot}OH + dye \longrightarrow$ intremediates $\longrightarrow CO_2 + H_2O$ ……...(1.8)

[57, 64])

The acts as the primary cause of organic species mineralization in the photocatalytic reactions. The photoexcitation of ZnO semiconductor by proper UV light irradiation, the primary degradation of dye is caused by the hydroxyl radicals generated through the previous processes.

It is worth noting that the presence of adsorbed oxygen molecules prevents the recombination of the photo generated electron-hole pairs.

1.4 - Advanced Oxidation Processes (AOPs):

These a set of chemical treatment procedures designed to remove organic (and sometimes inorganic) materials in water and wastewater by oxidation through reactions with hydroxyl radicals ($^{\cdot}OH$).

The first AOP based water purification/treatment in full scale was proposed in early 1980s[65], AOPs are characterized as best water treatment/purification processes that involve generation of hydroxyl

radical ($^{\cdot}OH$) in sufficient quantity to affect water purification at standard temperature and pressure[66, 67].

The significant advantage of AOPs over all existing chemical and biological processes is that they are totally "environmental-friendly" as they neither transfer pollutants from one phase to the other (as in chemical precipitation and adsorption) nor produce massive amounts of hazardous sludge[68]

AOPs : Consists of various techniques for the generation of reactive oxygen species and these are shown in Figure (1.6)[69].

Fig. (1.6):Classification of Advanced Oxidation Processes

1.5 -Coordination chemistry:

Coordination chemistry is the branch of chemistry that study coordination complexes. Such complexes are formed by bonding an ion or a central metal atom (Lewis acid) which has empty orbitals that are able to receive electrons from donating groups (Lewis base) [70].

A coordination bond differs from a covalent bond in that a covalent bond is formed when each atom shares an electron, while a coordination bond is formed when an electron pair carrier atom is able of donating the

electronic pair to a metallic ion containing an empty orbital to accept it. The coordination number is the number of electrons awarded, and most coordination compounds have the numbers 2, 4, and 6 and thus take the shapes of linear, tetrahedral, square planar and octahedral [71].

Inorganic Chemistry is involved in many fields, where some coordination compounds are found in biological systems, such as chlorophyll. Additionally, they can be used as catalysts since its compounds form a wide variety of colors, Coordination Chemistry has a place in the field of art, as artists used several coordination compounds as pigments, one of which is Prussian blue, which is made up of iron (II) and iron (III) [70]. A cyanide ligand holds them together Several metals are used as therapeutic, diagnostic, and pharmaceutical agents. Metals such as arsenic, gold and iron have been used to treat a variety of human diseases since antiquity [72].

Medical applications use a simple salt of the metal itself in some cases, such as the therapeutic use of lithium in bipolar disorders. However, the number of metal-based drugs is increasing all the time, Platinum anticancer drugs are among them "used as a component of nearly 50 percent of all cancer treatments"[73]

1.5.1 Chelate and Chelating Effect:

The chelate describes the groups that are capable to behave like two associating units. The process of chelation involves coordination of more than one sigma-electron pair donor group from the same ligand to a single central atom. The term polydentate is used to describe the number of ligand groups on a single chelating ligand [74].

Several factors of the stability are common in all chelate systems nd these which are the size and number of rings, substituents on the rings, and the nature of metal and donor atoms. In the macrocyclic complexes,

the degree to which the size of metal ion fits the space enclosed by the macro rings is a significant factor.

In chelation, five- and six-membered rings are most stable: coordination angles on the metal atoms prohibit the formation of three-membered rings and ring closure is improbable for rings having more than seven members.

In these latter systems, coordination in linear chains is a competing reaction. Formation of each additional ring by the same ligand contributes extra stability from the entropy effect of displacing coordinated solvent molecules. Substituents on a ring may also produce steric hindrance or otherwise alter the availability of the donor atom electrons for coordination. The stability constants are usually influenced by more than one of the parameters that are known to affect chelate stability. In some cases, the size of ring, number of rings for similar donor atoms, and whether one or more ligand molecule forms the rings will influence the chelate stability[75]

The chelate effect refers to the preference of metal ions to form comp-lexes with chelating ligand rather than non-chelating ligands where the two types of ligands can form bonds of similar strength. The chelating effect is affected by enthalpy and entropy contributions[76].

In general, for any stability constant as well as for their differences, the following thermodynamic relationship can be expressed as(Eq.9)

$$\Delta G^{\circ} = -RT \ln \beta = \Delta H^{\circ} - T\Delta S^{\circ} \quad \text{.....(1.9)}$$

With increasing of β, ΔG° becomes more negative, due to more negative enthalpy term ΔH° or more positive entropy term ΔS°. Factors ΔH° and ΔS° can operate in the same or different directions, the sum effect being decisive.

The following enthalpy contribution can be considered: ligand repulsion, ligand distortion and crystal field stabilization energy[77] .

The activity factor means that the chance of coordination of the other end of the ligand is proportional to its effective local concentration around the metal ion. In diluted solution, this is much higher than the average ligand concentration because the other end is located in a relatively small volume immediately surrounding the metal ion[78].

1.6 - Schiff bases:

Schiff bases contain azomethine group (-RC=N-), It is prepared by condensation of carbonyl group (aldehyde or ketone) with primary amines, it is nucleophilic addition forming a hemiaminal, generally Schiff base formation under acids or base catalysis upon heating as in the scheme (1.1) [79].

The aromatic aldehydes particularly with the effect of conjugation system form stable Schiff bases, but the aliphatic aldehydes are unstable and easily polymerize [80].

Schiff bases are currently being studied extensively due to their ease of synthesis, various structures with wide range of color, and they have sparked a lot of interest in the thermochromic material field[81]. These Schiff bases are made by combining a primary amine with an aldehyde or ketone and releasing water[82-84].

This combination is stable under both oxidation and reduction conditions[85]. The structure of any Schiff base is containing the significant azomethene group (C = N) in which it can coordinate with the metal ion through the pair of electrons provided by the N atom.[86] Because of their ability to form strong bonds with metal ions, Schiff bases are an important ligands in coordination chemistry[87]. Schiff bases are considered one of the important areas that researchers are focusing on, due to their use in many applications such as antibacterial, antifungal[88] anti-inflammatory[89] anti-tumor[90] and antiviral[91].

It has many other applications in addition to the biological ones, such as catalytic effect, corrosion inhibiting effect and industrial and electronic applications [92] .

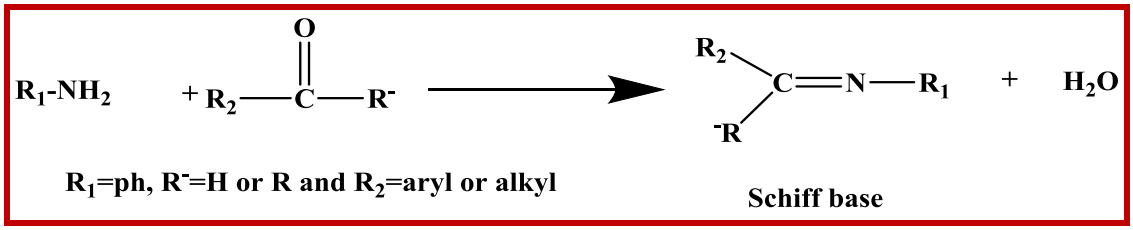

Scheme .(1.1)-: Formation of Schiff base

1.6.1- Classification of Schiff Bases:

Schiff bases are classified according to the number of Schiff bonds in the igand in to the following groups:

Monodentate Schiff Bases: These ligands contain one Schiff bond [93], an example of such Schiff bases is shown in the Structure (1.1)

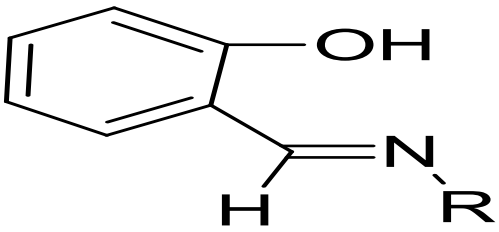

Structure (1.1): Monodentate Schiff base

Bidentate Schiff Bases: These ligands contain two Schiff bonds[94]. As given in Structure(1.2)

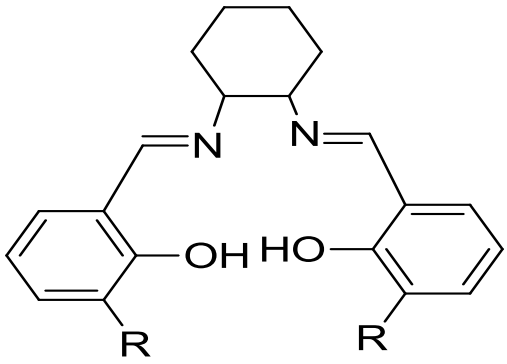

Structure (1.2): Bidentate Schiff base

Polydentate Schiff Bases: These ligands contain more than two Schiff bonds [95, 96] . Structure (1.3) shows such Schiff base type:

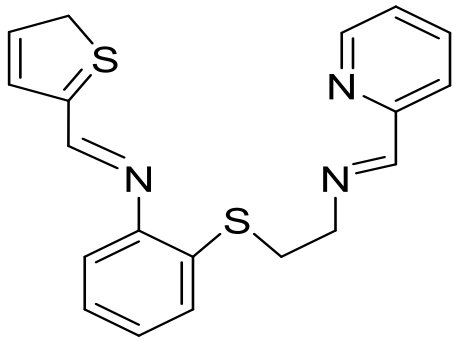

Structure (1.3): Polydentate Schiff base

1.7 - Dyes:

Dyes, unlike most organic compounds, have color because they have a chromophore structure consisting of an extended conjugated system of [p- electrons], often bearing groups with an electron acceptor or donor that can absorb light in the visible spectrum (400–700 nm).

They can be classified based on their chemical structures into several groups, including azo, anthraquinone, quinone , phthalo cyanine, sulphur andtriarylmethine[97].

Azo dyes absorb visible light due to their chemical structure, which is defined by one or more azo groups (–N=N–).

Azo group can besubstituted by benzene or naphthalene groups, which can contain avariety of substituents such as methyl (–CH3), chloro (–Cl), nitro ($–NO_2$),amino ($–NH_2$), carboxyl (–COOH), and hydroxyl (–OH), resulting in avariety of azo dyes .

Azo dyes account for the majority of all textiledyestuffs produced due to their low cost of synthesis and ease of use,stability, and color variety when compared to natural dyes.

Dyes are widely used in industries such as textiles, paper, leather,cosmetics, food and pharmaceuticals. The improper discharge of textiledye effluent containing azo dyes into aqueous ecosystems reduces

sunlight penetration, which reduces photosynthetic activity, dissolved oxygen concentration and has acute toxic effects on aquatic flora and fauna, resulting in environmental problems. Adsorption, oxidation, filtration, ozonation, microorganisms and enzymatic methods have all been used to remove synthetic dyes from waters and wastewaters in order to reduce their environmental impact.

Other common chromophoric configurations include azo (-N=N-), carbonyl (-C=O); carbon (-C=C-); carbon-nitrogen (>C=NH or -CH=N-); nitroso (-NO or N-OH); nitro(-NO_2 or =NO-OH); and sulphur (C=S) (, The chromogen, which is the aromatic structure normally containing benzene, naphthalene, or anthracene rings, is part of a chromogen-chromophore structure along within an auxochrome Generally, the dyes used in the textile industry are basic dyes, acid dyes, reactive dyes, direct dyes, azo dyes, mordant dyes, vat dyes, disperse dyes, and sulfur dyes where azo derivatives dyes are the major class of dyes that are used in the industry today[98].General classification of dyes are shown in Figure(1.7)

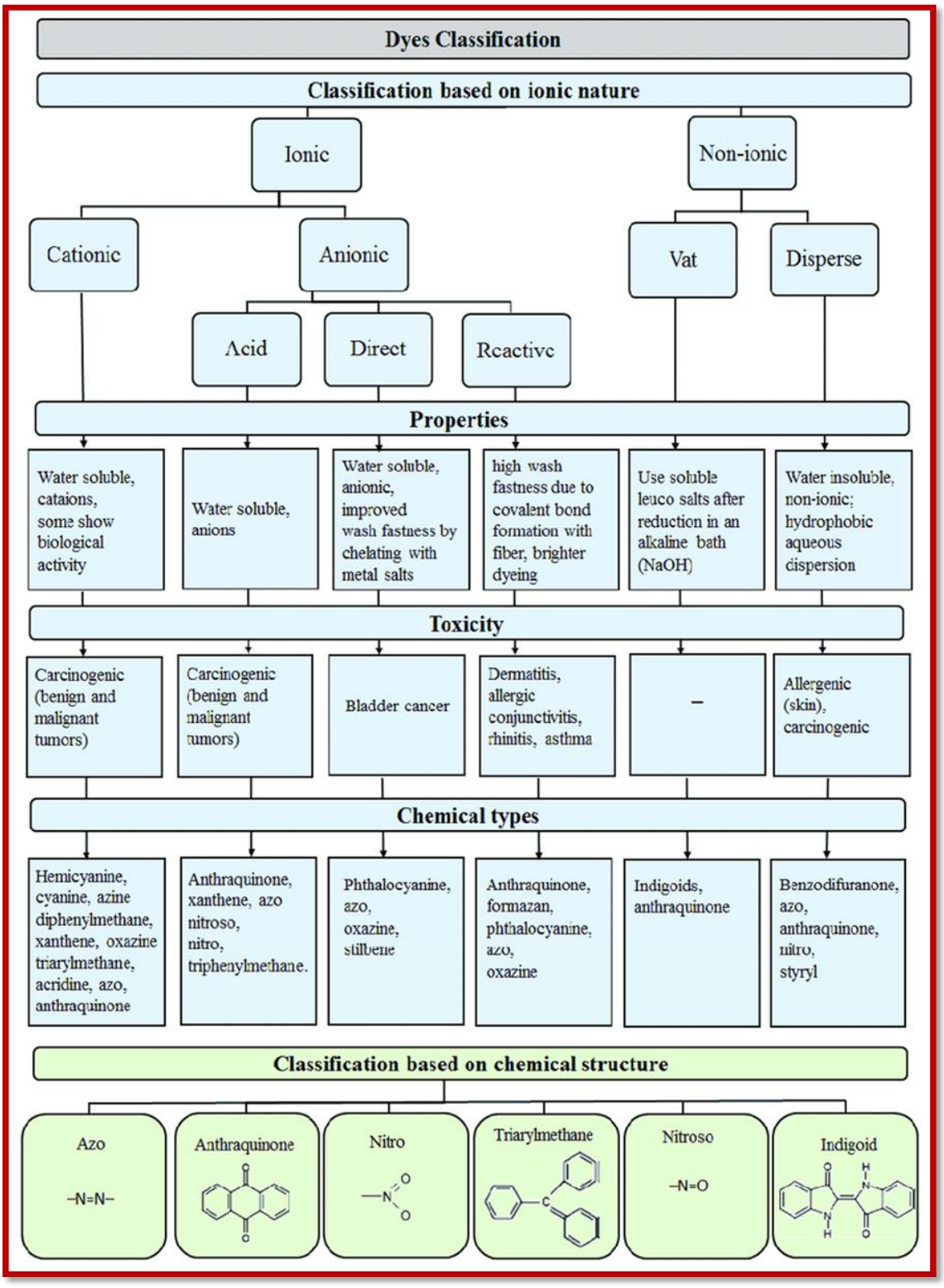

Fig.(1.7) -Classification of dyes based on ionic charge with corresponding properties, chemical types and some of the reported toxicity impacts (in blue), and based on chemical structure with corresponding chromospheres [99].

1.7.1 - Alizarin Yellow G Dye(AYG) :

Alizarin yellow G (AYG) is a bright, clear yellow with earthy undertones. Despite the name, this oil paint contains no AYG lake and is completely permanent. AYG is a well-known textile dye and an acid-base indicator that is also used in histology, dyeing, and the development of nutritive medium[100, 101]**.**

It has a wide range of applications in the context of increased chemical stability in aqueous medium, and the scope of discharge to waterbodies and related contamination is large. In the preparation of nutritional media, the acid-base indicator AYG is often utilized. According to studies, dye removal from aqueous solutions is pH dependant and can be accomplished by irradiating the sample with 369 nm radiation utilizing micro ZnO particles [102].

Because it stains free calcium and certain calcium compounds a red or light purple hue, AYG is commonly used as a staining agent in biological research. AYG is still used as a commercial red textile dye, but to a smaller level than before. There are very few photodegradation research on the azo dye AYG in the world [103].

1.7.1.1-Product Information of AYG Dye:

Name:

Alizarin Yellow G(AYG)

Synonyms:

- Metachrome Yellow
- Salicyl Yellow
- 2-Hydroxy-5-(3-Nitrophenylazo)Benzoate Sodium
- 5-(3-Nitrophenylazo)Salicylic Acid, Sodium Salt
- Acid Chrome Yellow 2GW
- Acid Chrome Yellow GG
- Alizarin Yellow
- Alizarin Yellow G
- Alizarin Yellow G Sodium Salt

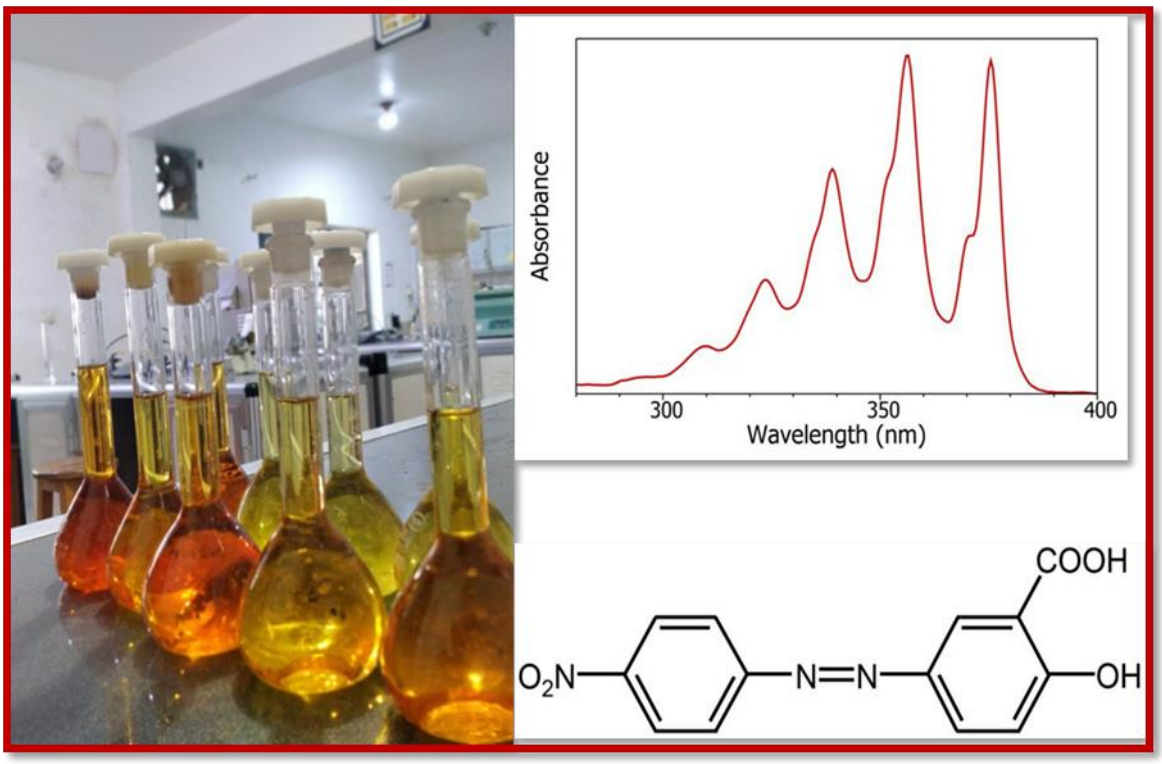

Fig. (1.8) Alizarin Yellow G Dye (AYG) [104]

1.8-A Review of Studies:

This review article seeks to describe recent research studies on the photoelectrocatalytic color breakdown and the production of ZnO-nps that have received a lot of interest in the previous decade.

.**Muhammad Amirul Islam, *et al* in .(2011):** The Succeeded Under Uv And Visible Light Irradiation, In such a liquid ZnO emulsion, the photocatalytic degradation of a heteropolyaromatic dye (Methylene Blue) was investigated. After 6 hours of UV light irradiation, the catalytic procedure resulted in a net decolorization and mineralization (50 M Mb) of about 98 and 89 percentages, resp.Meanwhile, After 8 Hours Of Visible Light Irradiation (10 M Mb), Decolorization And Mineralization Were Around 95 Ercent and 77 Percent, Respectively[105].

K. M. Joshi* *et al* in .(2012): the most active photocatalysts are nanosized TiO_2 and ZnO. the reference molecule for the experiment was methylene blue. degradation through photocatalysis. TiO_2 and ZnO have the ability to completely eliminate methylene blue dye is a dye that is used to make methylene blue. the impact of numerous process characteristics such as the initial state on the effect of concentration, contact time, catalyst dosage, and photocatalysis was used to remove dye in the presence of TiO_2 and ZnO. semiconducting materials were investigated. before and after deterioration of XRD and SEM[106].

R. Saravanan [a] *et al* in (2013): A simple thermal breakdown approach was used to make pure ZnO nanorods. The ZnO was made by calcining zinc acetate dihydrate directly. X-rays diffraction confirms the hexagonal structure of ZnO . SEM and TEM examinations were used to determine the form and size of the nanorods. XPS was used to analyze the

surface component and oxidation states of a ZnO sample. The estimated absorption coefficient values of Nanoparticle during UV light irradiation reveal that the photocatalytic activity may be high[107].

Jing Miao [A] , *et al* in. (2014): From being successfully used as a photocatalyst in aqueous solutions using a type of commercial nanosized catalyst, the equipment needed decomposition on Mordant Black 11, and Azo dye, was investigated with Visible light light (ZnO). To describe nanosized ZnO, researchers utilized UV–Vis Attenuated Total Spectrum, x-rays refracted, transmission electron, x-rays powder diffraction, and other techniques. the effects of catalyst dosage, initial dye concentration, initial PH value, and irradiation intensity on decolorization rates[108].

Keyvan Bijanzad [A], *et al* in. (2015): Hollow microblocks of as a new coordination chemical, [Zn(Anic)2] was produced using 2-aminonicotinic acid and zinc (II) nitrate tetrahydrate. the chemical composition of the zinc complex, was determined using fourier transform infrared spectroscopy and elemental analysis. the produced zinc complex was used as a precursor to create ZnO nanostructures after calcining at 550 °c for 4 hours. the x-ray diffraction pattern of the final product confirmed the production of a pure ZnO composition with a hexagonal structure. furthermore, ftir investigations showed that after the calcination step, the ligand peaks of 2-aminonicotinic acid were no longer present. diffuse reflectance spectroscopy was used to determine the band gap energy of the generated ZnO, which was found to be around 3.19 eV[109].

Saloni Sood,[A] *et al* in. (2016): in this study, the ZnO nanoparticles thermal decomposition of the zinc oxalate precursor $ZnC_2O_4.{}_2H_2O$ was used, which was synthesized using a simple solution-free

mechanochemical technique. the oxalate precursor decomposes in two phases, yielding zinc oxide nanoparticles, according to thermogravimetric analysis/differential thermal analysis. the ZnO nps were studied using fourier transform infrared, powder X-rays Diffraction, Transmission Electron Microscopy, and UV-Visible methods. according to the XRD Pattern, the hexagonal Wurtzite phase of ZnO nanoparticles had a high crystallinity. according to rietveld's refinement of the Xrd Pattern, the average grain size of the as-manufactured nanoparticles was 13 nm. The photocatalytic activity of as-prepared ZnO nps was investigated using methyl orange[110].

Hamide Barfeie *et al*. in. (2018): Bidentate NO was used to make four new bis-chelate ML_2 complexes (M= $Cu^{2+,}$ $Ni^{2+,}$ $Zn^{2+,}$ $VO^{2+,}$ and L= 1-[Furan-2-ylmethylimino)methyl]naphthalene-2-olate). The Schiff base ligand was studied using spectral and analytical methods. CuL_2, NiL_2, and VOL_2 crystal structures were determined using single crystal X-ray analysis. The Schiff base ligand is a bivalent ligand that attaches to the metal core via N and O atoms. VOL_2 complexes have a distorted square-pyramidal coordination geometry, whereas NiL_2 and CuL_2 complexes have a distorted square planar coordination geometry. The thermal analysis and thermal deterioration of the complexes in question were looked into. TGA, XRD, and SEM tests found the followi and SEM analyses revealed that they were transformed to metal oxides in the form ofform of nanoparticles (NiO, CuO, ZnO and V_2O_5)[111].

Krishnaswamy Kanagamani, *et al* in. (2019): they've been successful because of its vast application in numerous healthcare domains, phytomediated production of metal oxide nanoparticles has become a prominent study focus in nanotechnology. uv–visible

spectroscopy, scanning electron microscopy ,energydispersive x-ray spectroscopy ,fourier transform infrared spectroscopy ,x-ray diffraction ,transmission electron microscopy , and selected area electron diffraction studies were used to characterize the synthesized ZnO-nps [112].

Suhad Kareem Abass[1],*et al* in. (2020): a new novel in the mixed-ligand genre in this study, a binuclear Co complex of schiff base was synthesized. melting points, Uv-vis spectra, FTIR spectra, and magnetic susceptibility measurements were used to characterize the complex, which were then compared to metal and ligand solutions. based on the "metal:ligand" stoichiometry, the schiff bases and the Co ion form a binuclear complex with a molar ratio of 1:2. photodecolorization [113].

Hanadi A.Katouah, *et al* in . (2021): this work employed the thermal breakdown of unique Co(II) and Zn(II) schiff base complexes to make Co_3O_4 and ZnO nanoparticles. condensation of 4-amino-5-ethyl-4H-1,2,4-triazole-3-thiol with 4-(dimethylamino)benzaldehyde and 2,4-dihydroxybenzaldehyde, respectively, yielded the schiff bases e1 and e2. condensation of schiff bases with $CoCl_2•_6H_2o$ and $ZnCl_2$, respectively, yielded the Co and Zn complexes. different tools were used to characterize the schiff bases, complexes, and nanoparticles, including 1HNMR, FTIR, CHNS elemental analysis, TGA thermal analysis, XRD, TEM, and Uv–vis spectrophotometer. the photocatalytic degradation of crystal violet dye in aqueous media under uv illumination in the presence of hydrogen peroxide was performed using Co_3O_4 and ZnO nanoparticles [114].

Asma S.Al-Wasidi ,*et al* in. (2022): a novel Zn(II) and Co(II) schiff base complex was created by refluxing 2,3-naphthalenedicarboxaldehyde, metal(II) chloride (metal = Zn or Co), and l-phenylalanine ZnO and Co_3O_4 nanoparticles were generated by thermal breakdown of Zn(II) and Co(II) complexes, respectively. a range of instruments were used to characterize the products, including CHNS, conductivity, FTIR, XRD, TEM and Uv–vis spectrophotometer [115].

1.9- The aims of the present Work:

1-synthesis of ligands (L_1 and L_2)

2-Synthesis of zinc schiff base complexes

3- synthesis of ZnO nanoparticles *via* thermal decomposition method.

4- the study characteristic of nano particales using XRD, SEM, TEM EDX,FTIR,TGA,and,BET.

5- study the photo activity of nano particales using dyes.

6- study different parameter such as effect of dye concentration , effect of mass of catalyst, effect of temperature, effect of addiction hydrogen pyroxide H_2O_2,effect of Intensity effect of pH .

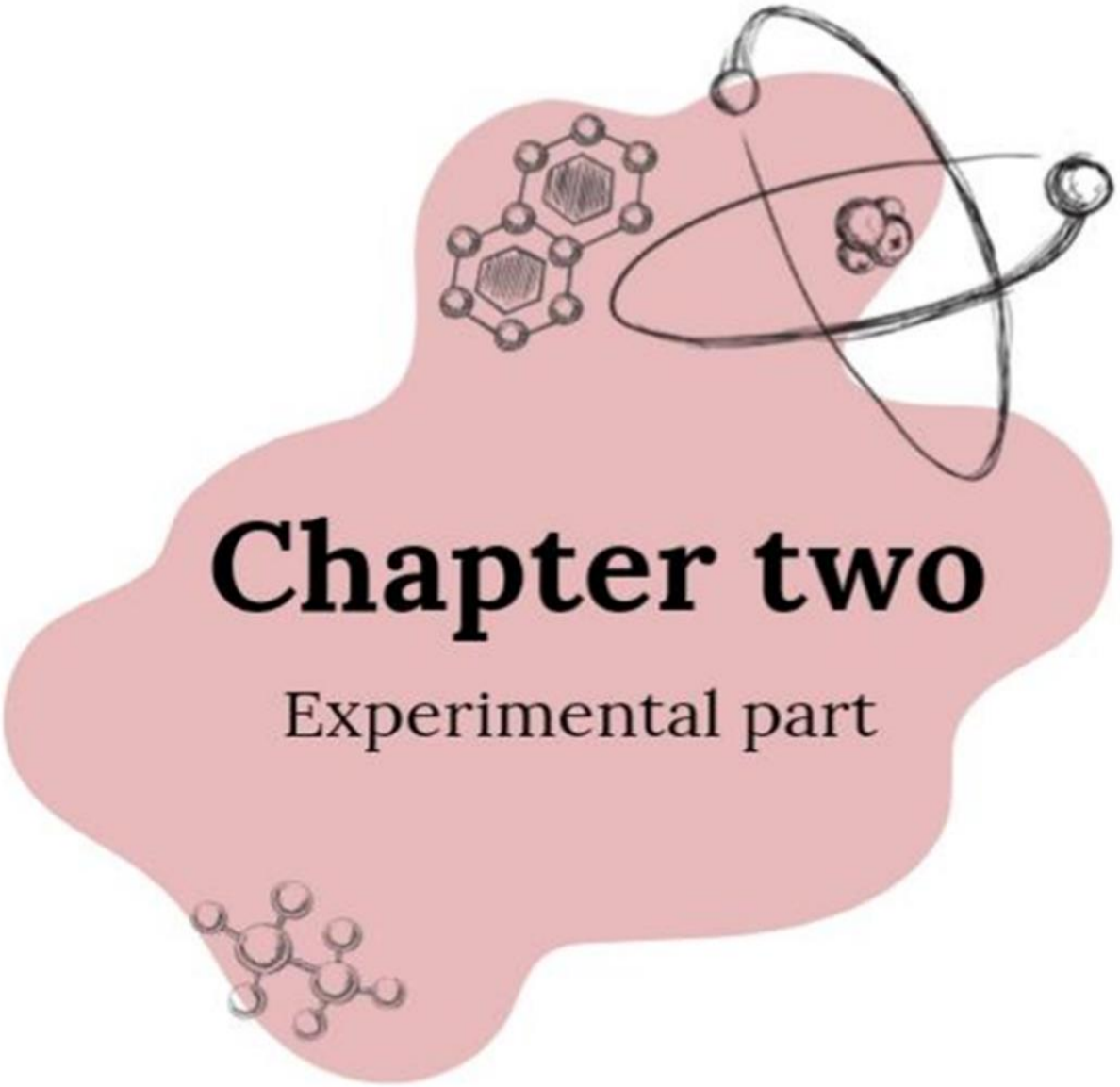

Chapter two

Experimental part

2.1- Chemical Reagents:

Table(2.1) lists all commonly used laboratory chemicals and reagents .These ingredients were utilized without any additional purification.

No	Material	Chemical formula	Molecular weight $g.mole^{-1}$	Supplier	Percentage%
1.	Salicylaldehyde	$C_7H_6O_2$	122.12	Sigma-Aldrich	98
2.	Benzyl amine	C_7H_9N	107.16	Sigma-Aldrich	98
3.	Zinc Acetate di hydrate	$Zn(CH_3COO)_2$. $2H_2O$	219.49	Sigma-Aldrich	98
4.	Glacial acetic acid	$C_2H_4O_2$	60.05	BDH	98
5.	2,5-Dihydroxybenzaldehyde	$C_6H_7O_3$	138.12	Sigma-Aldrich	98
6.	Absolute Ethanol	C_2H_5OH	46.07	Sigma-Aldrich	99.8
7.	Diethyl ether	$(C_2H_5)_2O$	74.12	GCC	99.8
8.	N.N Dimethyl Form amide (DMF)	C_3H_7NO	73.10	CDH	99.9
9.	Hydrogen peroxide	H_2O_2	19	Merck	30
10.	Hydrochloric acid	HCl	36.5	CDH	35
11.	Potassium bromide	KBr	119.01	Merch	98

12.	Sodium hydroxide	NaOH	40	Fluke	98
13.	Barium sulphate	$BaSO_4$	233.38	Merck	97
14.	Dimethyl sulfoxide DMSO	C_2H_6OS	78.13	CDH	98
15.	Alizarin yellow G	$C_{13}H_8N_3NaO_5$	309.12	BDH	97

2.2- Instrumentation:

2.2.1- Decomposition and Melting Points:

Melting points of ligands and their complexes were measured using electrothermal capillary apparatus (stuart–smp30) at laboratories of Department of Chemistry College of Science for Women, University of Babylon.

2.2.2- U.V-Visible spectrophotometer(Uv-vis):

The electronic spectra of ligands and their metal complexes were reported on an (1650-UV SHIMADZU spectrophotometer) in the range of (200-1000) nm and concentration (1×10^{-3}M) at department of Chemistry College of Science for women, University of Babylon.

2.2.3- Fourier Transform Infra-Red spectrophotometer (FTIR):

The FT-IR spectra were recorded at the department of Chemistry College of Science for Women, University of Babylon, and use a (8400 S-FTIR SHIMADZU spectroscopy) in the band KBr disk (4000-400) cm^{-1} for ligands and complexes.

2.2.4- Nuclear Magnetic Resonance (^{1}H-NMR and ^{13}C-NMR) spectroscopy:

The spectra of Nuclear Magnetic Resonance (^{1}H and ^{13}CNMR) were documented on 300 MHz NMR Spectrometer Bruker, Germany, using the internal standard tetraethyl saline (TMS) and DMSO-d^6 as a

solvent; measurements were conducted at Isfahan University of Technology (IUT) Iran.

2.2.5- Molar Conductivity Measurements:

Electrolytic conductivity calculating by using WTW conductivity meter, of metal complexes solutions (1×10^{-3}M) in DMSO solvent at 25°C in laboratories at Department of Chemistry , College of Science for Women, University of Babylon.

2.2.6- Scanning electron microscopy(SEM):

The size and morphology for the nanoparticle complexes were characterized by using scanning electron microscope (SEM) TESCAN, MIRA3, France) at University of Tehran, Iran.

2.2.7- X-ray diffraction(XRD):

The primary approach for identifying the crystalline solid structure is X-rays diffraction. Using X-rays diffraction experiments to characterize (XRD6000, Shimadzu, Japan). Iraqi Ministry of Science and Technology The mass data spectra were measured on a (Shimadzu model GCMSQP2010Ultra).

2.2.8- Thermal Gravimetric Analysis(TGA):

DTG-60, Shimadzu, Japan, was used for thermogravimetric (TGA and DTA) analysis. The experiment was carried out in an argon environment at a heating rate of 10 ^{o}C/min. measured samples were collected at the University of Babylon College of Science for Women.

2.2.9 Transmission Electron Microscopy(TEM):

TEM analysis was carried out utilizing 912AB, Leo, Germany, at the University of Tehran, Iran.

2.2.10 Energy Dispersive X- ray Analysis (EDX – Elemental):

This analysis was performed using EDX, Zeiss, Germany. The data were selected at the University of Tehran , Iran.

2.2.11-UV-visible spectrophotometer with Lisper diffuse reflectance accessory:

This technique used to measure band gap energy of manufactured ZnO Nano**,** was carried out using (UV-1700) SHIMADZU spectrophotometer and that recorded at Babylon University / Collage of Science for women /Chemistry Department**.**

2.2.12- Bruner–Emmett–Teller(BET):

The Scherer (BET) hypothesis attempts to describe the physical adsorption of gas molecules on a solid surface and serves as the basis for an important analysis technique for estimating the specific surface area of materials. The samples were collected using the Nanos ORD at Haskarsazan, Iran.

2.3- Synthesis of ligands , their Complexes and ZnO nanoparticle:

2.3.1- Synthesis of Ligands (L1 and L2):

Ligands were prepared according to the following procedure. An equimolar quantity of 2-hydroxy benzaldehyde (5ml, 0.047mol) for ligand (L_1) or 2,5-di-hydroxy benzaldehyde (6.49 g, 0.047 mole) for ligand (L_2) m.p. of 105-115 ^{o}c was added to a suspension of benzyl amine (5.ml, 0.047mol) in ethanol, then the reaction mixture was heated under reflux stirred for 6 hours. The solvent was withdrawn under reduced pressure, resulting in a solution, and then 10 ml of diethyether was added using a separating funnel to obtain an oil yellow product. The precipitate was dried in air to obtain a Schiff base (L_1) m.p. of 35-38 ^{o}C . The preparation

method is depicted in scheme (2.1), yield = 64% [116].

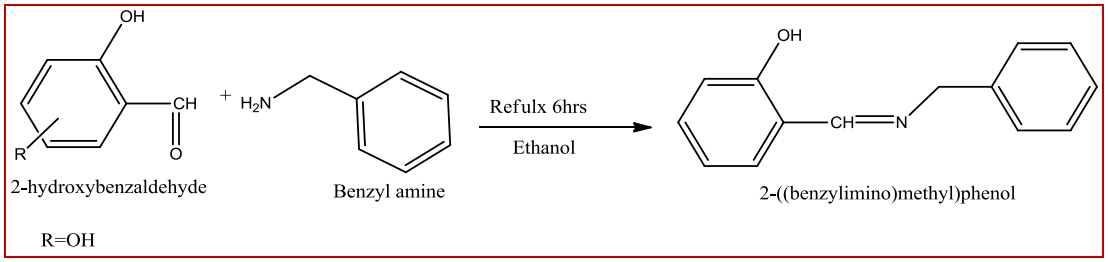

scheme (2.1): Synthesisof Ligands (L_1 and L_2)

2.3.2- Synthesis of Zn(II) Schiff complexes:

The chelate complexs were synthesized in the (M: L) ratios (1:1) and (1:2) by adding an ethanoic solution of the ligands listed in Table (2.2) to an aqueous solution of zinc acetate dehydrate. The mixture was heated under refluxed stirred for 4 hours, the colored solid precipitane was formed after cooling to room temperature and the product were filtered, dried and then recrystallized from hot ethanol[114].

Table (2.2): Complex Symbol, Complex Formula, Metal Salt, Weight (G)Metal Salt, Weight (G) Ligands:

Complex symbol	Complex formula	Metal salt	Weight (g)Metal salt	Weight (g) ligands
C_1	$[Zn(L_1)(H_2O)_2].2CH_3CO_2H$	$Zn(CH_3CO_2)_2.2H_2O$ (1:1)	10.48	10
C_2	$[Zn(L_1)_2].2CH_3CO_2H.\ 2H_2O$	$Zn(CH_3CO_2)_2.2H_2O$ (1:2)	5.19	10
C_3	$[Zn(L_2)(H_2O)_2].2CH_3CO_2H$	$Zn(CH_3CO_2)_2.2H_2O$ (1:1)	2.87	3
C_4	$[Zn(L_2)_2].2CH_3CO_2H.\ 2H_2O$	$Zn(CH_3CO_2)_2.2H_2O$ (1:2)	1.44	3

2.3.3- Synthesis of ZnO Nanoparticles:

Zinc oxide nanoparticle (NP) was obtained by directly calcining the yellow powder of Zinc Schiff base complex. Approximately 2 g were poured into a metal specimen heated to 700 ˚C in an electrical furnace at 10 C/min in air for 5 hours The ZnO NP produced in Scheme (2.2) was washed in ethanol to eliminate any leftover impurities before being air dried. [117, 118] .

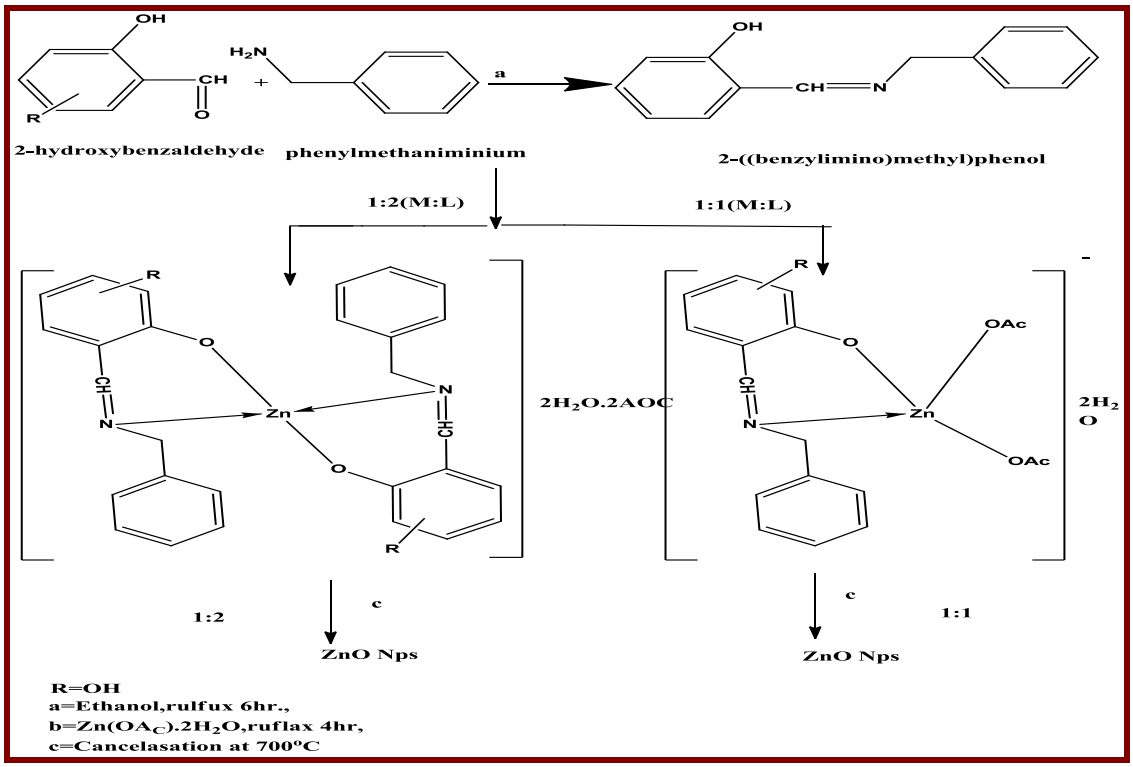

Scheme (2.2): Synthesis of ZnO Nanoparticles

2.4- Photocatalytic Reactor Set up:

Figure. (2.1) shows the photocatalytic degradation system that was used to carry out all photocatalytice experiments .

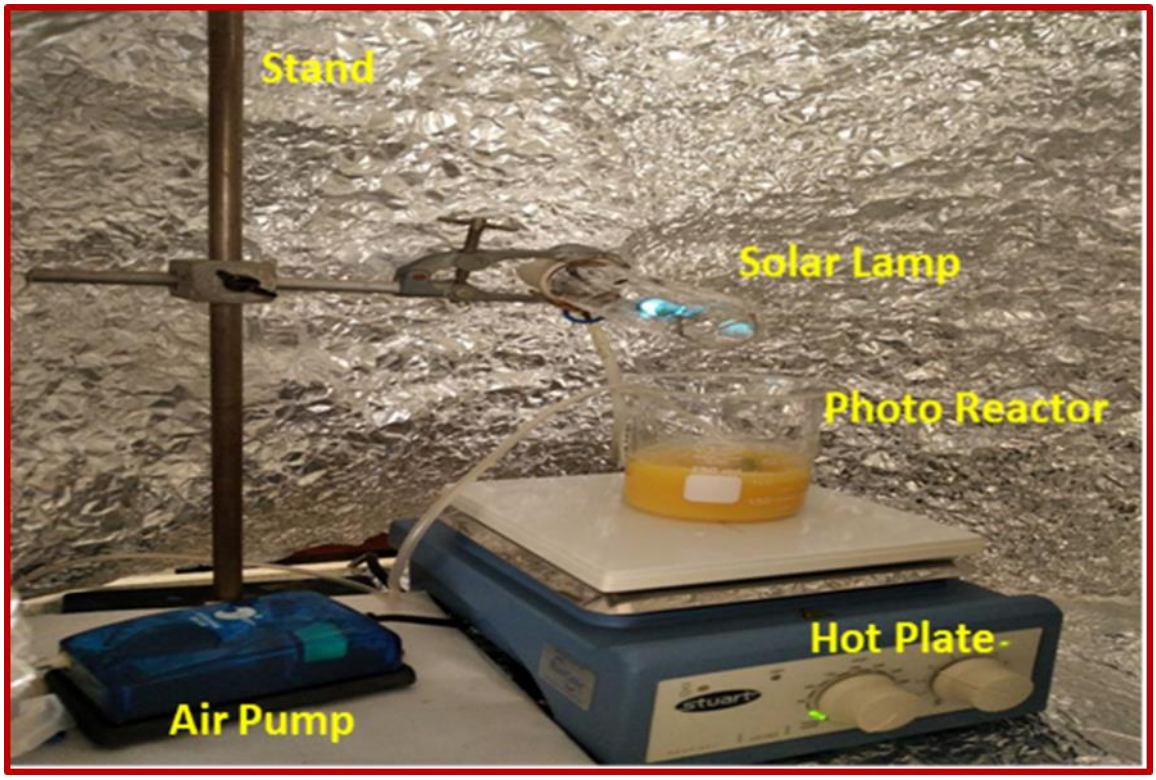

Fig.(2.1) :Optical Photo for Main Parts of The Photocatalytic Degradation System .

2.5- Parameters effecting on photocatalytic degradation process:

measurement of the reaction rate constant the response time following adsorption equilibrium can be expressed as follows:

K.t = Ln (Ao / At) ……..(2.1)

Where At and Ao are the reactant concentrations at times t = t and t = 0 plot of ln (Ao / At) vs t yields a slope of k.[119, 120]

2.6- Thermodynamic Parameters:

2.6.1-Determination the activation energy:

The activation energy can be calculated using Arrhenius Law[121].

$$K = Ae^{-Ea/RT} \quad \text{.....(2.2)}$$

$$\ln K = \ln A - Ea/RT \quad \text{.....(2.3)}$$

where : K is apparent rate constant,

T is temperature of reaction,

Ea is the apparent activation energy,

R is the gas constant, and

A is a frequency constant[122].

2.6.2- Determination enthalpy of activation and entropy of activation:

The $\Delta H°$ and $\Delta S°$ values can be calculated from the Eyring equation:

$$\ln(k/T) = -\Delta H / R \cdot 1/T + (\ln k_B / h) + \Delta S / R \quad \text{.....(2.4)}$$

where:

k is apparent rate constant.

K_B = Boltzmann's constant $1.381 \cdot 10^{-23}$ J.K^{-1}

T absolute temperature in degrees Kelvin (K)

h = Plank constant 6.626×10^{-34} J·s

R universal gas constant 8.31441 J mol^{-1} K^{-1}.[123]

2.6.3- Determination of Gibbs free energy:

The free energy $\Delta G°$ is calculated by equation.[124]

$$\Delta G° = \Delta H - T\Delta S° \quad \text{.....(2.5)}$$

2.7 photocatalytic degradation:

2.7.1- Photocatalytic degradation of AYG Dye:

Different experiments were carried out with different concentrations of ZnO Nano partial (0.02, 0.04, 0.13 and 0.6 g.) in this study. Throughout all of the studies, the concentration of AYG was kept constant. AYG irradiation with a 9 mW/cm^2 solar lamp at 298.15K. The reaction vessel was airated with a $10cm^3$/min air bubble .

2.7.2- Effect of the Initial Concentration substrate on photocatalytic degradation process using constant mass of coupled of ZnO Nano particles:

Various studies were carried out with varying beginning substrate concentrations of AYG (10, 20, 30, and 50 ppm) and a constant mass of 0.13 g of ZnO nanoparticle. A 9 mW/cm^2 solar lamp is used for the photocatalytic degradation process.

At 298.15K, the reaction vessel is filled to the brim with a rate flow of air bubble was $10cm^3$ / min.

2.7.3- Effect of pH on the photocatalytic degradation process using ZnO Nano Particles.

A series of experiments were conducted in the pH different value in (3.89,6.20,8.74, and 9.85) using HCl and NaOH (0.1M) to control on the effect of pH on dye removal efficiency over nanocomposite. 0.13g. ZnO nanoparticle with 100 ml of 10 ppm aqueous solution of AYG dye at room temperature continual stirring for an extended period of time under normal air conditions 80 minutes.

2.7.4- Effect of Temperature on the photocatalytic degradation process using ZnO Nano particles:

A series of experiments were conducted to investigat the effect of changing temperature (281, 294, 301, and 308 K) on the photocatalytic degradation at optimum conditions of 0.13 g. mass of ZnO nanoparticle and 10 ppm initial concentration of AY G dye, with an air flow rate of 10 cm^3/ min.

2.7.5 - Effect of intensity on the photocatalytic degradation process using ZnO Nano particles:

A series of exepermental were conducted to investogate the Intensity range in the rang (1, 3, 5, and 7) mw to control the effect of 0.13 g.intensity on dye removal efficiency on nanoparticle was suspended ZnO with 100 ml of 10 ppm medium An aqueous solution of AYG dye at room temperature with continuous stirring for a long period of time under normal air conditions for 80 minutes.

2.7.6 - Effect of hydrogen peroxide on the photocatalytic degradation of AYG dye process using ZnO Nano particles:

Different experiments were carried out with different volumes of hydrogen peroxide (0.5, 1.5, 5, and 7 ml) in this study in the concentration of AYG remained constant. AYG irradiated with 9 mW/cm2solar lamp at 298.15 K, the reaction vessel being filled with an air bubble at a rate 10 cm3/min.

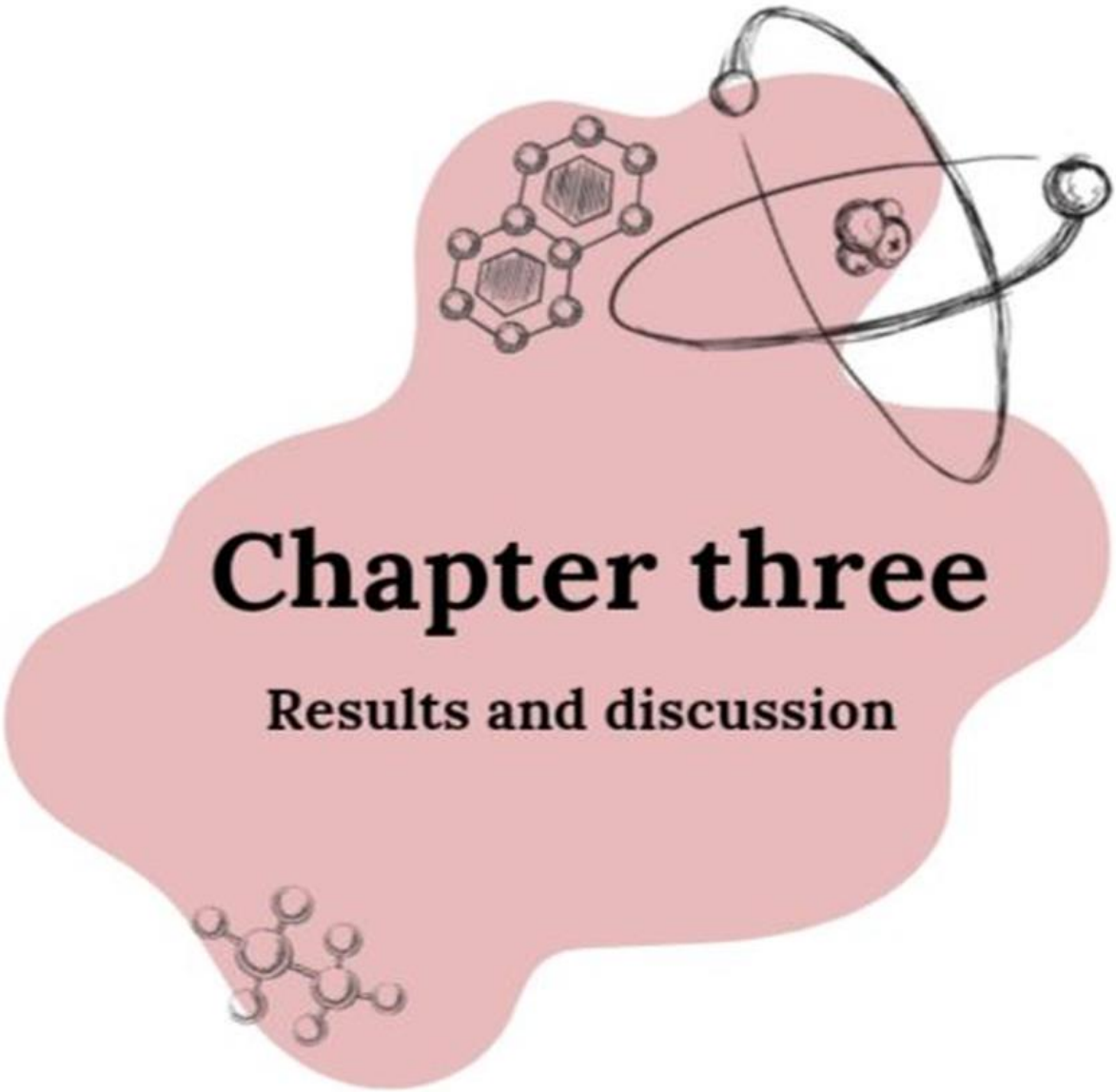

Chapter three

Results and discussion

3.1- FT-IR Spectra:

3.1.1- FT-IR Spectra of Salicylaldehyde:

The FT-IR spectrum of this compound, Figure.(3.1).This spectram shows one stretching band at (1666.6 cm^{-1})for carbonyl group and stretching broad band at (3182 $cm^{-1)}$ due to υ (O-H) group also two stretching bands υ (C=C) aromatic at (1597 and 1579 cm^{-1})[125]

3.1. 2- FT-IR Spectra of Benzyl Amine:

The FT-IR spectrum of Benzyl amine is shown in Figure.(3.1). This spectram two stretching bands at (3270 cm^{-1}) and (3290cm^{-1}) attributable to the two weak bands of (asym. and sym. NH_2 group) respectively, and the bending band at (1604 cm^{-1}) due to υ(N-H) ,but the small band observed at (3084 cm^{-1}) owing to (C-H Aromatic). As it has been noted that two vibrations bands at (2916 cm^{-1}) and (2858 cm^{-1}) due (asym. and sym. group υ(CH_2)) respectively, while two stretching vibration bands of υ (C=C) aromatic showed at (1494, 1452 cm^{-1}) [126, 127].

3.1.3-FT-IR Spectra of Schiff Base Ligand 2-(Benzylimino)Methyl)Phenol (L1) and Their Complexes:

The FT-IR spectrum of the (L_1) ligand shows in the Figure.(3.1). several changes compared to the spectrum of starting material. The existence of hydrogen bond either of intermolecular to happen as it was proven from exist are a band in the range (3061) cm^{-1} due to ν(O-H) of the phenol group as well as shows absence of the absorption bands at (3270 cm^{-1}) and (3290cm^{-1}) due to υ(NH_2) in the spectrum of (Benzyl amine) and new stretching vibration band at (1631 cm^{-1}) was assigned to υ (C=N) group confirm the formation of Schiff base L_1 ligand[125].

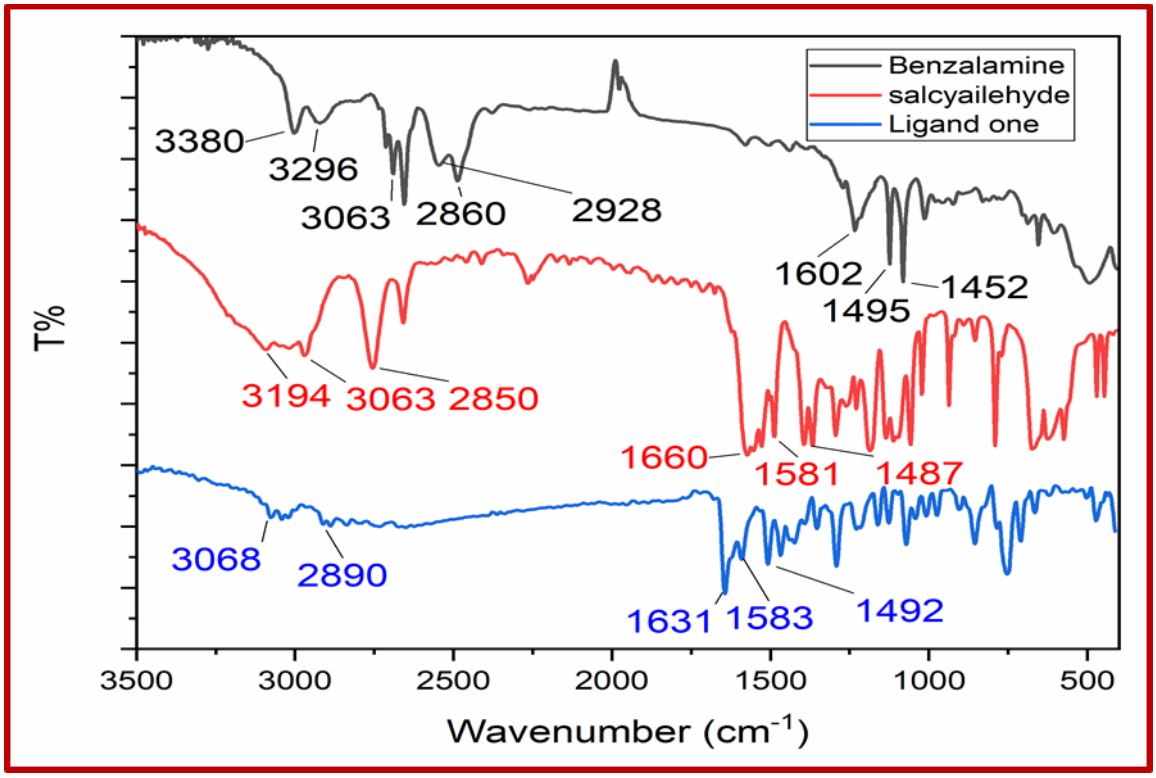

Fig.(3.1):FT-IR spectra for Benzyl Amine,salcyaildehyde and ligand One

3.1.4 - FT-IR Spectra of 2,5- Dihydroxy Benzaldehyde:

The FT-IR spectrum of this compound is shown in Figure.(3.2) This spectram shows one stretching band at (1653.05 cm^{-1})for carbonyl group and stretching brod band at (3296-3230 cm^{-1}) due to υ (O-H) group of group alsoshowes two stretching bands of υ (C=C) aromatic at (1597 and 1579 cm^{-1}) [126] .

3.1.5 - FT-IR Spectra of Schiff Base ligand 2-((benzylimino)methyl)Phenol (L_2) and their Complexes:

The FT-IR spectrum of the (L_2) ligand shows in Figure.(3.2). whoch exhibited several changes compared to the spectrum of starting material. The existence of hydrogen bond either of intermolecular to happen as it was proven from exist of a band in the range (3300) cm $^{-1}$ due to ν(O-H) of the phenol group as well as showed absence of the absorption. Bands at (3270 cm^{-1}) and (3290cm^{-1}) due to υ(NH_2) in the spectrum of (Benzyl amine) and new stretching vibration band at (1643 cm $^{-1}$) was assigned to υ (C=N) group confirm the formation of Schiff base L_2 ligand [126, 128]

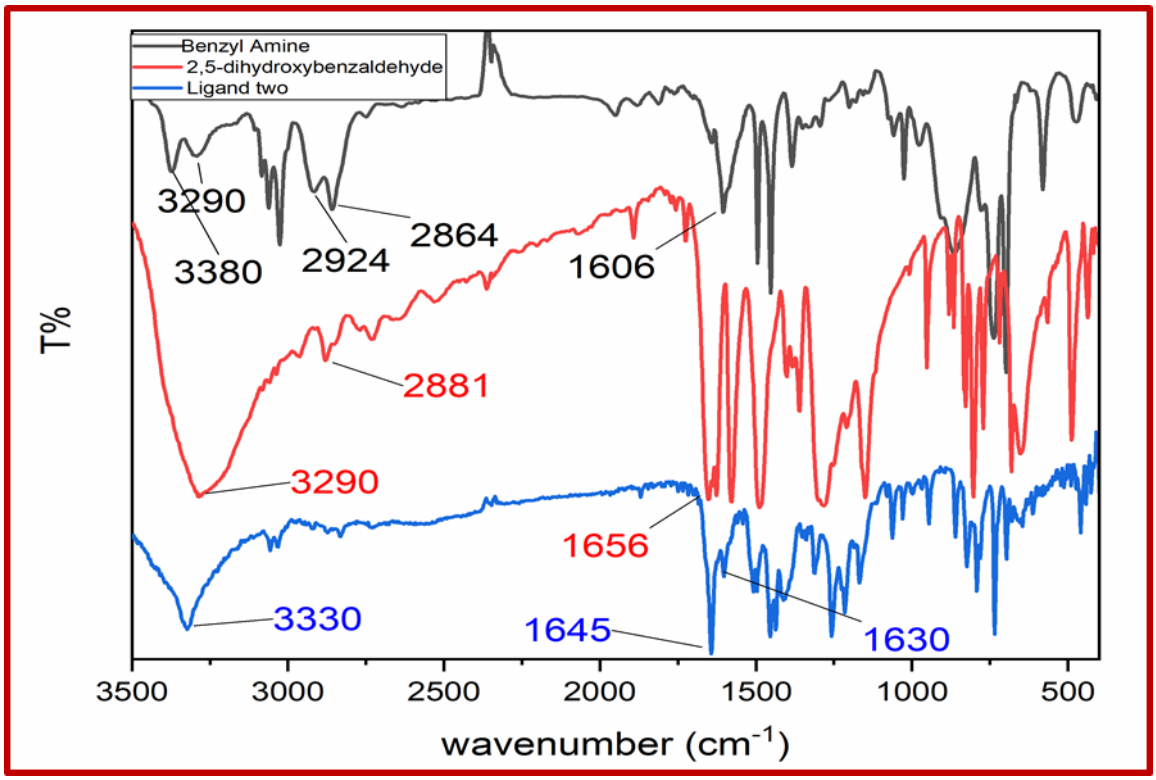

Fig.(3.2) FTIR spectra of benzyl Amine,2,5-dihydroxybenzaldehyde and ligand two

3.1.6-FT-IR spectra for C_1 to C_4 complexes :

Verification of the complexes structure can be easily realized by comparing the spectra of free ligand L_1 sites involved in chelation with their complexes. The comparison revealed that absorption bands appearing in the FT-IR spectra of ligand change in chelation, These peacks are shown in Table(3.1) and Figure.(3.3).

The shift of υ (O-H) and(C=N) imine for azomethane group in their positions and change the shape or intensity of band compared with the ligand (L_1) due to the coordination of this ligand with the metal ions , and gave an indication that the complexes were formed.

In some complexes the water entered in lattice or coordinated with metal and exhibited broad band (3100-3500) $cm^{-1.}$ The significant stretching vibrations of L_I and its complexes are listed in Table(3.1).

The comparison revealed that absorption bands appearing in the FT-IR spectra of ligand change in chelation,see Table(3.1) and Figure.(3.3).

The shift of υ (O-H) and(C=N) imine for azomethane group in their positions and change the shape or intensity of band compared with the ligand (L_2) due to the coordination of this ligand with the metal ions , and gave an indication that the complexes were formed.In some complexes the water entered in lattice or coordinated with metal and exhibited broad band (3100-3500) cm^{-1}[129-131].

The significant stretching vibrations of L_2 and its complexes are listed in Table(3.1).

Table (3.1) FTIR peaks for ligands(L_1 and L_2) and their complexes

Symbol of compound	υ(O-H)(cm^{-1})	υ(C=N)(cm^{-1})	υ(M–O) (cm^{-1})	υ(M–N) (cm^{-1})
L_1	3000-3170	1631	-	---
C_1	3000-3082	1621	476	325
C_2	3100-3600	1625	447	319
L_2	3000-3170	1631	-	---
C_3	3000-3082	1621	476	325
C_4	3100-3600	1625	447	319

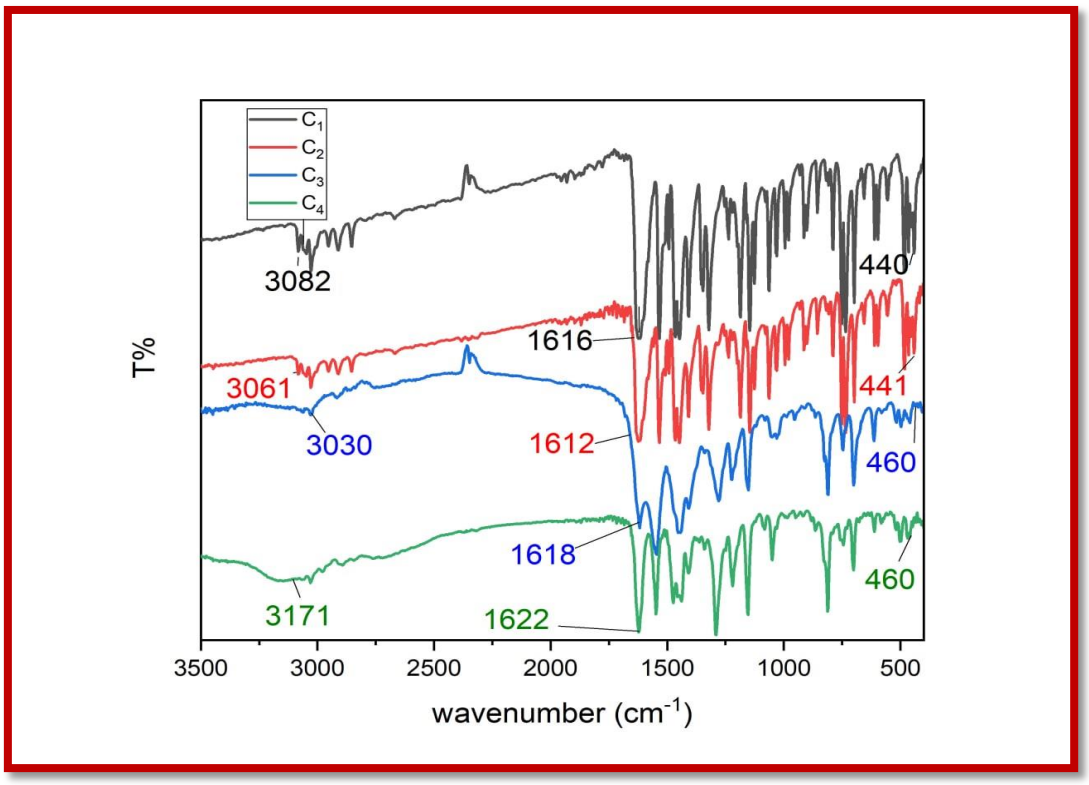

Fig.(3.3)-FT-IR spectra for C_1 to C_4 complexes

3.2. ^{1}H-NMR Spectra

3.2. 1-^{1}H-NMR Spectra of (L_1):

The ^{1}H-NMR chemical shifts (ppm) exhibited for the above mentioned compounds showed a good support results to the suggested structures .

The signal assignments for the ^{1}H-NMR spectra of Schiff base (ligand L) in DMSO-d_6 are shown in Figure. (3.4). The Schiff base proton was detected as a key singlet (s, 1H, CH=N), 8.7ppm (1H). The aromatic protons exhibited chemical shifts at 7.2-7.4 ppm, (m,7H, ArH) and 6.8 - 6.9 ppm, (m,1H, ArH). The O-H proton singlet had a significant peak at 13.48 ppm (s,1H,) in the spectra (1H) and methylene group at 4.5 ppm (s,2H,)[116, 132].

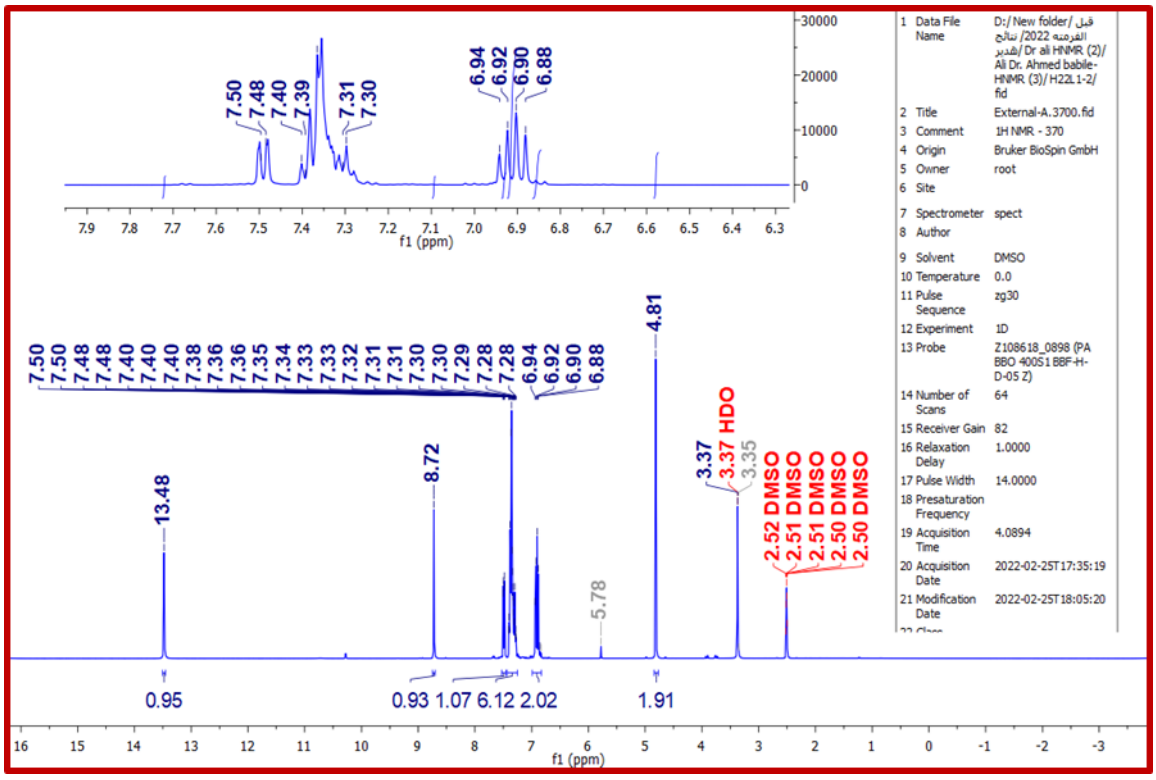

Fig. (3.4): ^{1}H-NMR Spectra for L_1

3.2.2- ^{1}H-NMR Spectra of (L_2):

The ^{1}H-NMR chemical shifts (ppm) exhibited by the above mentioned compounds showed a good support results to the suggested structures .

The signal assignments for the ^{1}H-NMR spectra of Schiff base (ligand L_2) in DMSO-d_6 are shown in Figure. (3.5). The Schiff base proton was detected as a key singlet (s, 1H, CH=N), 8.62ppm (1H). The aromatic protons exhibited chemical shifts at 7.2-7.4 ppm, (m,7H, ArH) and 6.8 -6.9 ppm, (m,1H, ArH). The O-H proton singlet had a significant peak at 9.02ppm and 13.48 ppm (s,1H,) in the spectra (1H) and methylene group at 4.5 ppm (s,2H,)[116, 132]

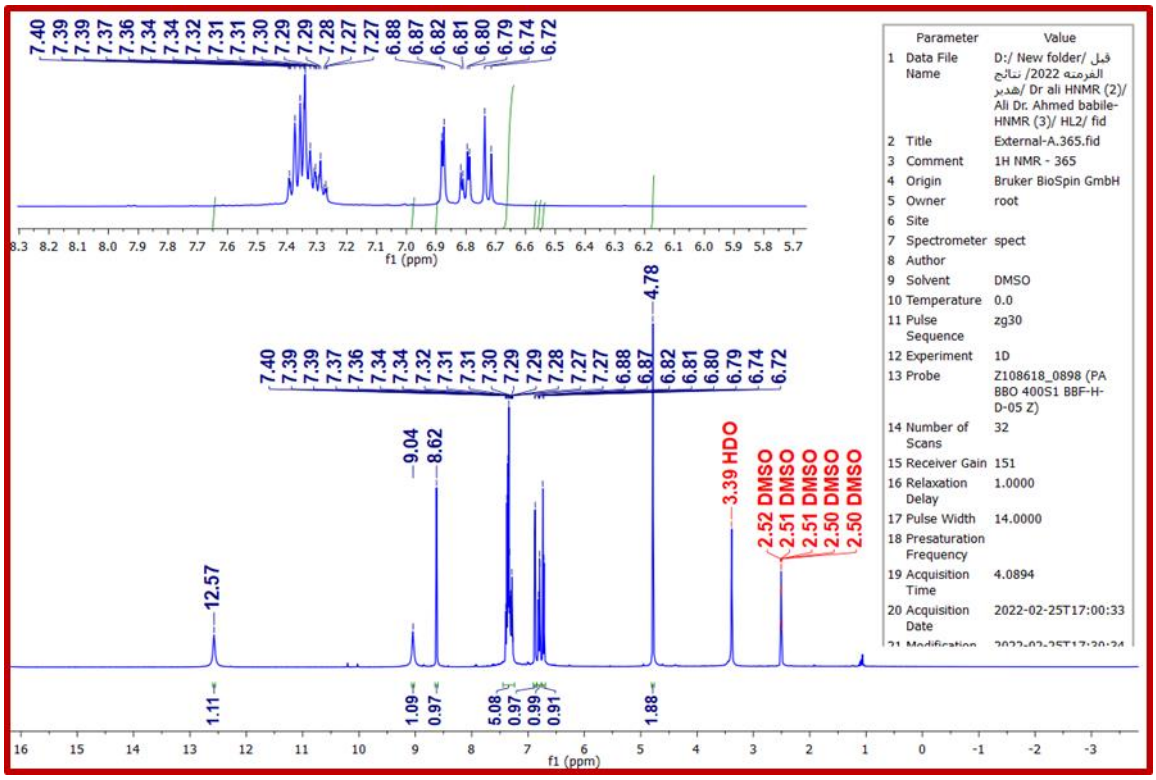

Fig. (3.5): ^{1}H-NMR Spectra for L_2

3.2.3- ^{13}C-NMR spectra of L_1 :

The ligand's ^{13}C-NMR spectra are shown in Figure.(3.6) distinguishing feature of the ligand's spectra was the presence of the (N=CH) azomethine group, which appeared at 166ppm. The carbon of hydroxyl group was at 153.49ppm (C-OH). The carbons in aromatic compoing were at 149.88ppm (Carom), 139.28ppm (CHarom), 129.03ppm (CHarom), 128.23ppm (2C, CHarom), 127.60ppm (CHarom), 120.48ppm ($_2$C, CHarom), 119.12ppm (Carom), 117.37ppm (CHarom), 117.06ppm (CHarom) and 62.83ppm (CH_2) [116, 132].

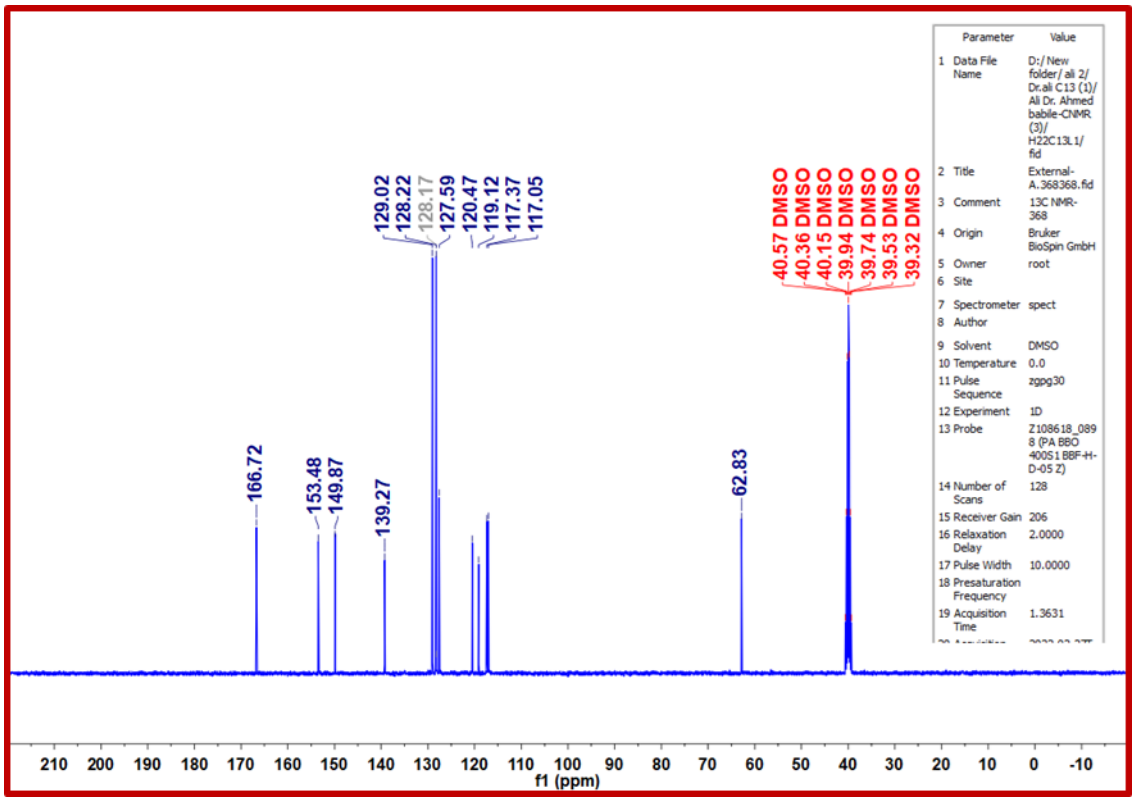

Fig. (3.6)^{13}C-NMR Spectra of L_1

3.2.4- ^{13}C-NMR Spectra of L_2:

The ligand's ^{13}C-NMR spectra are shown in Figure. (3.7). A distinguishing feature of the ligand's spectra was the presence of the (N=CH) azomethine group, which appeared at 166ppm. The carbon of hydroxyl group was at 153.49ppm (C-OH). The carbons in aromatic compounds were at 149.88ppm (Carom), 139.28ppm (CHarom), 129.03ppm (CHarom), 128.23ppm (2C, CHarom), 127.60ppm (CHarom), 120.48ppm (2C, CHarom), 119.12ppm (Carom), 117.37ppm (CHarom), 117.06ppm (CHarom) and 62.83ppm (CH_2).[126]

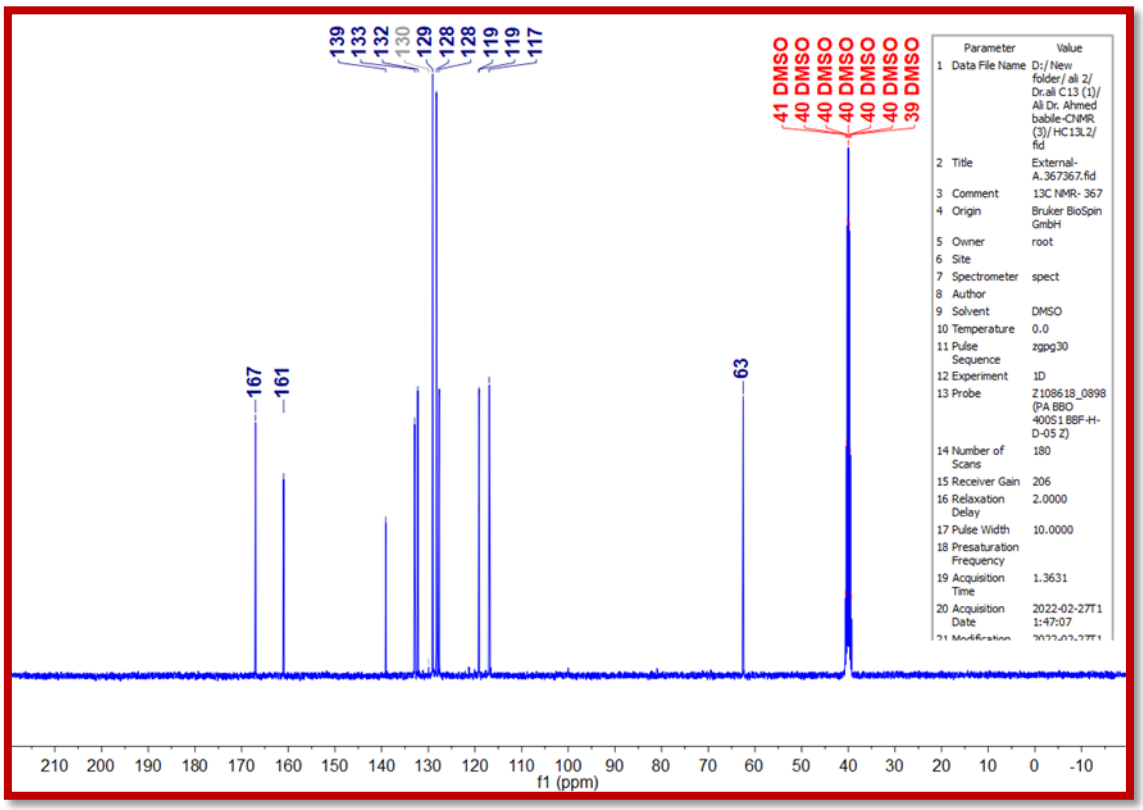

Fig. (3.7)^{13}C-NMR Spectra of L_2

3.3 Electronic spectra and molar conductance :

3.3.1 Electronic spectra of Schiff base ligands (L_1 ,L_2),(C_1-C_4) complexes and molar conductivity :

The UV-visible absorption spectra of ligand L in a DMF solution are presented in Figure.(3.8) and reported in Table (3.2). The electronic transitions were allocated at two bands at due to (π-π^*) transition and the (n–π*) transition[126]. The spectrum of the ZnL complexes in DMF solution exhibited are listed in table.(3.2). These absorption bands also exist in the spectrum of Zn(II) complex but undergo red shift. This shift in the spectra of the synthesized complex supports the coordination of the ligand to Zn(II) ion.The Zn(II) complex because of its d^{10} configuration does not show any d–d transition andpossibly having tetrahedral geometry[133]. The synthesized Zn(II) complex was dissolved in DMSO solvent and molar conductance of(1×10^{-3} M) solution was measured at room temperature Table(3.2). The molar conductance value indicates that the metal complex is a non-electrolyte[127].

Table (3.2): λ_{max} nm(Ʊ cm^{-1}), Assignment, Suggested geometry Malar conductivity $Ohm^{-1}.cm^2.mole^{-1}$ for the ligands and complexs

Symbol	λ_{max} nm(ʊ cm^{-1})	Assignment	Suggested geometry	Malar conductivity $Ohm^{-1}.cm^2.mole^{-1}$
L_1	270,(37037.03) 352,(28409.09)	(n–π*) (π-π*)	------	---
C_1	274.5,(36429.87) 375.0(26666.60)	(n–π*) (π-π*), CTML	T.d	14
C_2	274.5,(36429.87) 375.0(26666.60)	(n–π*) (π-π*), CTML	T.d	16
L_2	316,(31645.56)	(π-π*)	-----	---
C_3	328,(30487.80)	(π-π*), CTML	T.d	18
C_4	352,(28409.09)	(π-π*), CTML	T.d	13

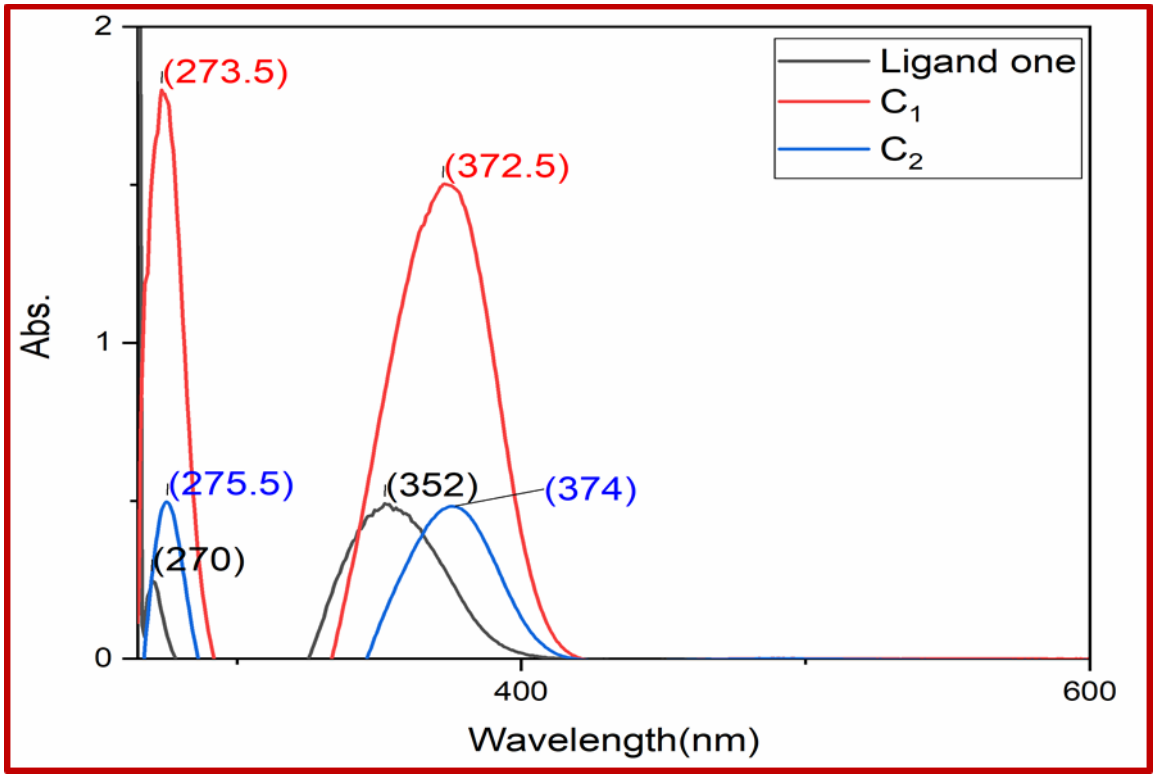

Fig. (3.8) Uv –visible for Ligand one and it's complexes

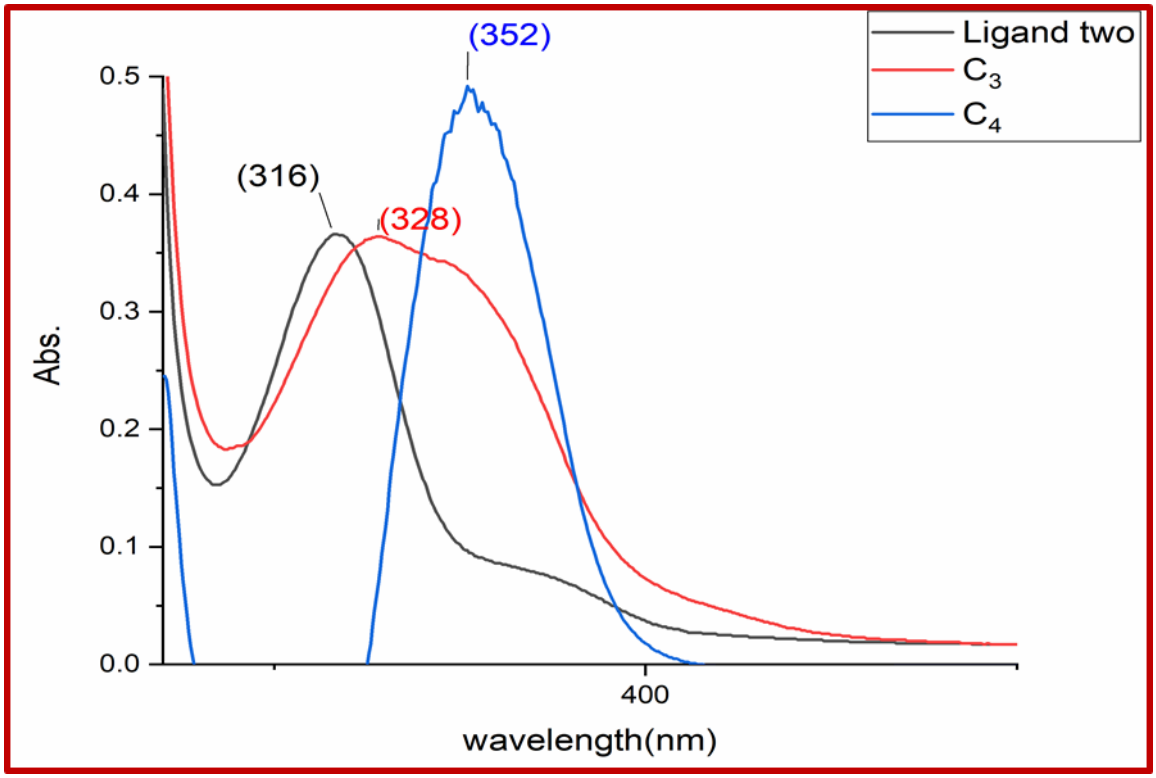

Fig. (3.9) Uv –visible for Ligand two and it's complexes

3.4- Thermal Gravimetric Analysis(TGA):

3.4.1- TGA of the Ligands and some their Metal Ion Complexes:

Thermal gravimatric analysis(TGA)of synthesized ligand and their metal complexes have been carried out under nitrogen gas with heatingat the range (25-800) °C and ramp rate of heating (10ºC/min). The thermal analysis was performed to expect the suggested structures of the ligands and their complexes. The thermal decomposition data for all the ligands (L_1 and L_2) and its metal complexes are shown in Table (3.3) and their thermographs are given in Figure.(3.10 to 3.15) respectively. From these results

The first stage which took place at temperature range of (25-180) °C and adsorbed H_2O include of water molecules (lattice water) or any lattice molecules such as ethanol in addition of some fragments [134].

The next stages include the decompose of organic speies of the ligands and their complexes may occurs in one or more steps [135].

The final stages involved the residual fragments of the ligands and the metal ion still coordinated to the remaining part of the ligands[136].

The average percentages of fragments were exhibited a good agreement between calculated and suggested values in addition of compatibility with elemental analyses[137].

Table (3.3): Thermal Decomposition Data L_1 and L_2, and their Zinc (II) Complexes:

No	Molecular formula and M.wt	Stage	Temp. rang of the Decomp. C°	Suggested Formula of loss	Mass loss%	
					Cal.	Found
L_1	$C_{14}H_{13}NO$ 211.26	1	221.82-262.49	$C_{14}H_{11}NO$	99.053	98.939
C_1	$[Zn(L_1).(H_2O)_2]2CH_3COOH$ 430.75	1 2 3	25-332.76 332.76-522.35 >522.35	$2CH_3COOH$, $2H_2O$, C_7H_8 C_6H_5 Residue ($Zn(C_6H_5O$)	57.573 17.643	54.962 19.206
C_2	$[Zn(L_1)_2(H_2O)_2].2CH_3COOH$ 642.01	1 2 3	25-225.08 225-331.71 > 331.71	$2H_2O$, CH_3COOH CH_3COOH, $2C_6H_5$ Residue ($Zn(C_6H_5O$)	14.797 38.00	14.692 39.71
L_2	$C_{14}H_{13}NO_2$ 227.26	1 2	25-257 220-327 > 327	-2OH -C=N,CH_2 Residue $2C_6H_5$	15 18.04	20.82 15.51
C_3	$[Zn(L_2).(H_2O)_2]2CH_3COOH$ 447.75	1 2 3	25-352	$2H_2O$ H_2O, $2CH_3COOH$ $2C_6H_5$	7.81 30.82 41.15	18.78 18.89 62.31
C_4	$[Zn(L_2)_2.(H_2O)_2]2CH_3COOH$ 676.01	1 2	25-225.88 291-579 > 579	CH_3COOH , $2H_2O$,	14.20 18.17 58.08	14.69 18.65 58.24

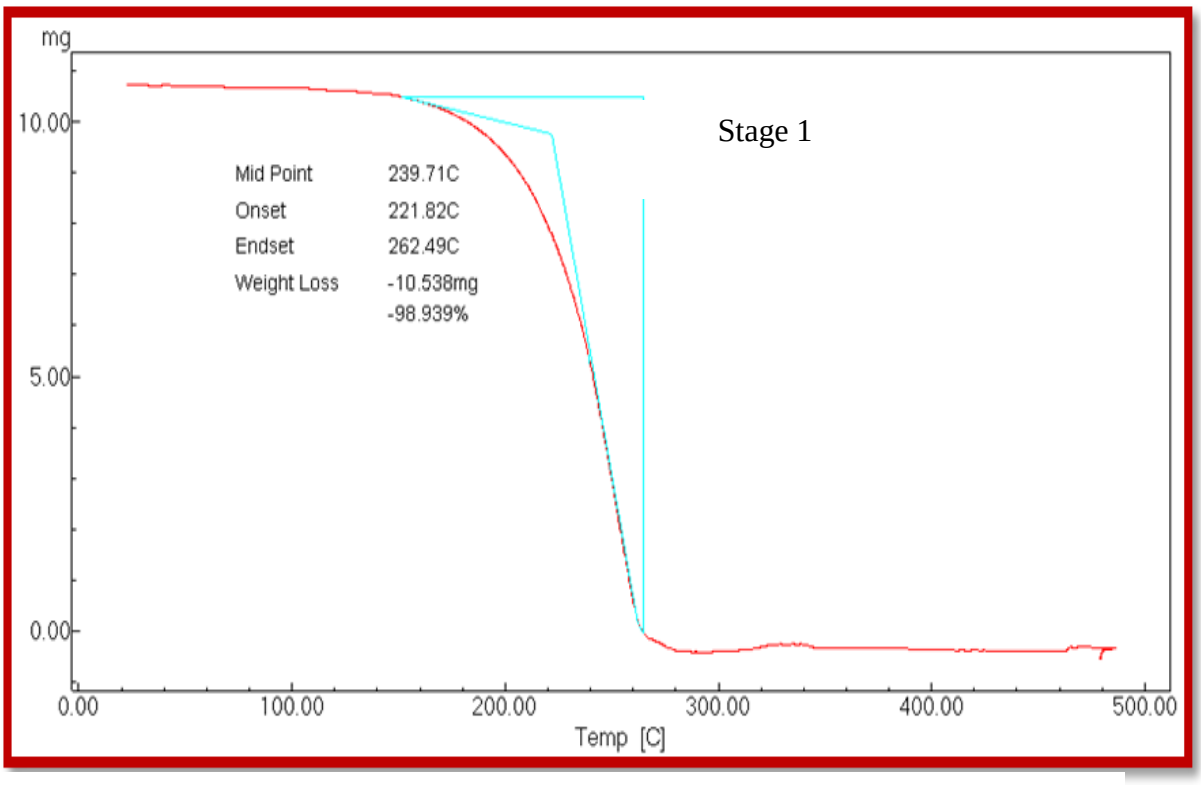

Fig. (3.10) TGA thermogram of L $_1$

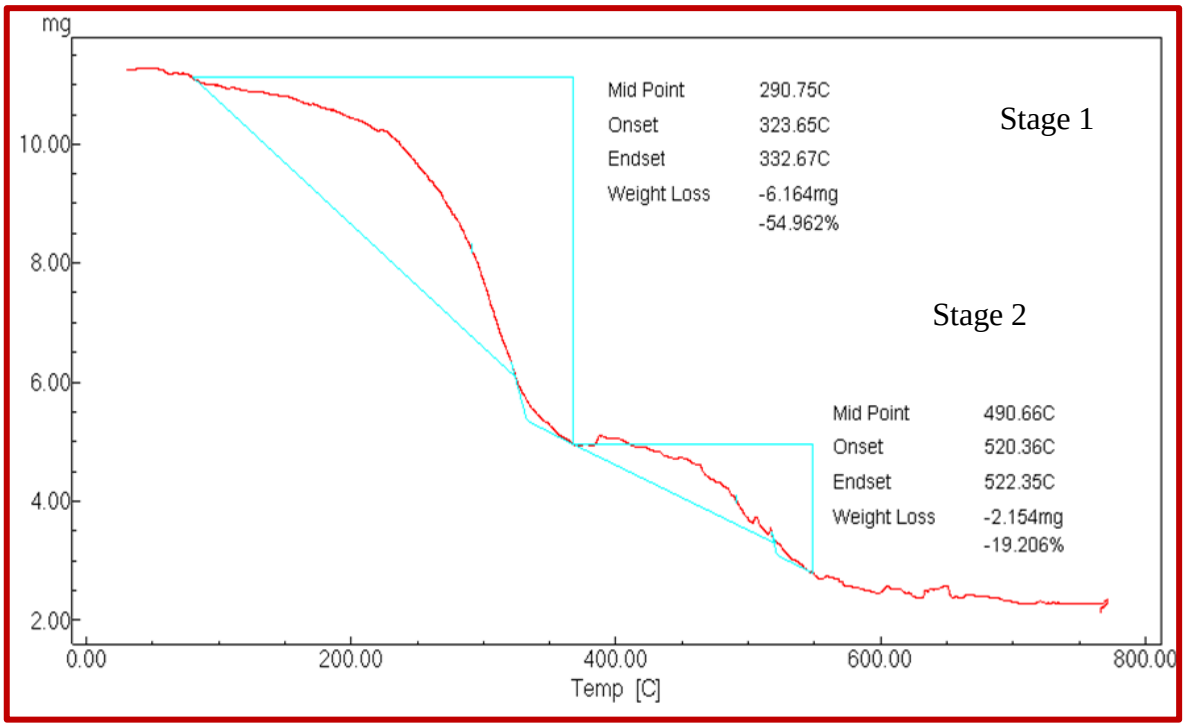

Fig. (3.11): TGA thermogram of C_1

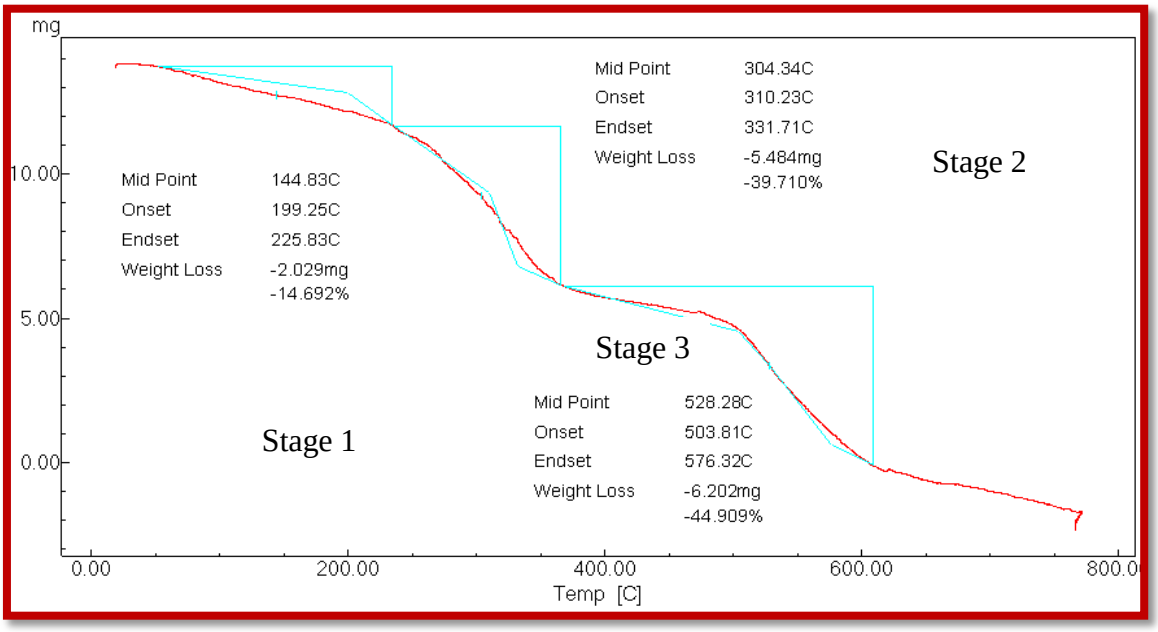

Fig. (3.12): TGA thermogram of C_2

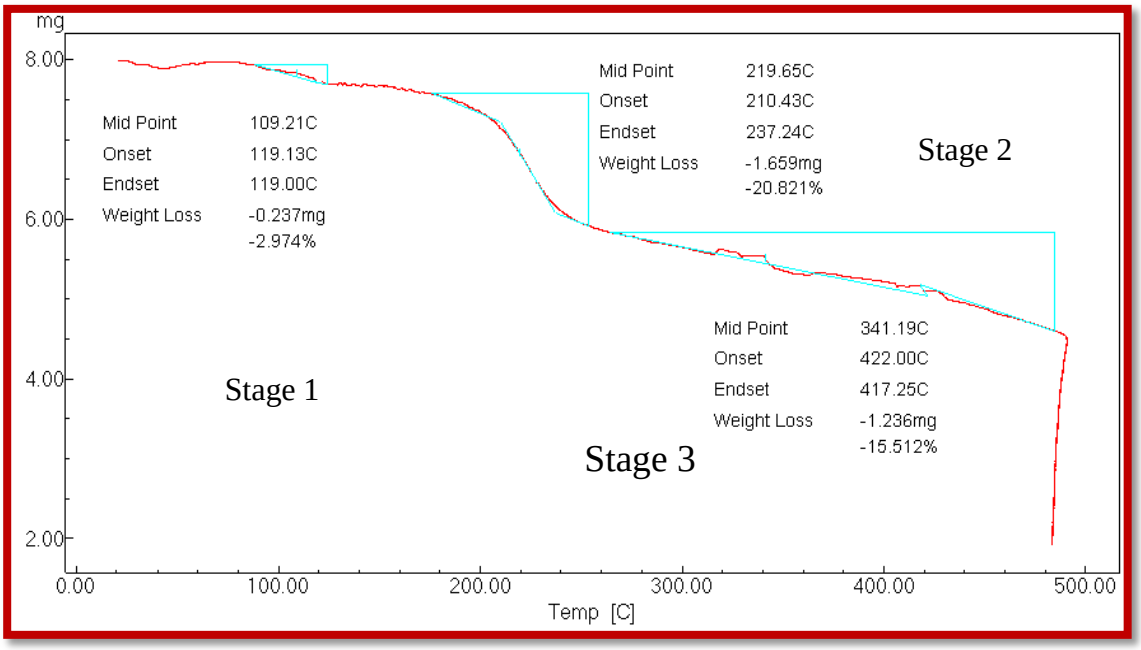

Fig. (3.13): TGA thermogram of L_2

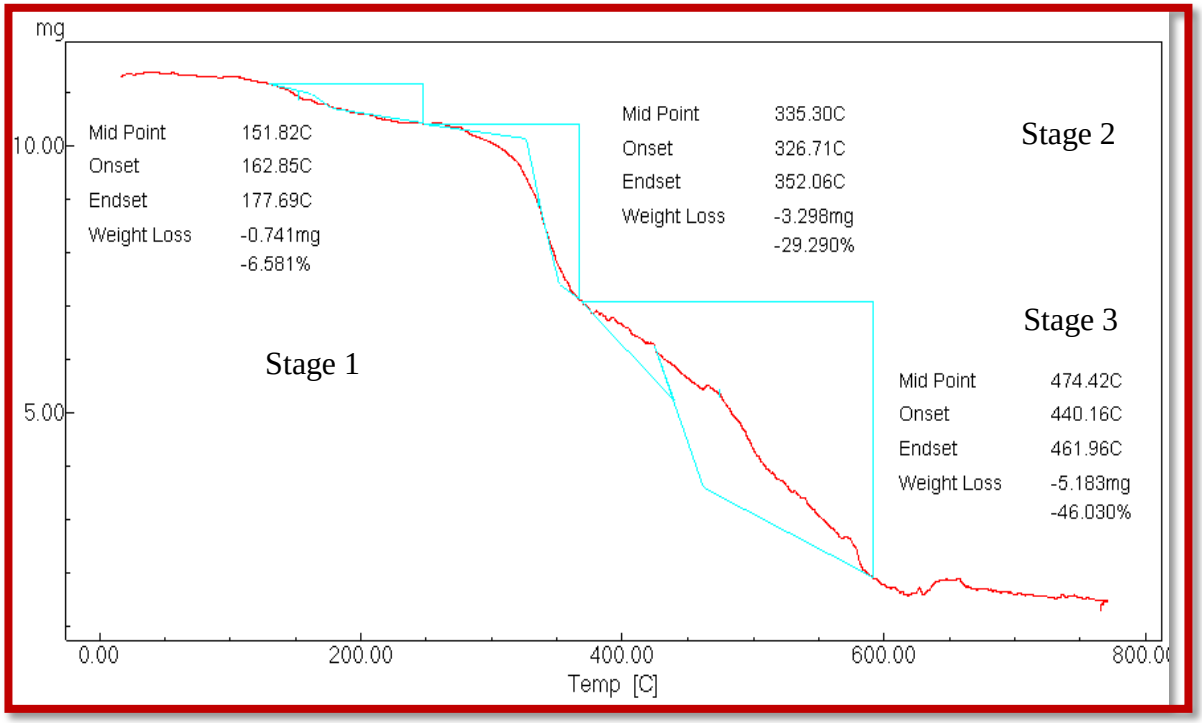

Fig. (3.14): TGA thermogram of C_3

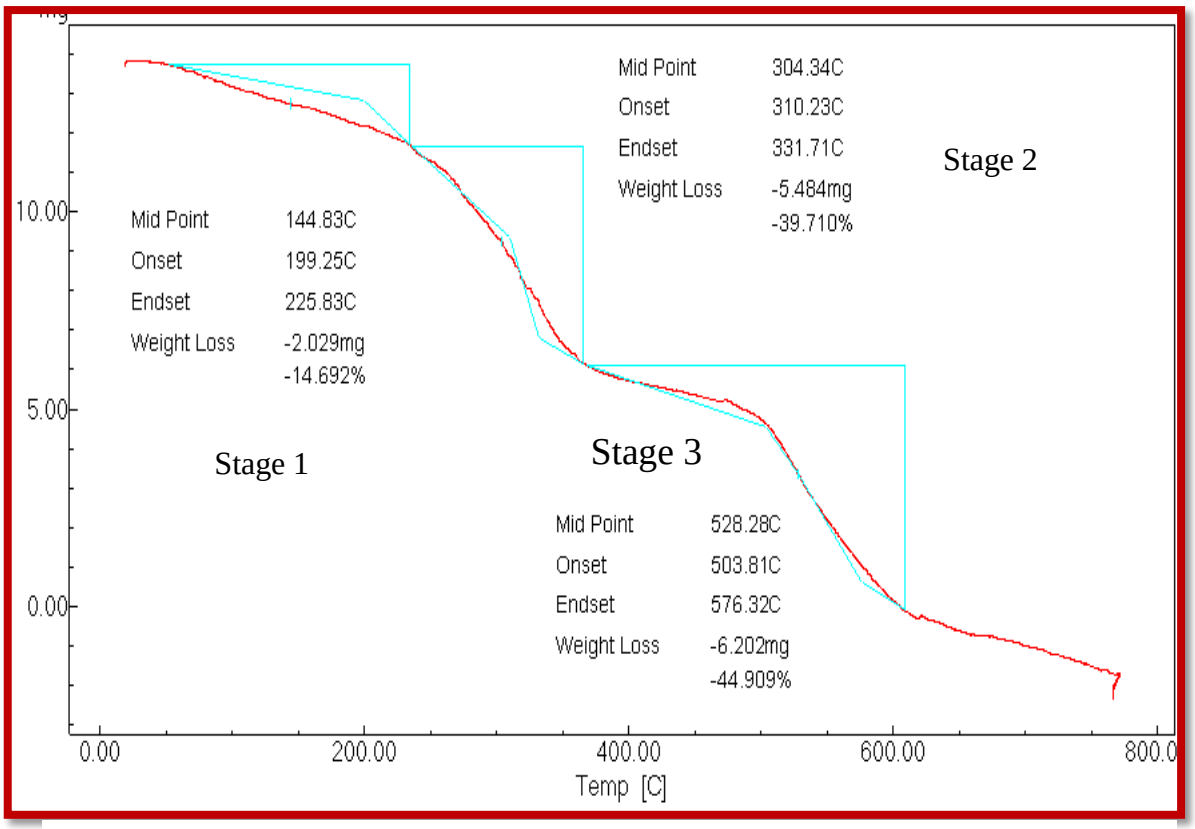

Fig. (3.15): TGA thermogram of C_4

3.5- Characterization of the Synthesized Znic oxide Nanoparticles :

Zinc oxide ZnO NPs were obtainede by calcining a typical complex for 5 hours at 700 ^{o}C. The nature of the obtained ZnO was validated using FTIR, UV -Vis Diffuse Reflectance, XRD, SEM, TEM, EDX, and BET pattern analysis.

3.5.1- FTIR for the Zinc Oxide Nanoparticles:

The FTIR pattern of the produced ZnO NPs is shown in Figure (3.16) on a scale of 4000 to 400 cm^{-1}. The absorption bands of ZnO nanoparticles for all synthesized in the rang at (490-440)cm^{-1} due to v(Zn–O). The FTIR spectra obtained clearly showed that ZnO NPs were synthesized.

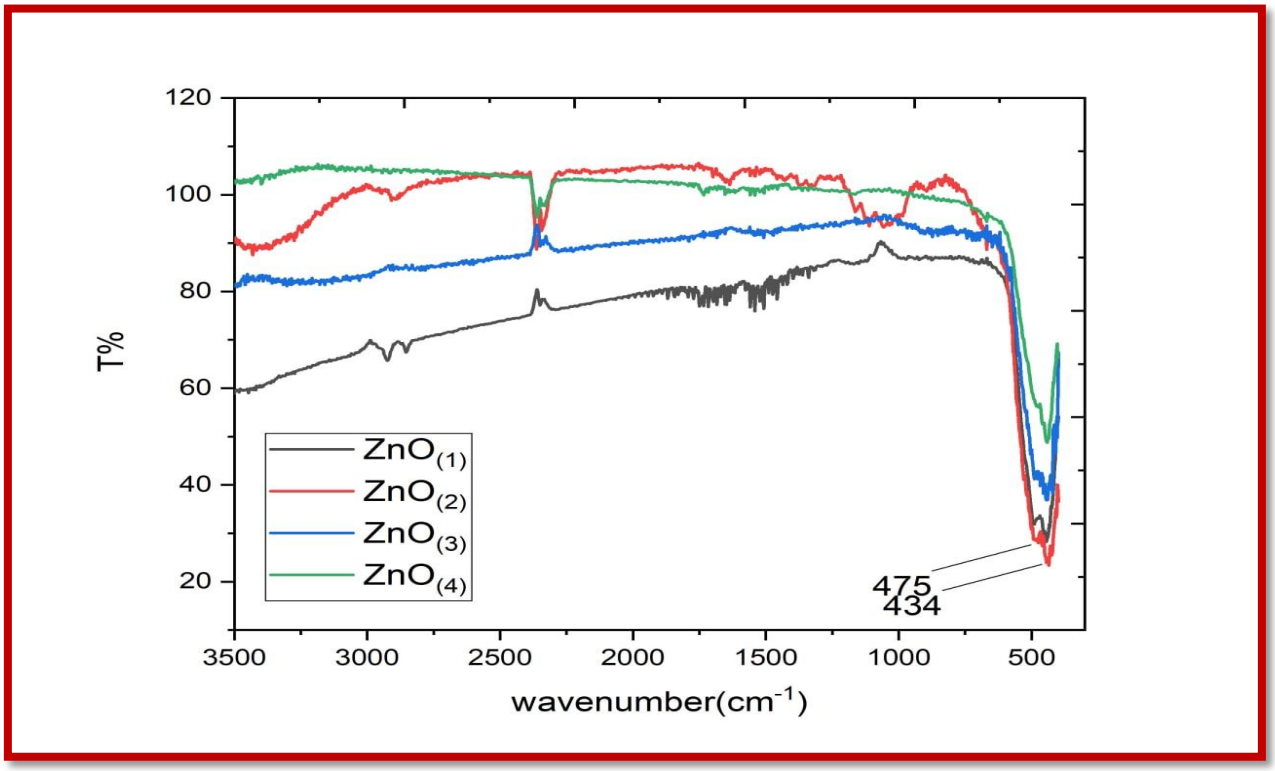

Fig. (3.16) FTIR spectra for ZnO from C_1 to C_4 Complexes

3.5.2- X-rays Diffraction (XRD) for Zinc Oxide Nanoparticles:

X-rays diffraction is the fundamental technique used to determine the crystalline solid structures and crystallite size, the X-ray beam incident on a sample and diffracted by the crystalline phases based on Bragg's law, as equation (1).

$$\mathbf{n\,\lambda = 2d\sin\theta} \ldots\ldots\ldots\ldots\ldots\ldots\ldots\ldots\ldots\ldots\ldots\ldots\ldots\ldots\ldots\ldots\ldots\ldots\ldots \quad (\mathbf{3.1})$$

Where:

n is the order of reflection,

λ the wavelength of X-Rays,

θ Bragg angle and d is the interplanar spacing[138, 139].

The main information included in a diffraction pattern are the shape, position of the peak and intensity . The X-ray diffraction patterns of represents the X-ray diffraction pattern of ZnO nanopowder

A definite line broadening of the XRD peaks indicates that the prepared material consist of particles in nanoscale range. From this XRD patterns analysis, peak intensity, position and width, full-width was determined at half-maximum (FWHM) data. The diffraction peaks located at 32.05°, 34.71°, 36.53°, 47.82°, 56.87°, 63.14°, 66.64°, 68.22°, and 69.36° have been keenly indexed as hexagonal wurtzite phase of ZnO[140, 141].

with lattice constants a=b=0.324 nm and c=0.521 nm (JCPDS card number: 36-1451) [142], and further it also confirms the synthesized nanopowder was free of impurities as it does not contain any characteristics XRD peaks other than ZnO peaks. The synthesized ZnO nanoparticle diameter was calculated using Debye-Scherrer formula[143].

$$D = K\lambda / \beta \cos \theta \quad \text{......(3.2)}$$

where 0.89 is Scherrer's constant, λ is the wavelength of X-rays, θ is the Bragg diffraction angle, and β is the full width at half-maximum (FWHM) of the diffraction peak corresponding to plane ⟨101⟩. The average particle size of the sample was found to be 49.36 nm which is derived from the FWHM of more intenses peaks corresponding to 101,100 and 002 plane located at 36.33°,32,05 and 34,71 using Scherrer's formula.

Table(3.4): The Crystallite Size (D) of ZnO nanoparticles from difference complexes

Nanoparticles	D(nm)	D (SEM)
ZnO(1)	49.36	84
ZnO(2)	45.92	44
ZnO(3)	42.59	41
ZnO(4)	44.6	43

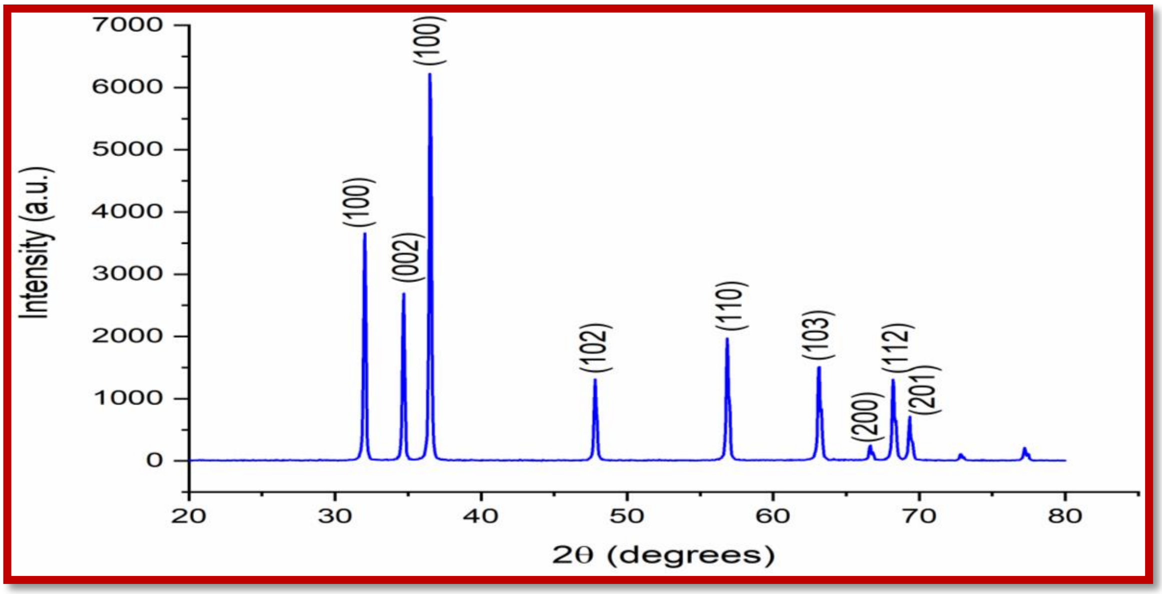

Fig. (3.17) X-ray Diffraction Pattern of the Zinc Oxide Nanoparticles Synthesis from C_1 Complex

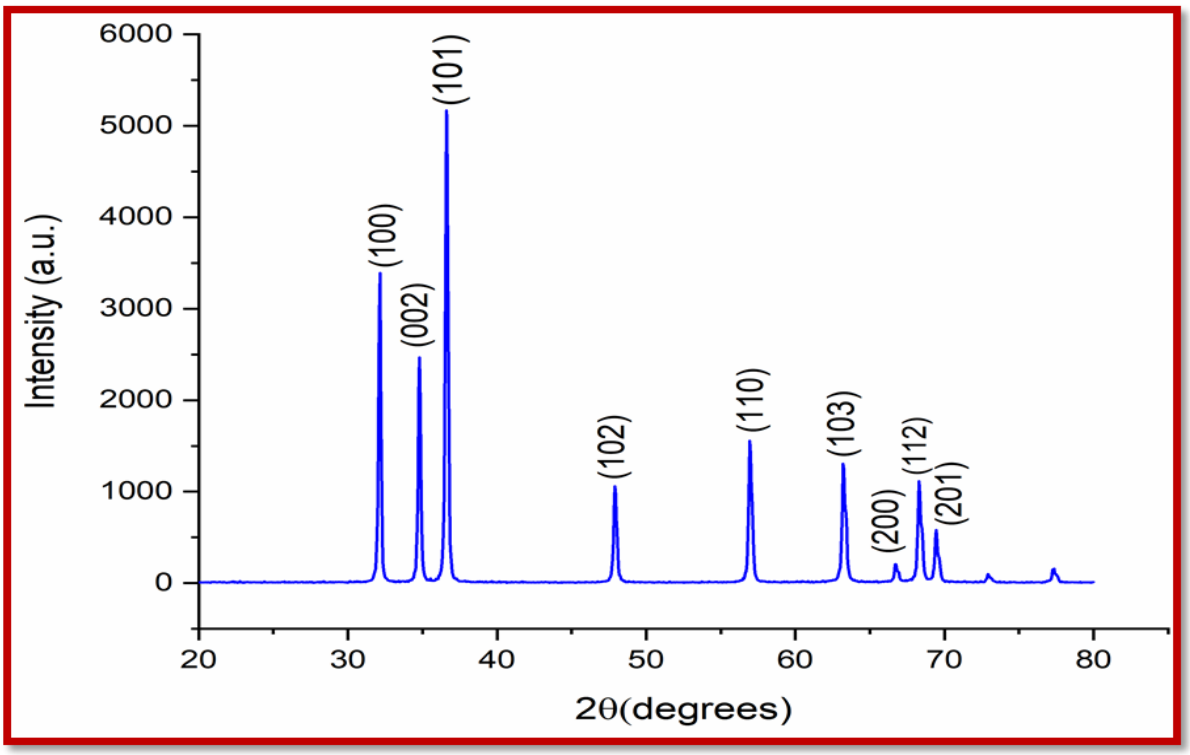

Fig. (3.18) X-ray Diffraction Pattern of the Zinc Oxide Nanoparticles Synthesis from C_2 Complex

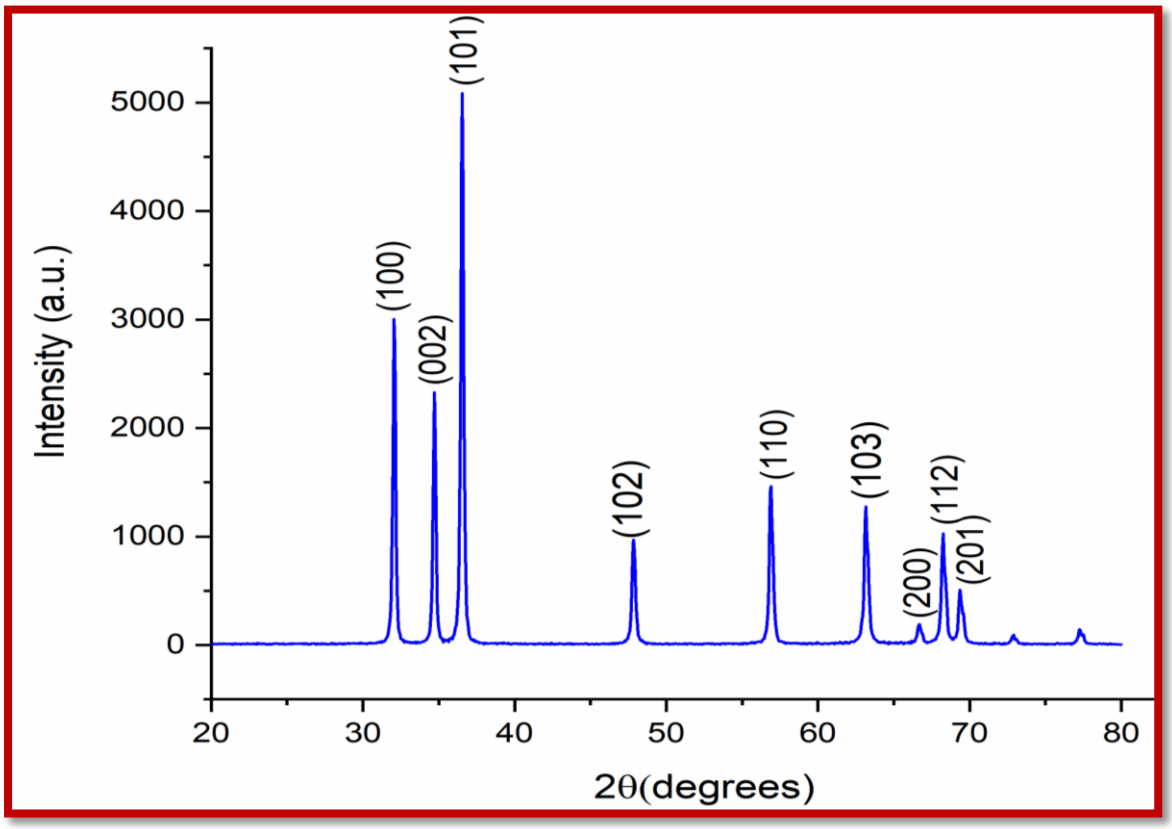

Fig. (3.19) X-ray Diffraction Pattern of the Zinc Oxide Nanoparticles synthesis from C_3 Complex

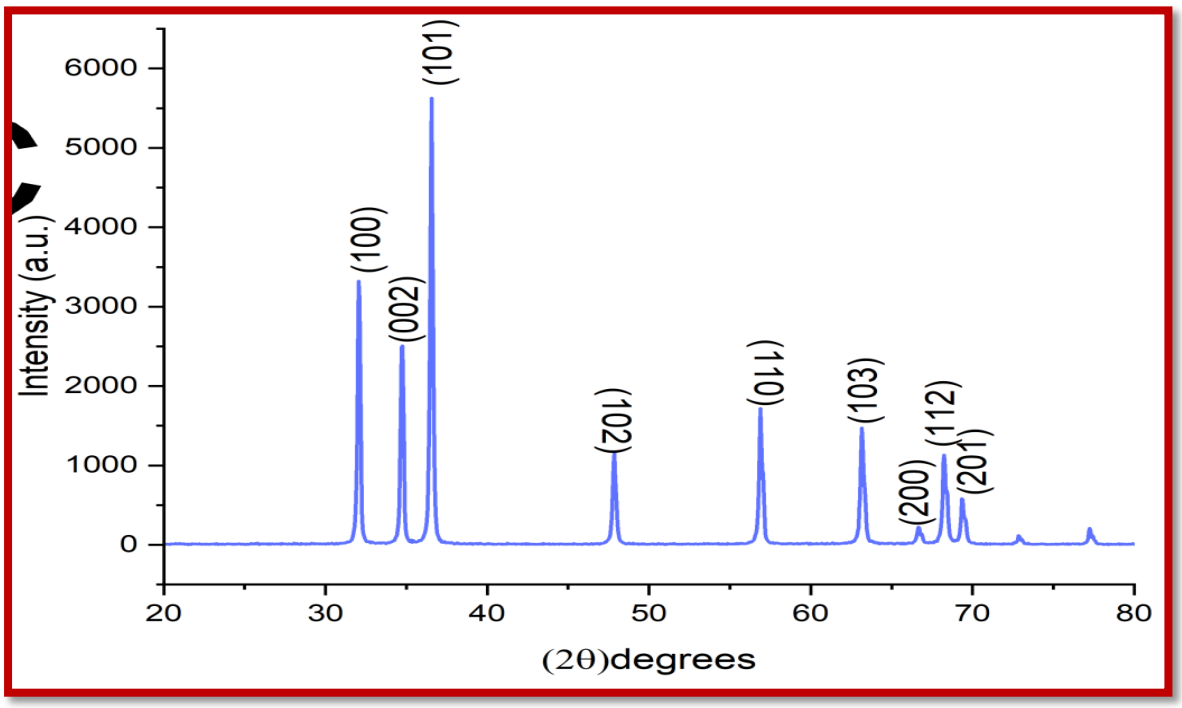

Fig. (3.20) X-ray Diffraction Pattern of the Zinc Oxide Nanoparticles Synthesis from C_4 Complex

3.5.3- Scanning Electron Microscopy (SEM) for Synthesis ZnO:

The morphology of ZnO nanoparticles sintered at 700 °C is shown figures. (3.21 to 3.24)was studied using scanning electron in microscopy (SEM) techniques to collect useful information about the structure of the produced nanoparticles. Gaussian and SEM pictures micrograph investigations showed irregular aggregated distribution and aspherical shape. According to the histogram, the average grain size was between 60 and 90 nanometers, and the grain size equaled the measured Gaussian at 49.36 nm.

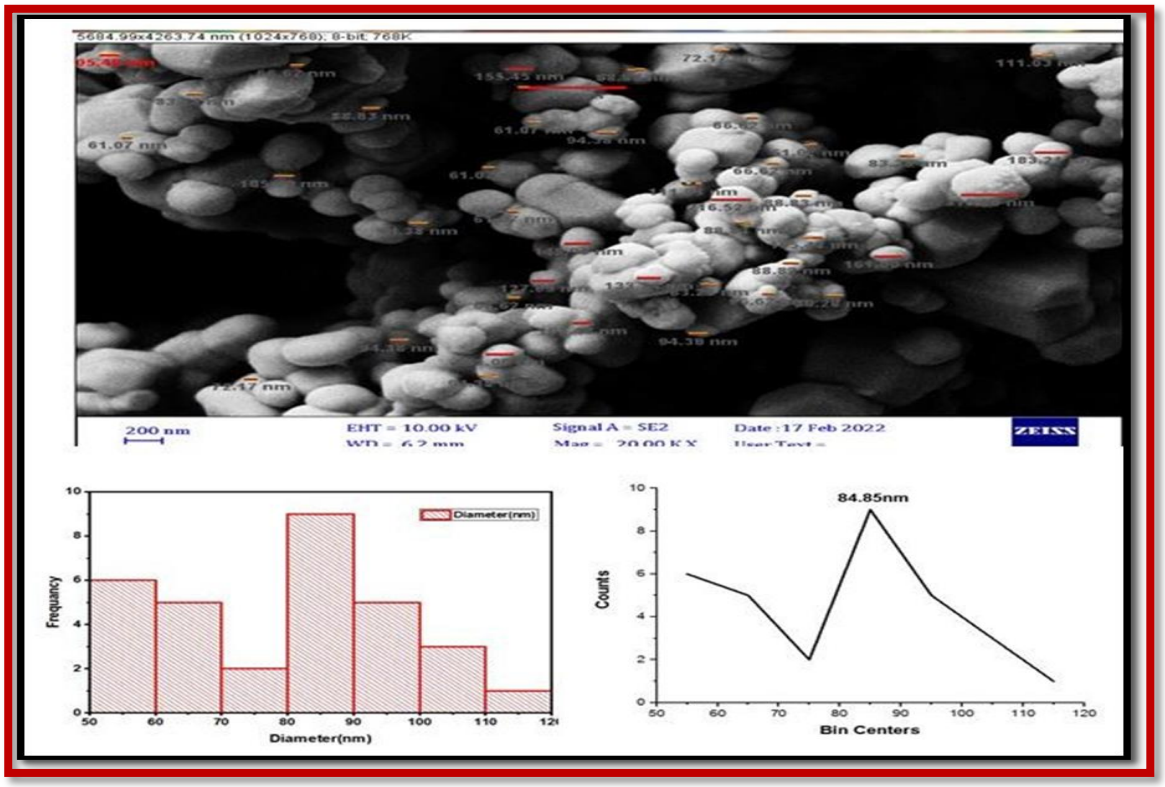

Fig. (3.21) SEM and Histogram of the Zinc Oxide Nanoparticles Synthesis from C_1 Complex

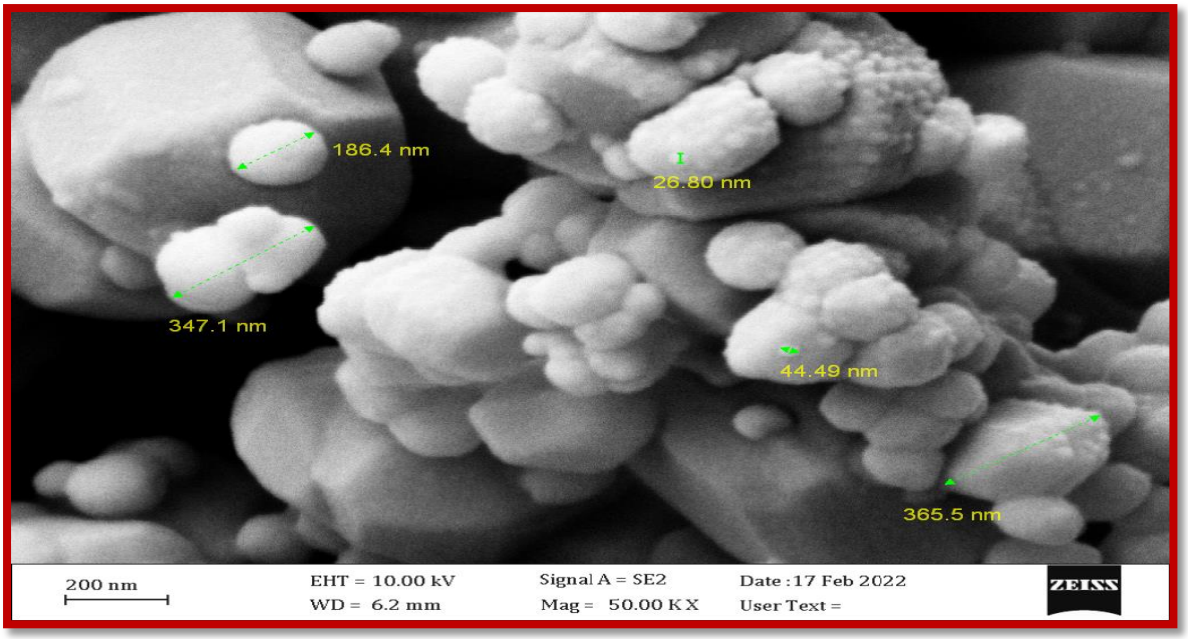

Fig. (3.22) SEM of the Zinc Oxide Nanoparticles Synthesis from C_2 Complex

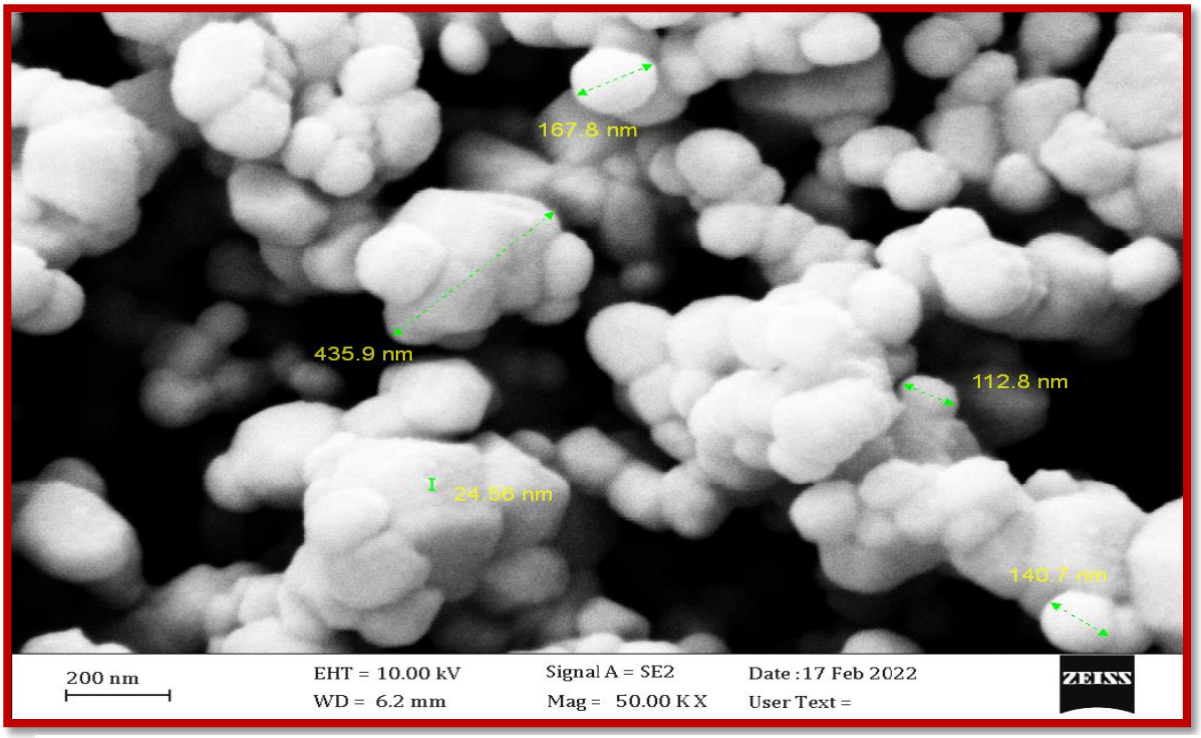

Fig. (3.23) SEM of the Zinc Oxide Nanoparticles Synthesis from C_3 Complex

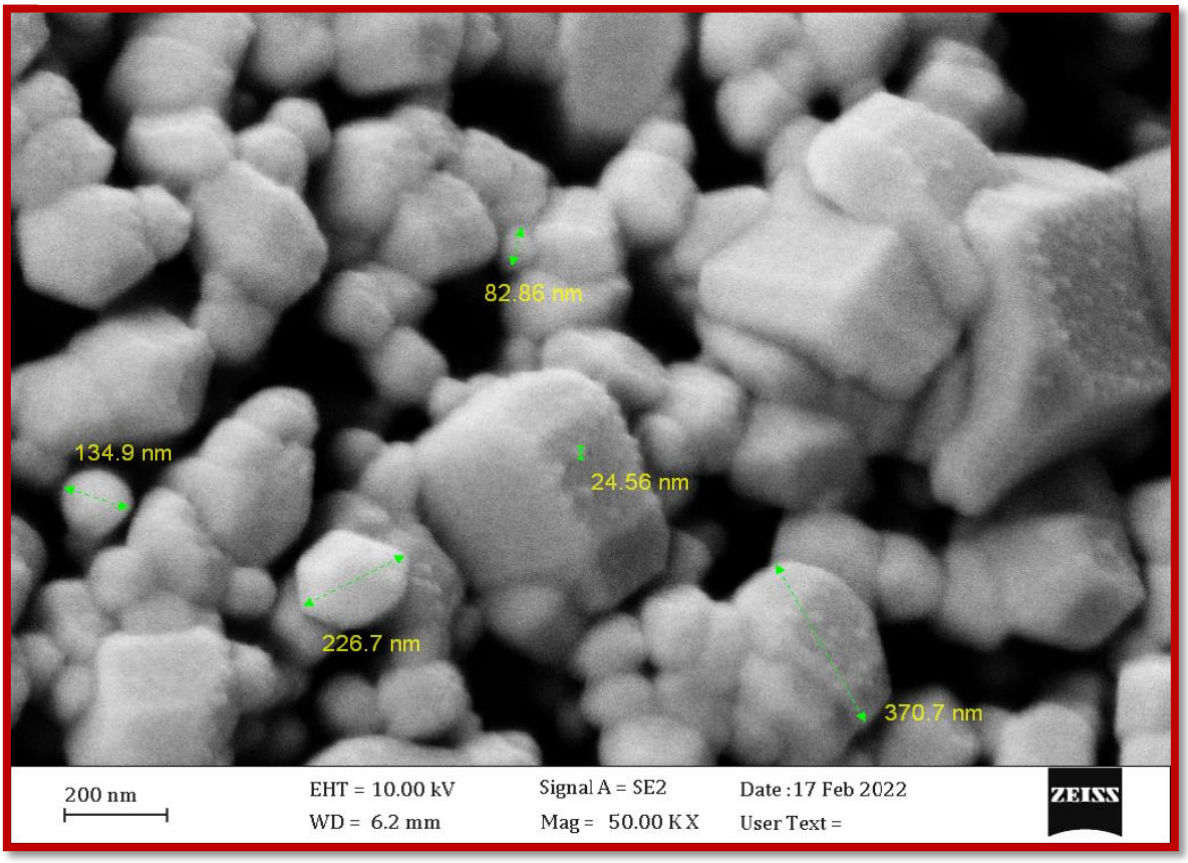

Fig. (3.24) SEM of the Zinc Oxide Nanoparticles Synthesis from C_4 Complex

3.5.4- EDX analysis of ZnO nanoparticles:

The production of ZnO NPs was investigated using EDX analysis. Various locations were concentrated during the EDX measurement. The relevant peaks are shown in Figures.(3.25 to 3.28). The EDX spectrum revealed the presence of ZnO in the produced nanostructure. The atomic percent values of Zn and O in the spectrum were listed in Table (3.5). In the synthesis samples, there was a presence of Zn and O dopants. There was no significant quantity of impurities found.

Table (3.5): EDX of zinc oxide nanoparticles from differences complexes:

ZnO	Zn%	O%
$ZnO_{(1)}$	86.7	13.3
$ZnO_{(2)}$	88.1	11.9
$ZnO_{(3)}$	86.9	13.1
$ZnO_{(4)}$	88.3	11.3

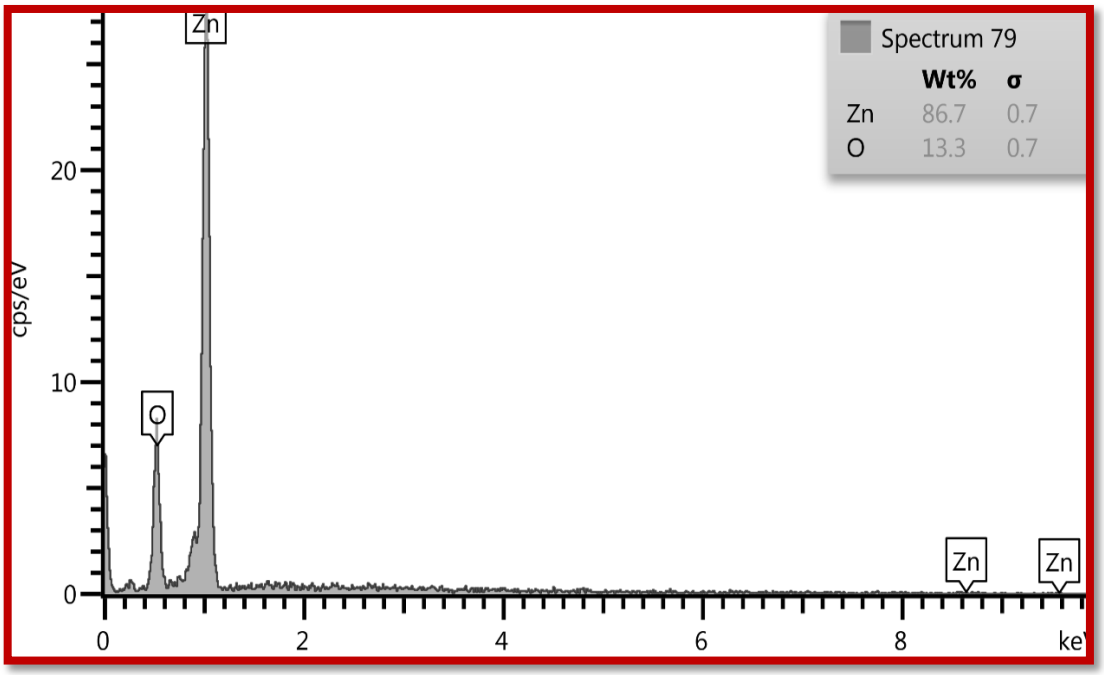

Fig. (3.25) EDX for Zinc oxide nanoparticles from C_1

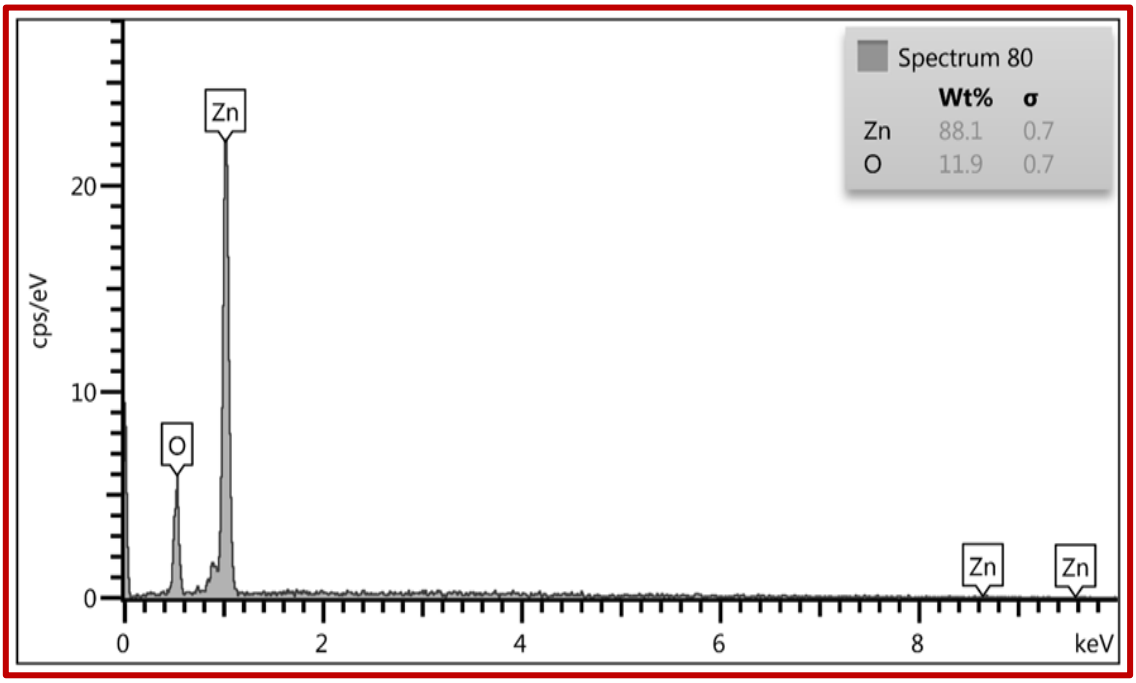

Fig. (3.26) EDX for Zinc oxide nanoparticles from C_2

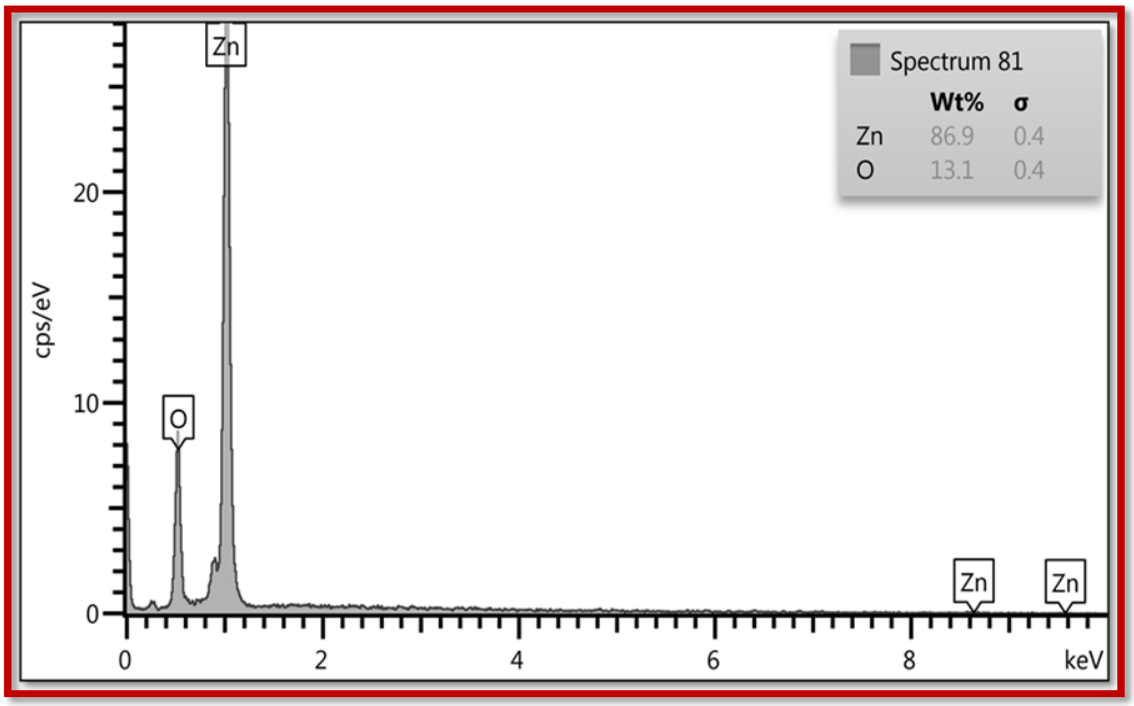

Fig. (3.27) EDX for Zinc oxide nanoparticles from C_3

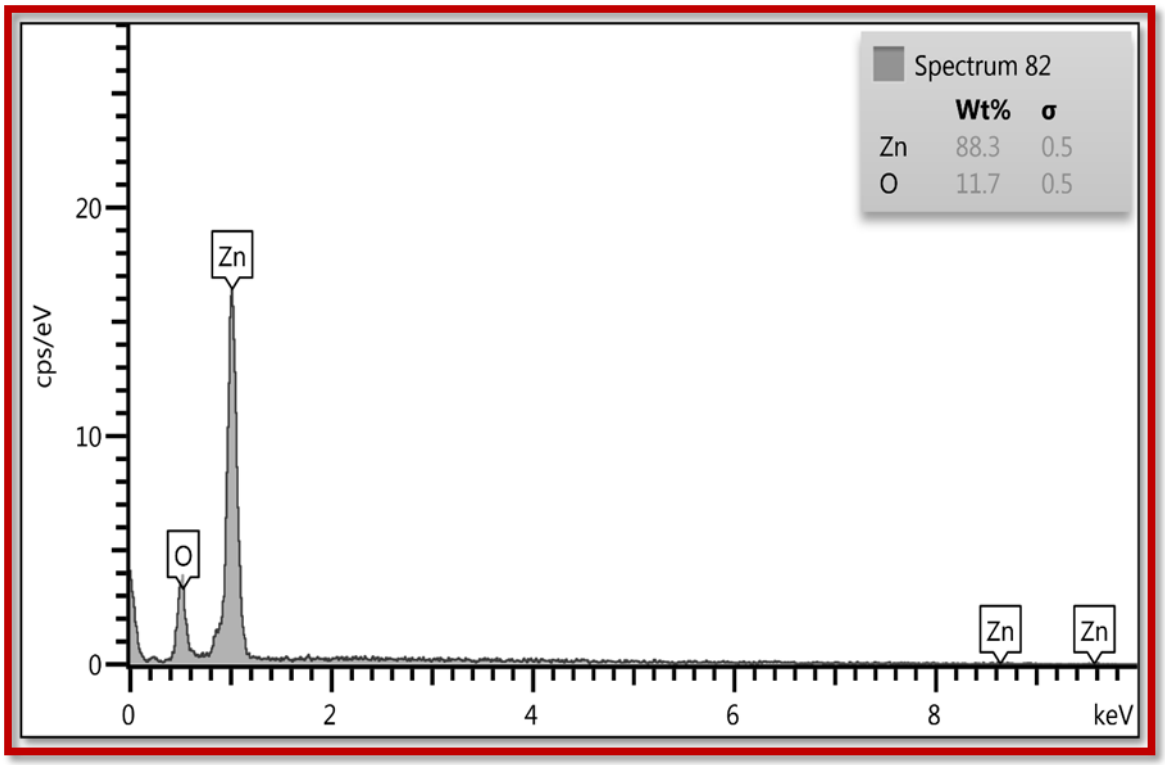

Fig. (3.28) EDX for Zinc Oxide Nanoparticles from C_4

3.5.5-Transmittance Electron Microscopy (TEM):

The TEM investigation was held to better understand the nanoparticles' crystalline properties and size, Figures.(3.29 to 3.32) showns TEM images of ZnO . The TEM images of ZnO showed that the particles were virtually hexagonal with a minor thickness variation, confirming the results that were obtaind by SEM [144] . The TEM morphology surface analysis is used to analyze the morphology of the surface of ZnO nanoparticles.

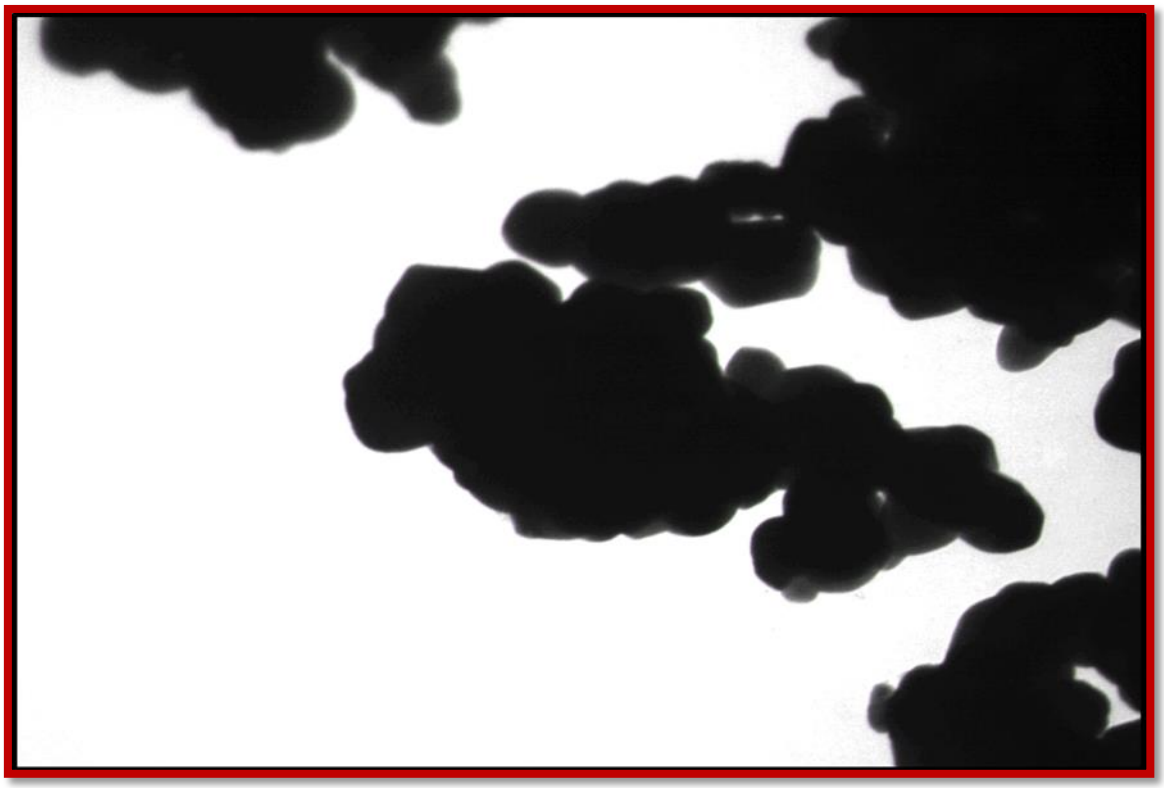

Fig.(3.29) Transmittance Electron Microscopy for ZnO NPs from C_1 complex

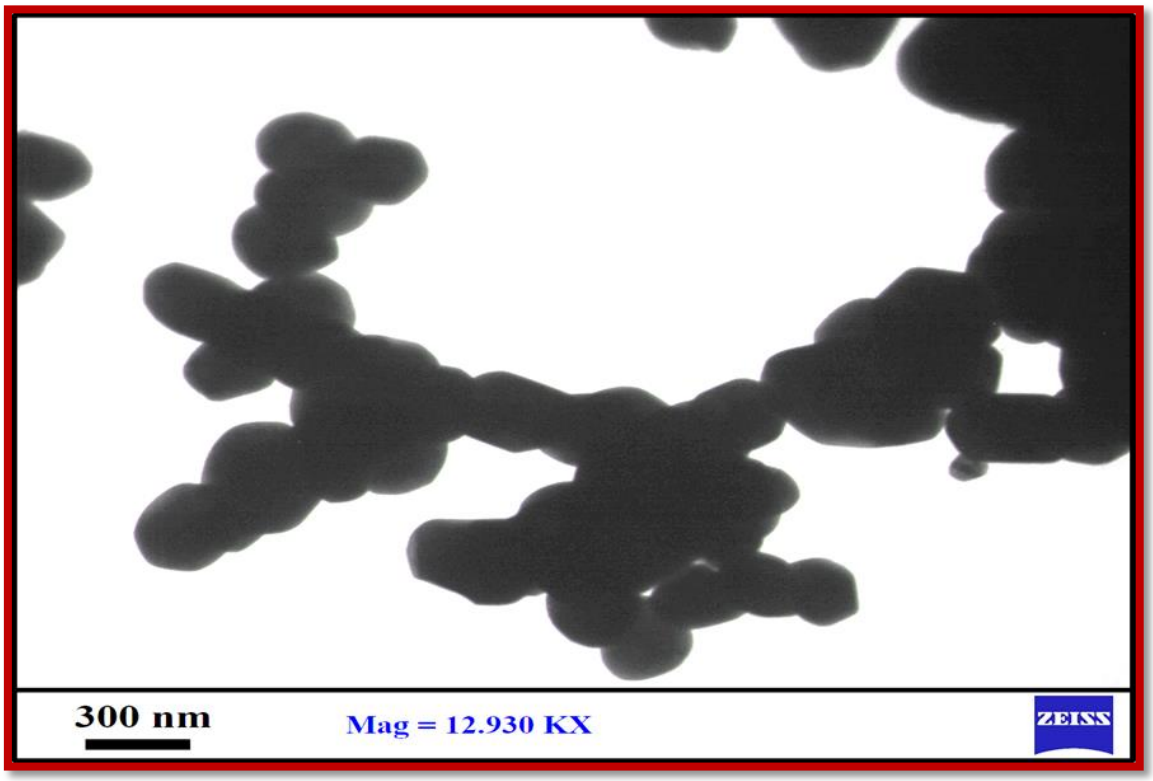

Fig.(3.30) Transmittance Electron Microscopy for ZnO NPs from C_2 complex

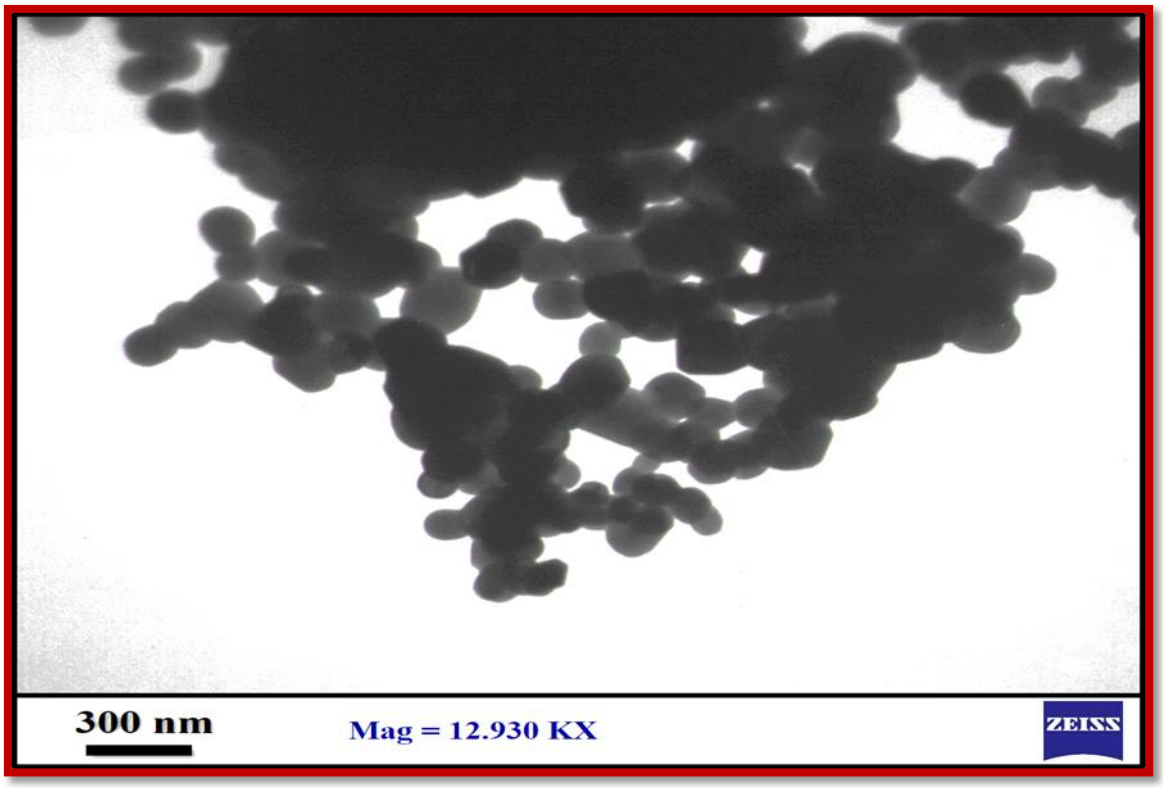

Fig.(3.31) -Transmittance Electron Microscopy for ZnO NPs from C_3 complex

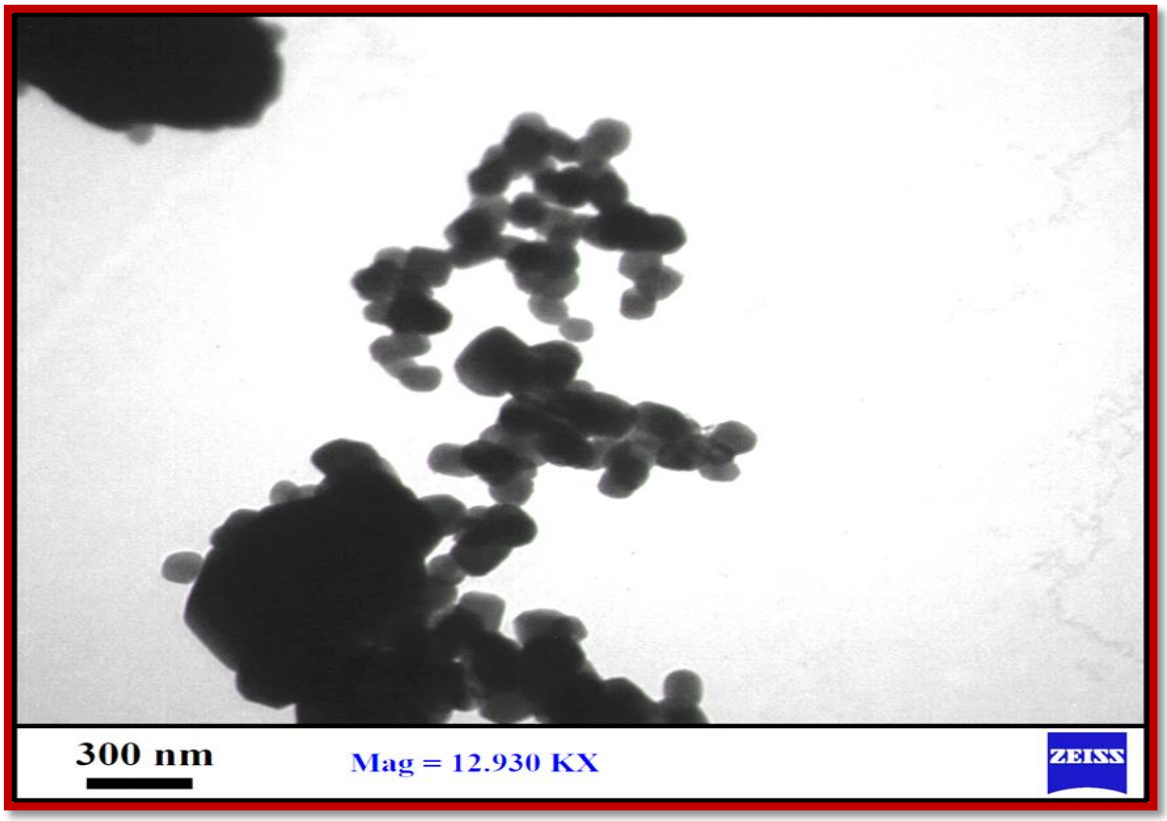

Fig.(3.32) -Transmittance Electron Microscopy for ZnO NPs from C_4 complex

3.5.6 - UV -Vis Diffuse Reflectance for spectroscopy ZnO Nps :

Diffuse reflectance spectroscopy (DRS) measures direct electronic band gap of ZnO. DRS works based on a principle that photon with energies greater than ZnO band gap will be absorbed . Absorption spectroscopy is powerful technique to explore the optical properties of nanoparticles.

The absorption spectra of ZnO nanoparticles for different thermal treatment temperatures in the UV and visible range are presented. All spectra showed absorption edges around 370-390 nm, which can be assigned to the intrinsic band-gap absorption of ZnO, owing to the electron transitions from the valence band to the conduction band (O2p→Zn3d) .

The Tauc method is a practical and basic approach for measuring a thin film material's characteristic optical band gap [29].The UV-VIS reflectance spectra of ZnO nanoparticles are shown in Figures (3.33 to 36), The band gap energy could can be calculated using the Tauc's relation.

The UV-VIS reflectance spectrum had a lower scattering effect than absorption. The optical band gap, which corresponded to a sharp reduction in reflectance at a certain wavelength, indicated that the particles in the sample were nearly evenly spread. The direct band gap energy (Eg) for ZnO nanoparticles was obtained by fitting the reflection data to the direct transition as shown in Equation(3.3).

$$(\alpha h\upsilon)^{\gamma} = A(h\upsilon - Eg) \ldots\ldots\ldots\ldots\ldots\ldots\ldots\ldots\ldots\ldots\ldots\ldots (3.3)$$

Where α is the absorption coefficient, hυ is the photon energy and Eg is the direct band gap. The direct band gap were measuremend by plotting when plotting (h)2 as a function of photon energy and projecting linear component of the curve to absorption equal to zero[145, 146].

Table(3.6) -The band gap energy from different complexes)

ZnO	Band gap energy (eV)
$ZnO_{(1)}$	3.17
$ZnO_{(2)}$	3.18
$ZnO_{(3)}$	3.20

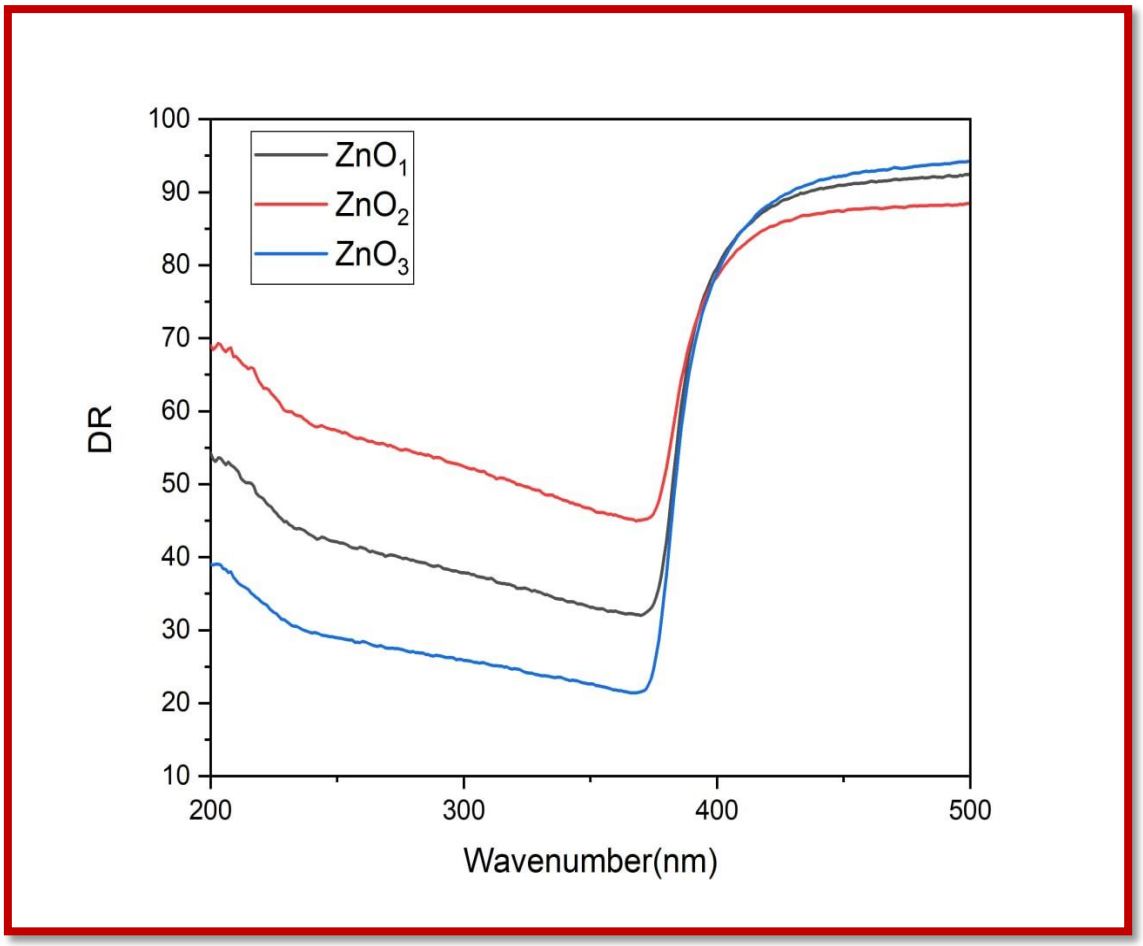

Fig. (3.33) Diffuse reflectance of Synthesis ZnO nanoparticles from difference complexes

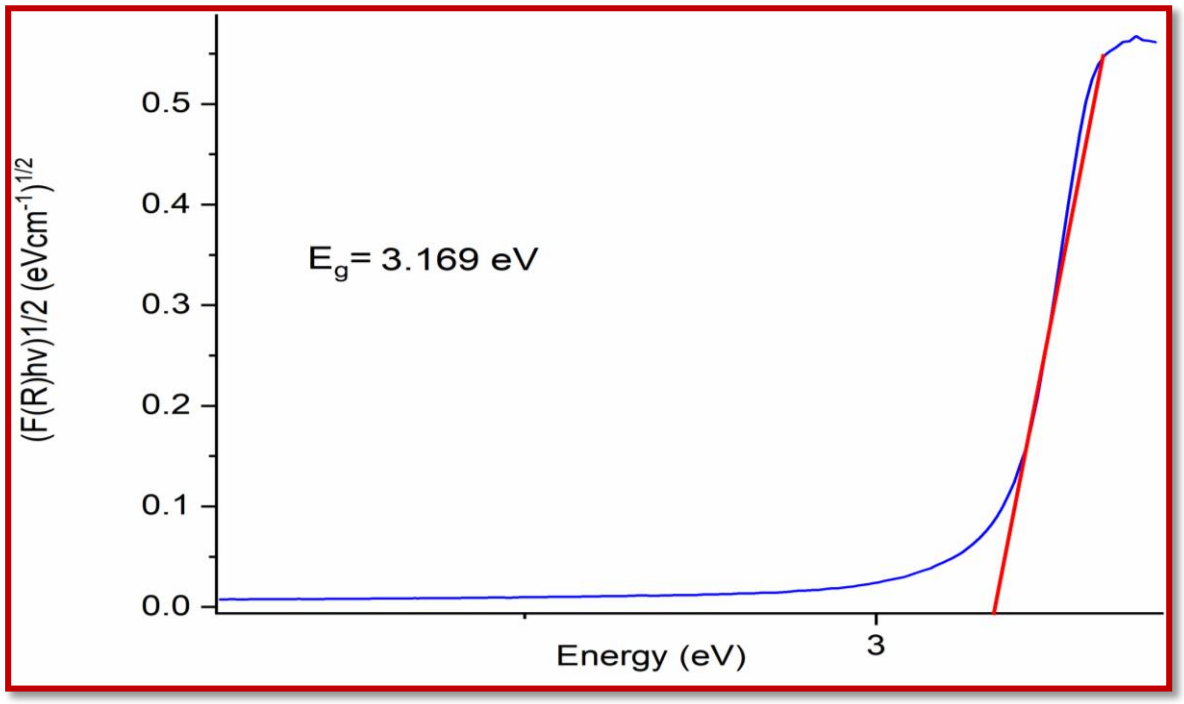

Fig. (3.34) Band gap energy of ZnO Nps from C_1 complex

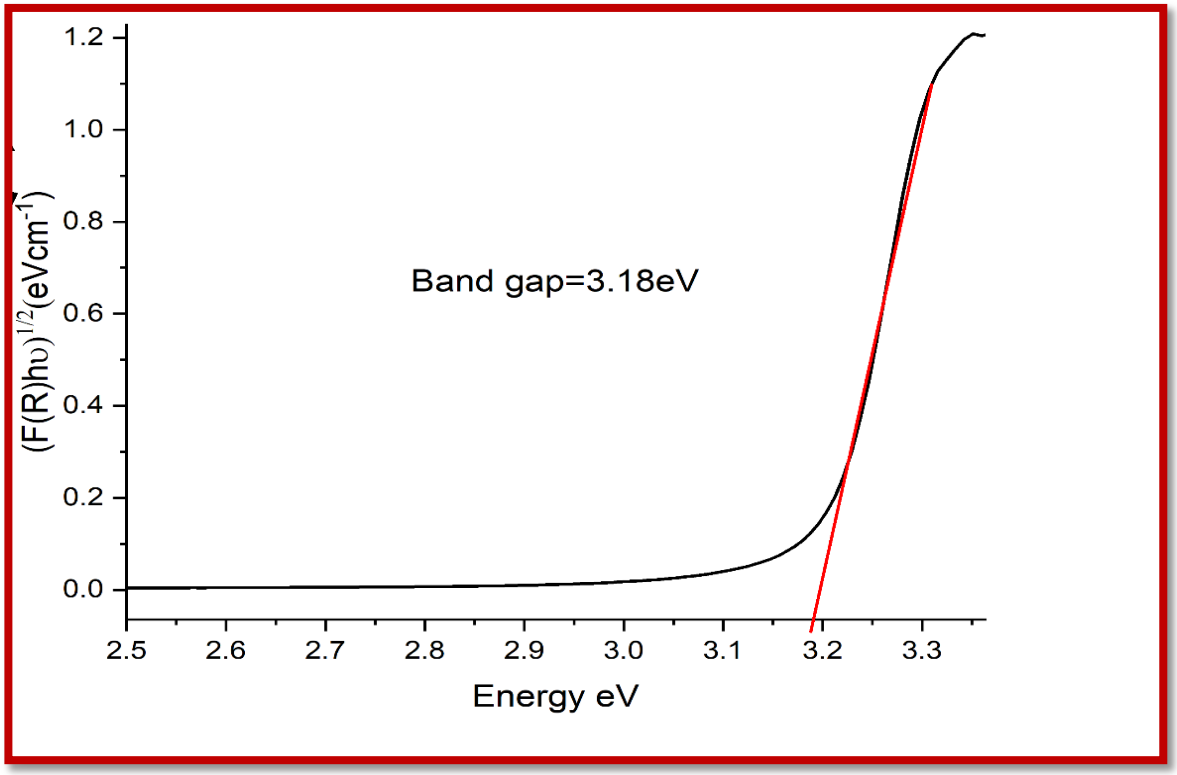

Fig. (3.35) Band gap energy of ZnO Nps from C_2 complex

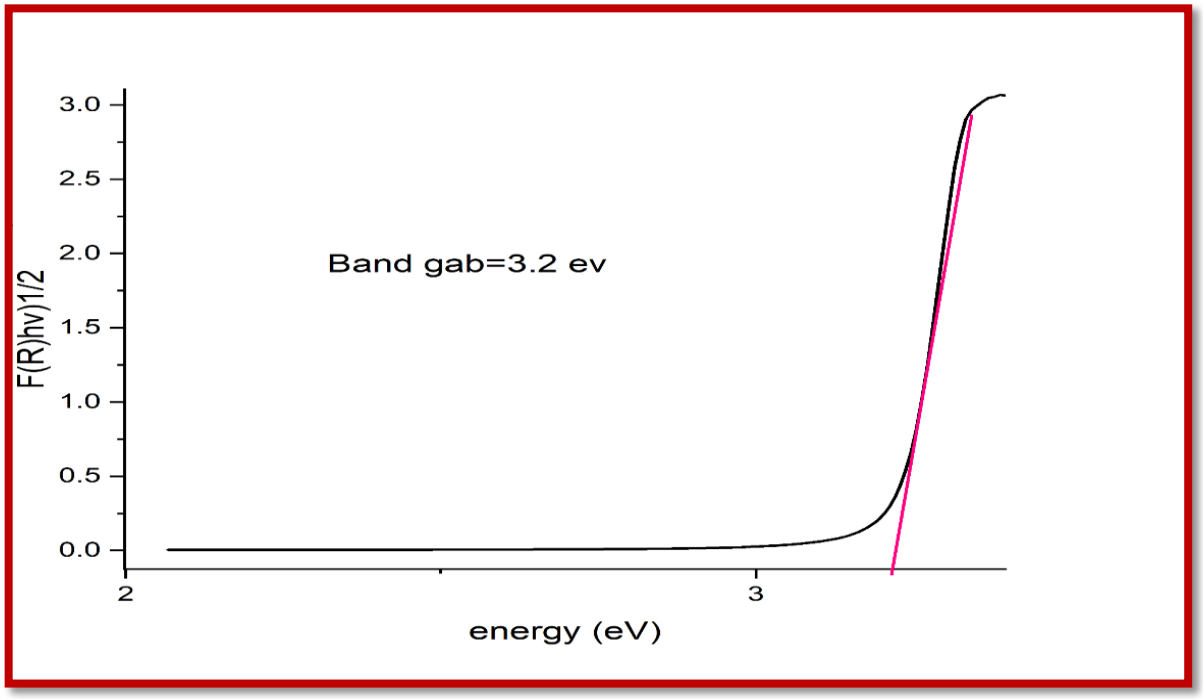

Fig. (3.36) Band gap energy of ZnO Nps from C_3 complex

3.5.7 - Surface Area Analyzer:

Brunauer–Emmett–Teller (BET) method was used for determine the surface area of a prepared ZnO nanoparticles calcined at 700°C, was investigated by using nitrogen adsorption-desorption isotherm , as shown in Figures.(3.37 to 3.38) display a Type-IV isotherm given by the IUPAC classification[147] From the results,a specific surface area and pore volume were obtained as 5.247 m^2 /g and 0.024166 cm^3 /g, respectively. The pore size was calculated as 18.421 nm. Thus synthesized ZnO Nanoparticles with larger surface area may provide active sites for photocatalytic degradation of pollutants[148].

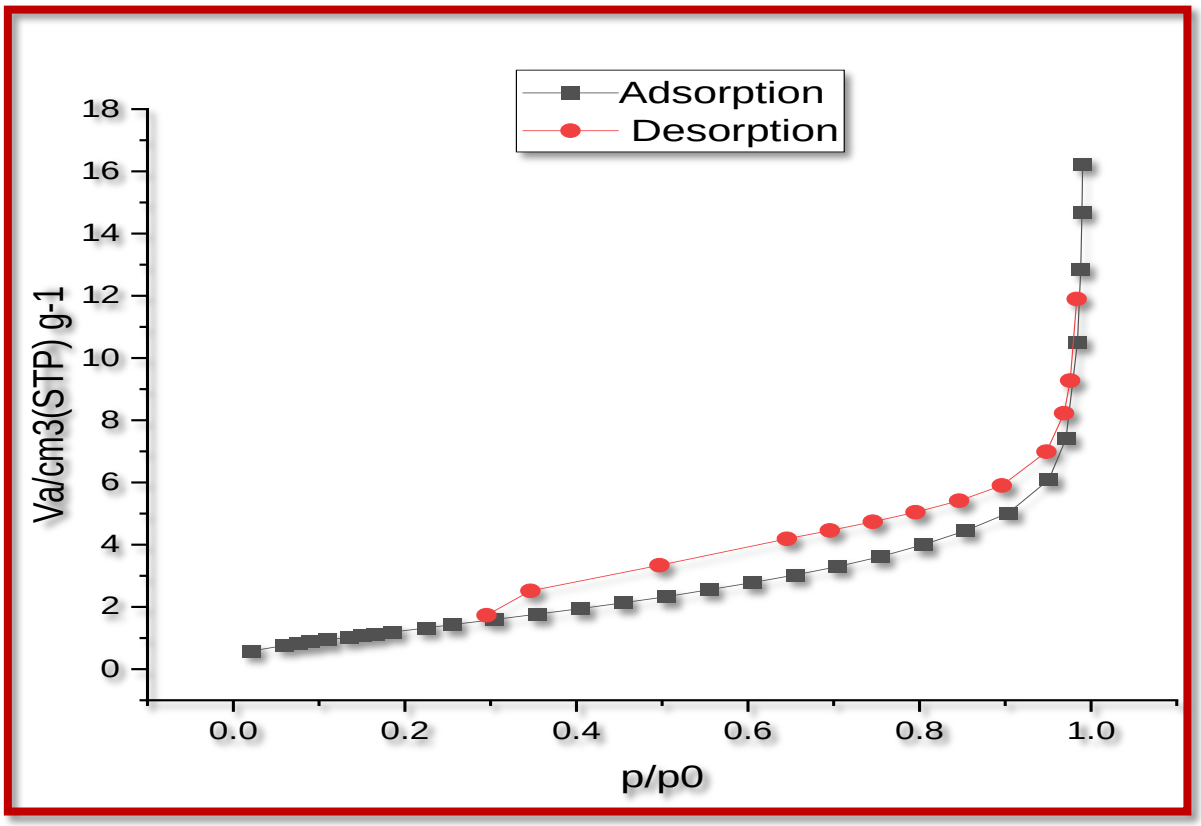

Fig. (3.37) Nitrogen adsoption-desorption isotherms for ZnO from C_1 complex

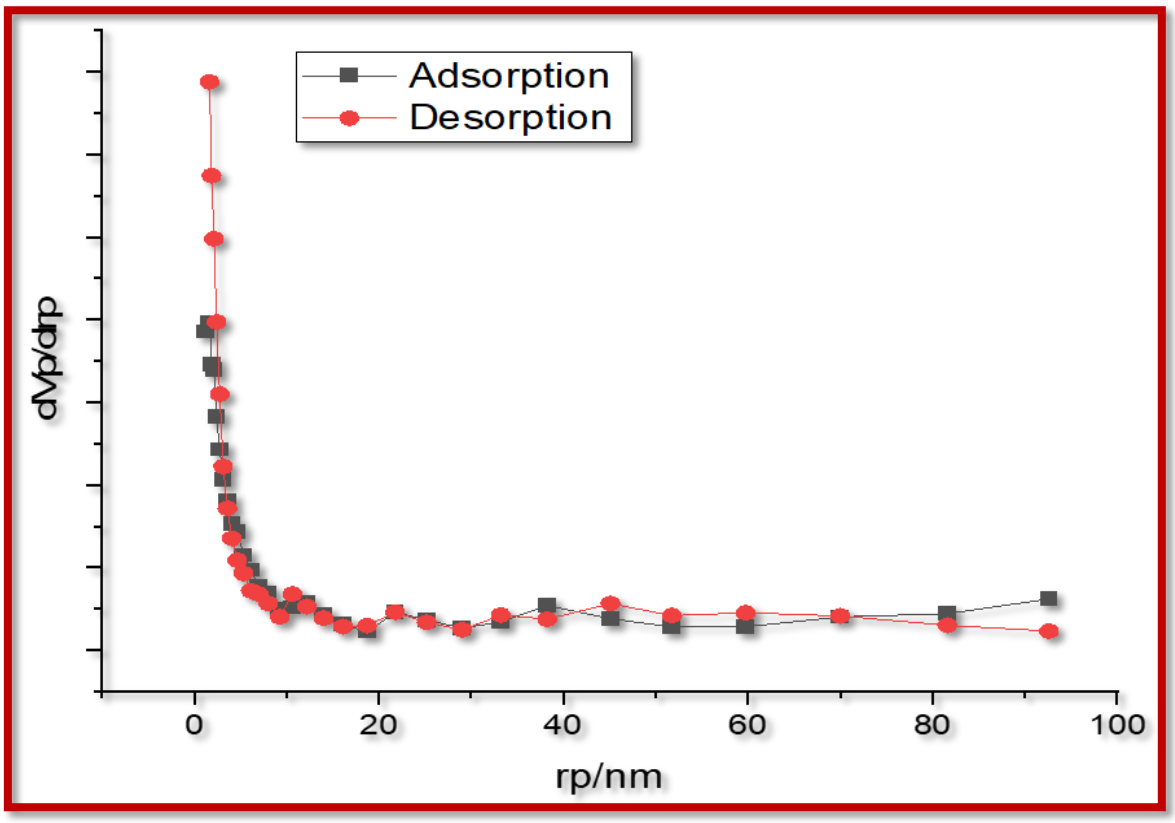

Fig. (3.38) Pore size distribution of ZnO nanoparticles from C_1 complex

3.6 Degradation of AYG dye by photo catalytic reaction over ZnO Nps :

3.6.1- Preliminary experiments:

Many experiments were carried out to reach the optimum conditions of the photocatalytic degradation processes. The first reaction has been done using 10 ppm of AY G dye with the addition of 0.13 g/100ml of ZnO nanoparticles under solar lamp and 10 ml/min Air flow rate in room temperature (photocatalytic process). The second reaction has been carried out using 10 ppm of dye in the dark using 0.13 g/100ml of ZnO nanoparticles (adsorption). The third reaction was performed using the same solution but without addition of ZnO nanoparticles under solar lamp(photolysis).

Figure. (3.39) depicts the results of AYG dye degradation in the precence of solar irradiation only (photolysis process) less than AYG dye degradation when adding amount of zinc oxide semiconductor to an aqueous solution without solar irradiation(adsorption process) .

In addition, AYG dye degradation in the presence of ZnO nanoparticales with solar lamp(photocatalytic degradation process) more than the two type above [149].

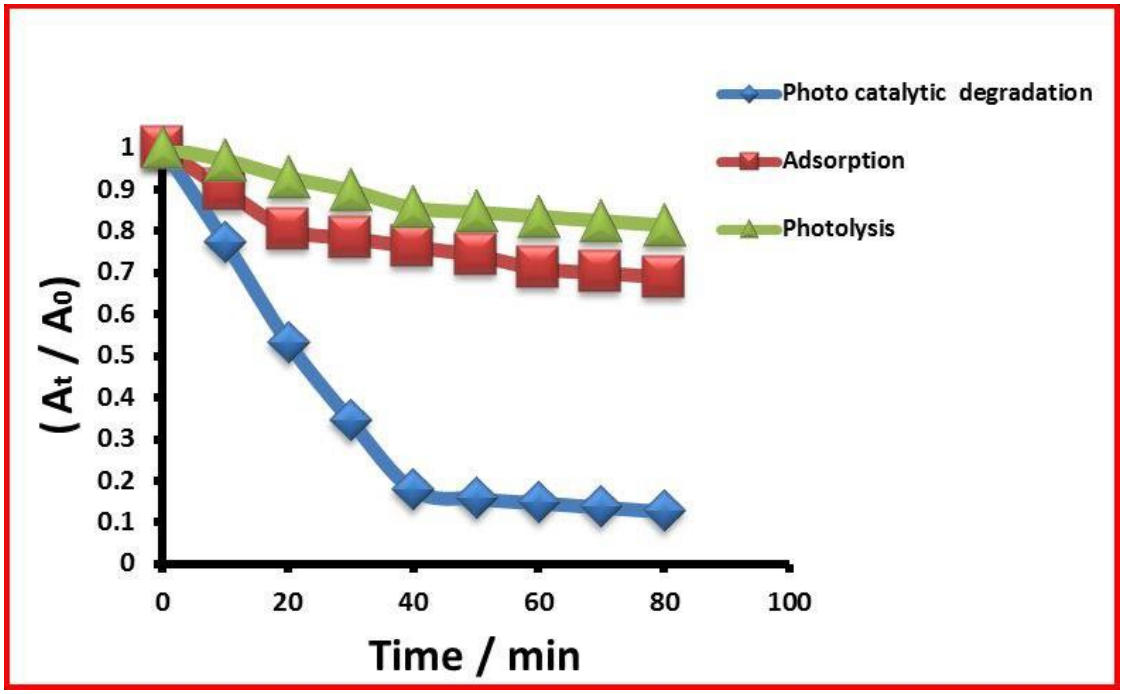

Fig.(3.39): The variation of PDE% of AYG dye with type of process.

3.6.2 Effect of different process on the photo-catalytic-degradation for AYG dye :

photocatalytic degradation of different types of pollutants such as AYG dye is reactions occurs on the surface of the semiconductors (TiO_2, ZnO, and many prepared nanocomposite), The parameters that affect on the surface properties of semiconductors normally have an impact on the photocatalytic degradation efficiency. In this part reviews different kind of parameters that was reported to affect the photocatalytic degradation efficiency of dyes.

3.6.2.1 Effect of the mass of ZnO nanoparticles on photo catalytic degradation of the AYG dye :

At ambient temperature, the effect of ZnO nanoparticle's mass on photocatalytic degradation of AYG dye was studied using 10 ppm dye as well as a flow rate of 10 ml/min air. When the mass of the ZnO Nano particles grows till it reaches 0.13 g /100 ml, the photo catalytic

degradation of AYG dye increases gradually, then drops gradually. The semiconductor may give the greatest absorption of light when the mass of ZnO nanoparticle's (0.13 g /100 ml) is used. Due decrease in photo degradation efficiency owing to a mass ratio of ZnO nanoparticle's, light absorption will be restricted to the early layers of AYG dye. more than 0.13 g/100 ml, and the other layers of solution will not receive photons. Furthermore, with high ZnO nanoparticle's loading, light scattering occurs. and because a result of the decreased photon intensity, light is strongly absorbed by the first few layers of solution, preventing light from traveling through the rest of the reaction vessel's layers. Table(3.7) and Figure. (3.40).

Many researchers have studied this effect and found that when the loading mass of ZnO nanoparticle's is less than the optimum value of 0.13 g /100 ml, the rate of photo degradation of AYG dye also decreases. This is because the quantity of mass of ZnO nanopartivales decreases, which means the surface area decreases, resulting in less light absorption ZnO nanoparticle's, resulting in a lower photo degradation rate [150] .

Table (3.7): The change in At/A0 with irradiation time on different masses of ZnO nanoparticle's.

Catalyst mass of ZnO g/100ml	0.02	0.04	0.13	0.60
Irradiation Time/min	At/A0			
0	1.00	1.00	1.00	1.00
10	0.90	0.83	0.68	0.96
20	0.74	0.61	0. 48	0.86
30	0.62	0.44	0.28	0.71
40	0.64	0.29	0.14	0.62
50	0.36	0.22	0.08	0.52
60	0.26	0.12	0.06	0.39
70	0.18	0.10	0.05	0.32
80	0.13	0.07	0.04	0.30

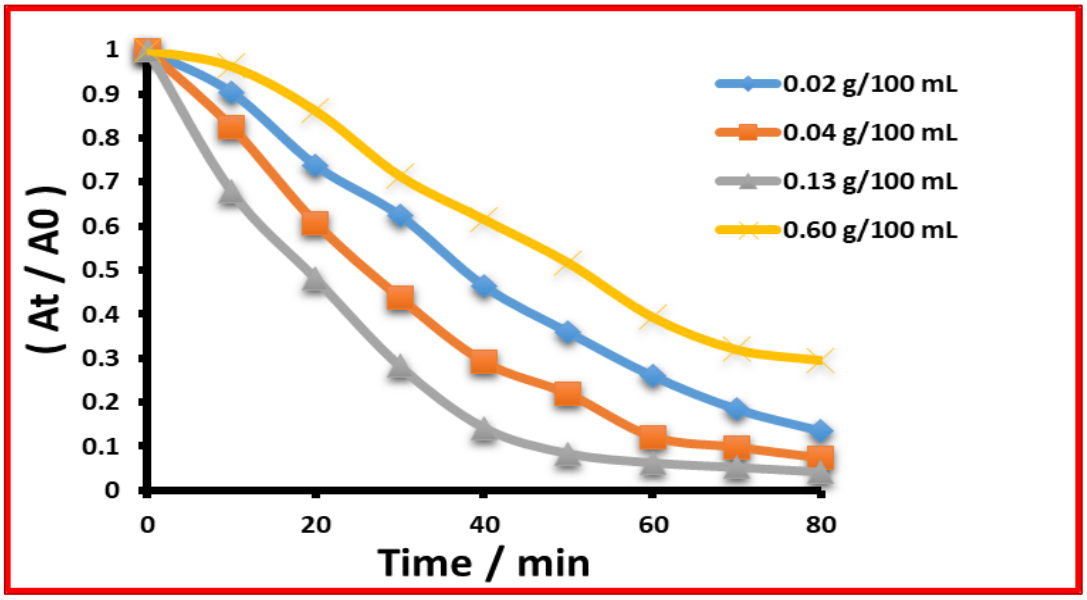

Fig. (3.40) : Variation in (A_t / A_0) with irradiation time at 10 ppm of the prepared dye .

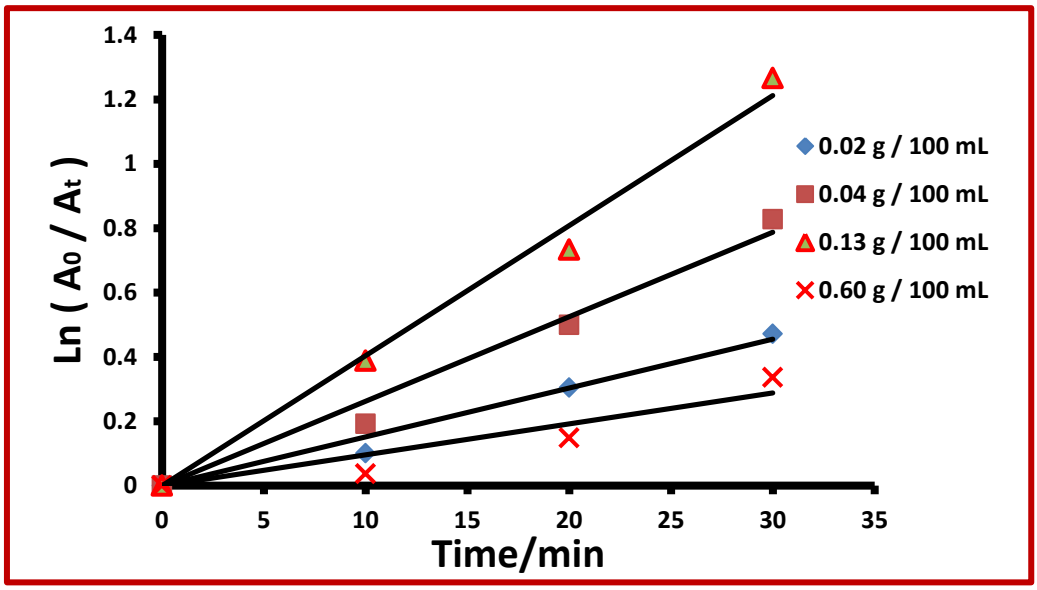

Fig. (3.41): Chang in Ln (A0 / At) through irradiation-time at different of the mass of ZnO nanoparticles using UV radiation.

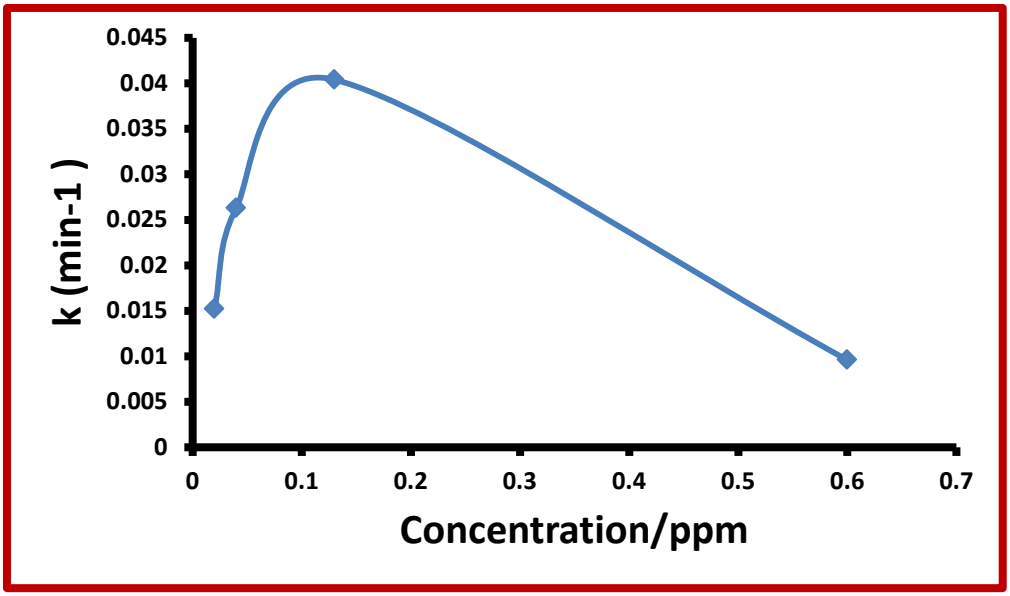

Fig. (3.42) : Effect of dye concentration on photo degradation rate constants using 10 ppm , 0.13 g/ 100 ml ZnO at constant K

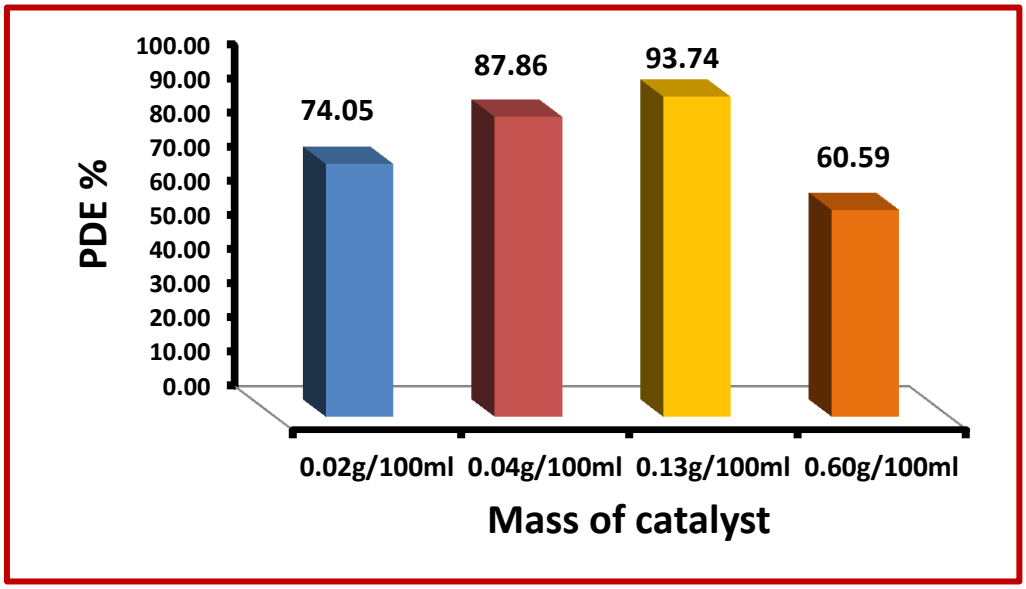

Fig. (3.43): Photocatalytic degradation efficiency using 10 ppm of AYG against mass of ZnO nanoparticles.

3.6.2.2- Effect of AYG dye initial concentration on the photocatalytic degradation process:

The effect of AYG dye concentration solution in the photocatalytic degradation processes in the range of (10-50 ppm) was investigate by keeping the other experimental conditions constant. Table (3.8) and Figure. (3.44) illustrate the findings. The rate of photocatalytic degradation reduced as the initial dye content was raised, according to these data. As the concentration of AYG dye in the solution declines, the path length of the photon entering the solution shortens. increase so the number of photons reaching to catalyst surface increase and hence rate of formation hydroxyl radicals and super oxide ions are increases thereby increasing rate of degradation[171-174].

Table (3.8): change of At /A0 through irradiation-time on different-concentration for AYG dye

Concentration of AYG dye/ ppm	10	20	30	50
Irradiation Time min	At/A0			
0	1.00	1.00	1.00	1.00
10	0.67	0.82	0.87	0.96
20	0.48	0.60	0.77	0.88
30	0.28	0.41	0.61	0.79
40	0.14	0.28	0.46	0.67
50	0.06	0.19	0.36	0.58
60	0.03	0.15	0.29	0.48
70	0.01	0.09	0.27	0.46
80	0.03	0.09	0.25	0.45

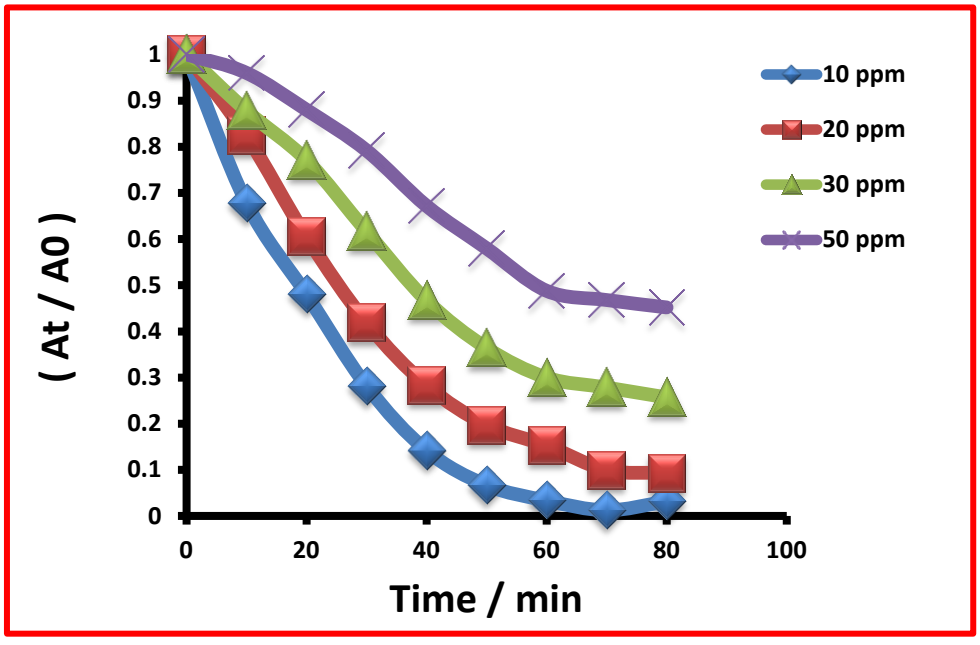

Fig. (3.44) : Variation in (At / A0)with irradiation time at different concentrations of dye

Langmuir–Hinshelwood rate expression has been successfully used for heterogeneous photocatalytic degradation to determine the relationship between the initial degradation rate and the initial concentration of the organic substrate. The rate of degradation of AYG dye at the surface is proportional to the surface coverage of AYG dye on the ZnO

The Langmuir–Hinshelwood model is expressed as Eq. (3.4)

$R = d_c / d_t = k_f Ka C /(1+ Ka C)$ …….....(3.4)

Where as:

R: Rate of reaction,

Kr: Rate constant (min^{-1}),

Ka: Langmuir adsorption constant,

C: Concentration (ppm), t: Time (min)

The Langmuir–Hinshelwood equation can be modified as (3.5)

$1/R = 1/K_f Ka C + 1/ K_f$ ……..……(3.5)

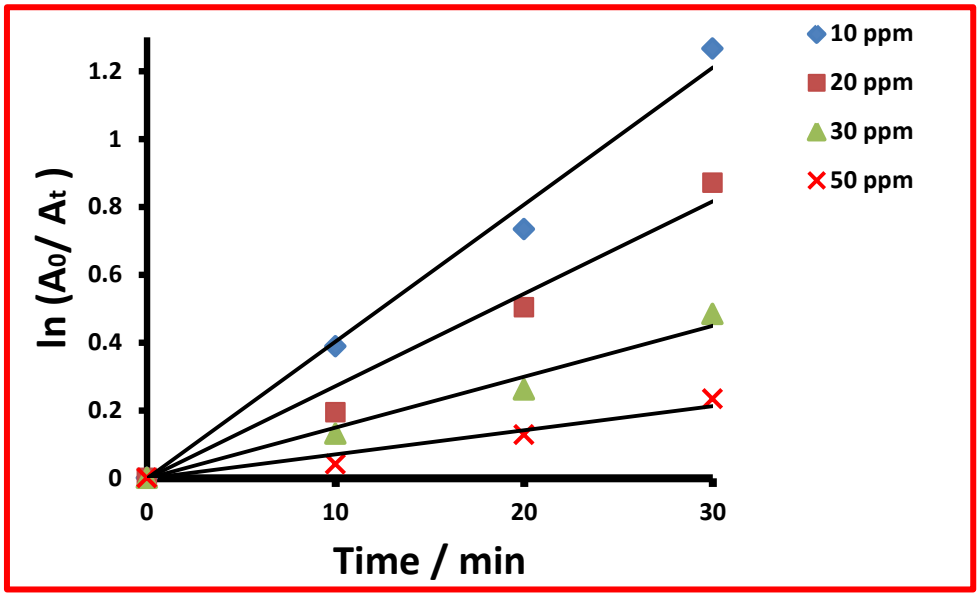

Fig. (3.45): Linear variation of ln A_O/A_t versus time for the photocatalytic degradation of AYG dye at different initial concentrations.

The results revealed that the photocatalytic reaction kinetics closely matched the Langmuir– Hinshelwood kinetics model. As a result, AYG absorption on the thin film surface is the regulating phase in the entire degradation process.

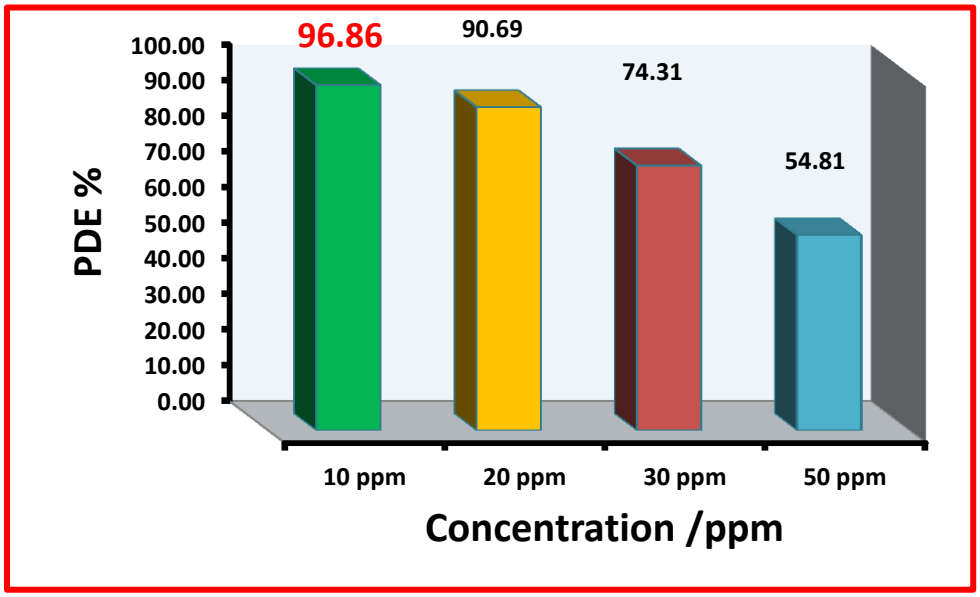

Fig. (3.46): Photocatalytic degradation efficiency using 0.13 g / 100 ml ZnO Nano particles against different concentration of AYG dye.

3.6.2.3- The effect of light intensity on photo degradation of AYG dye using ZnO nanoparticles :

Different experiments were accomplished to investigate the influence of light intensity on photocatalytic degradation of AYG dyeing in the range (1–7) mW/cm^2.By conservation other experimental conditions apply constant at initial AYG dye concentration of 10 ppm, prepared ZnO catalyst dosage was 0.13 g /100 cm^3, 10 cm^3 /min at room temperature, the flow rate of an: air bubble.

Table(3.9) and Figure (3.47) illustrate that when the light intensity rose , the dye breakdown process accelerated [150, 151]

This may be attributed to increased photons formation that is required for the electron transfer from the valence band to the conduction band of catalyst[152].

The light intensity 7 mW/cm^2 given the greater photo degradation efficiency which is equal to 92.43 %.

Table (3.9): The change of At/A0 through irradiation-time on different light intensity.

Light-intensity m W/cm2	1	3	5	7
Irradiation Time min	A_t/A_0			
0	1.00	1.00	1.00	1.00
10	0.96	0.92	0.89	0.80
20	0.92	0.84	0.74	0.55
30	0.84	0.73	0.58	0.39
40	0.72	0.58	0.43	0.26
50	0.62	0.45	0.29	0.17
60	0.51	0.39	0.25	0.16
70	0.50	0.36	0.24	015
80	0.50	0.34	0.23	0.14

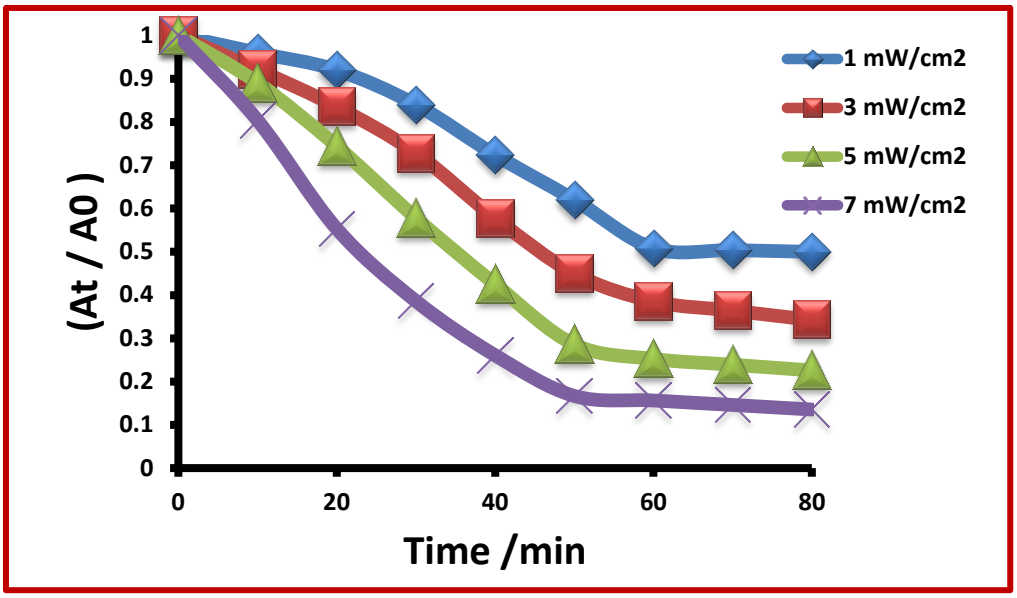

Fig. (3.47): Variation in (A_t / A_0) with irradiation time at different light intensity.

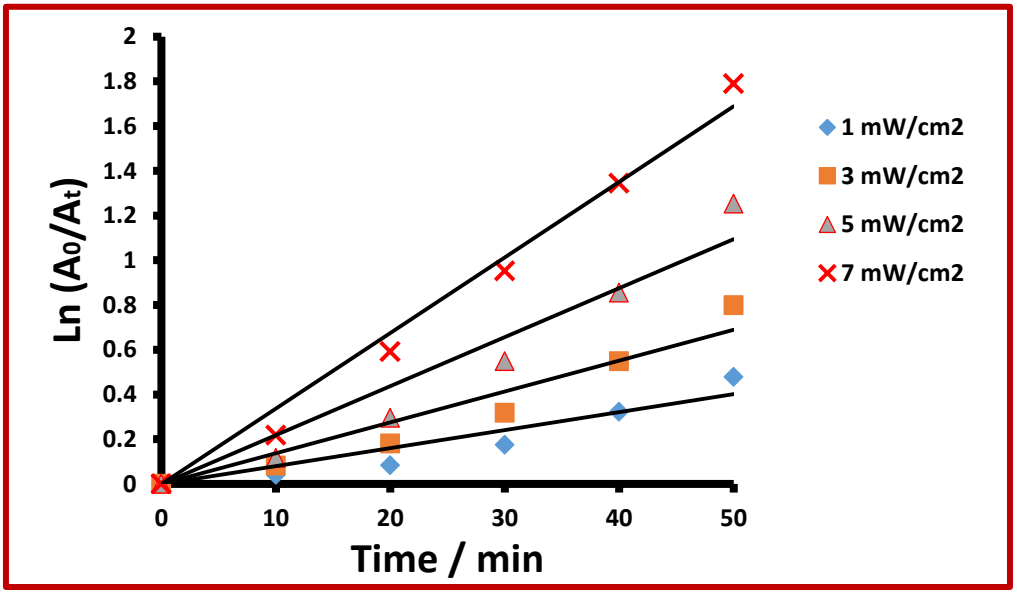

Fig. (3.48): Chang in Ln (A_0 / A_t) through irradiation-time at different intensity of light.

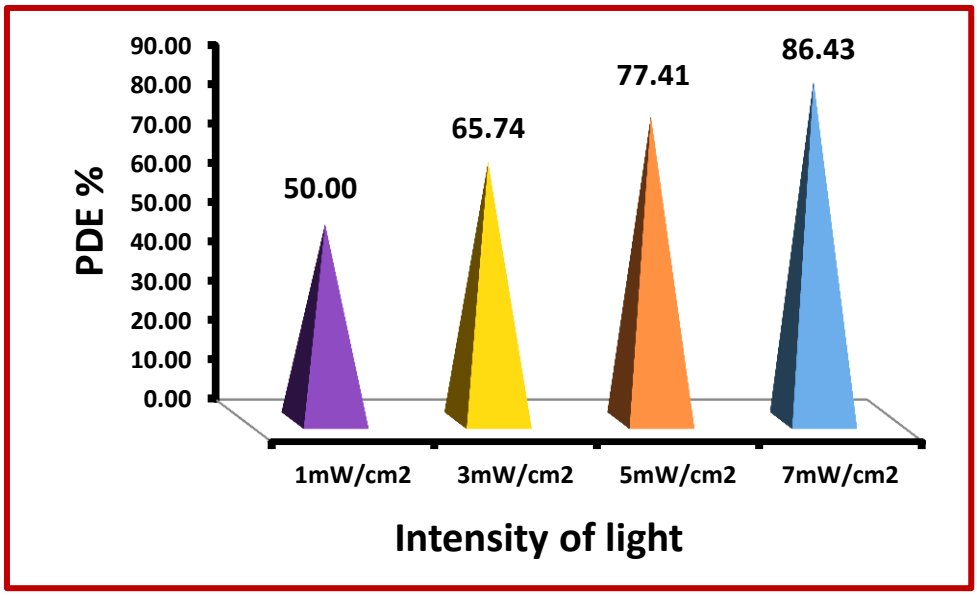

Fig. (3.49): Photocatalytic degradation efficiency using 0.13 g / 100 ml ZnO nanoparticles and 10 ppm of AYG dye for different light intensity.

3.6.2.4- Effect of pH on photocatalytic degradation of AYG dye:

The influence of the initial pH of the suspension solution on the ability to photo catalytically degradation AYG dye over 0.13 g /100 ml of ZnO nanoparticle was investigated in a series of experiments,10 ppm of AYG dye concentration. The practical experiments were carried out under pH solution (9.85, 8.75, 3.89 and 6.20).

As shown in Table(3.10) and Figure.(3.50) the optimum value of degradation AYG dye, was determined at pH=8.75.At pH in the acidic medium the surface of catalyst become acidic this lead to increase repulsion of dye molecules with catalyst surface, and hence decreases photocatalytic degradation efficiency [153-155].

While at higher pH function in the basic medium increase the attractive force between molecular dye and catalyst surface and hence increase photocatalytic degradation efficiency[155-158].

Table (3.10): change for At/A0 through irradiation-time on different pH Value .

Initial-pH solution	3.89	6.20	8.74	9.85
Irradiation Time/ min	A_t/A_o			
0	1.00	1.00	1.00	1.00
10	0.90	0.83	0.72	0.94
20	0.76	0.68	0.54	0.84
30	0.61	0.51	0.33	0.76
40	0.50	0.34	0.19	0. 69
50	0.44	0.29	0.15	0.62
60	0.38	0.22	0.11	0.57
70	0.35	0.19	0.09	0.52
80	0.32	0.17	0.08	0.44

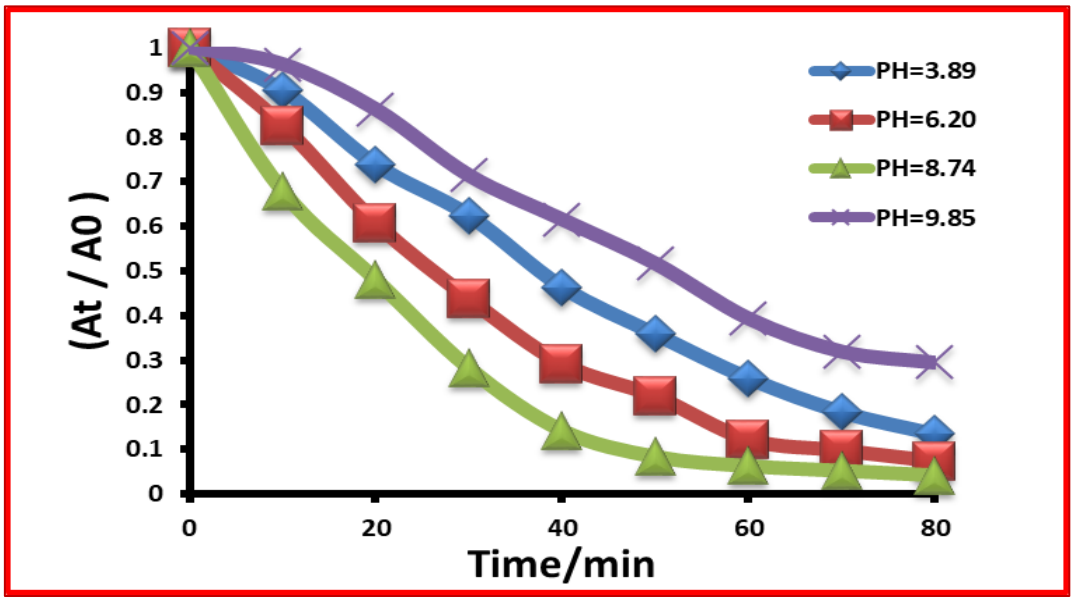

Fig. (3.50): Variation in (A_t / A_0) with irradiation time at different initial pH solution.

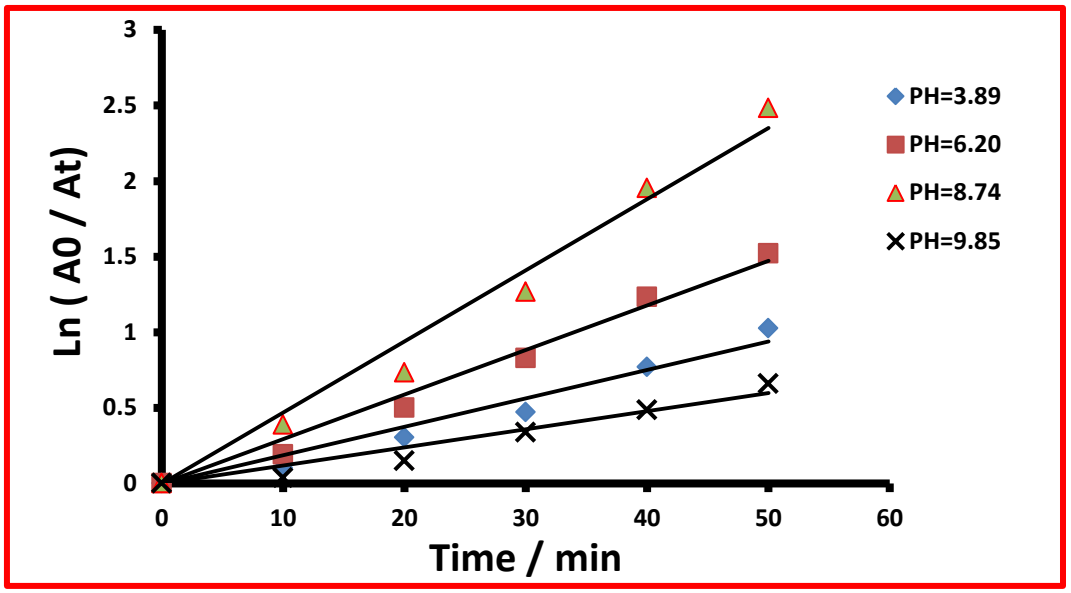

Fig. (3.51):Chang in Ln (A_0 / A_t) through irradiation-time at different-pH using UV radiation, initial AYG dye.

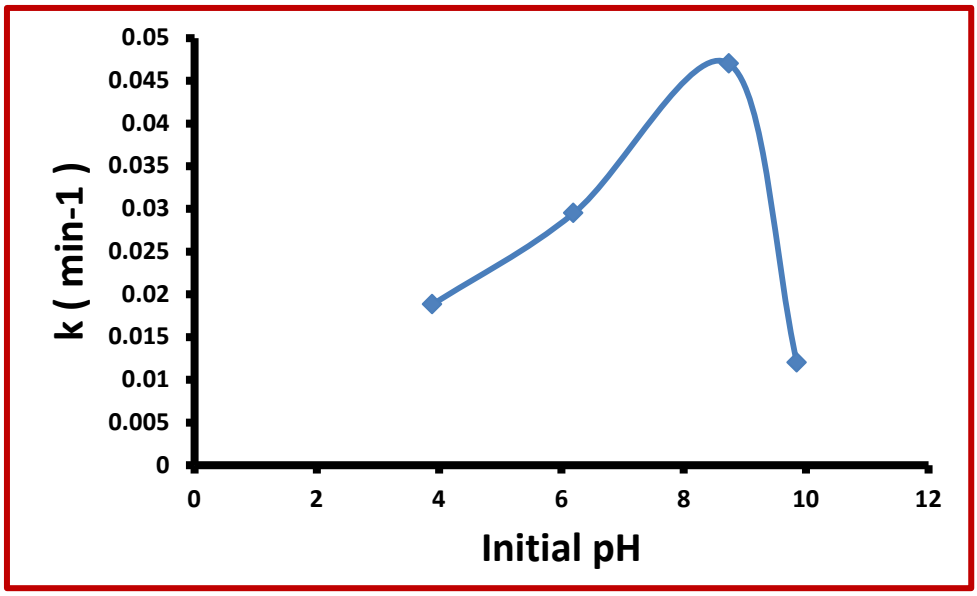

Fig. (3.52): Effect of pH on photo degradation rate constants

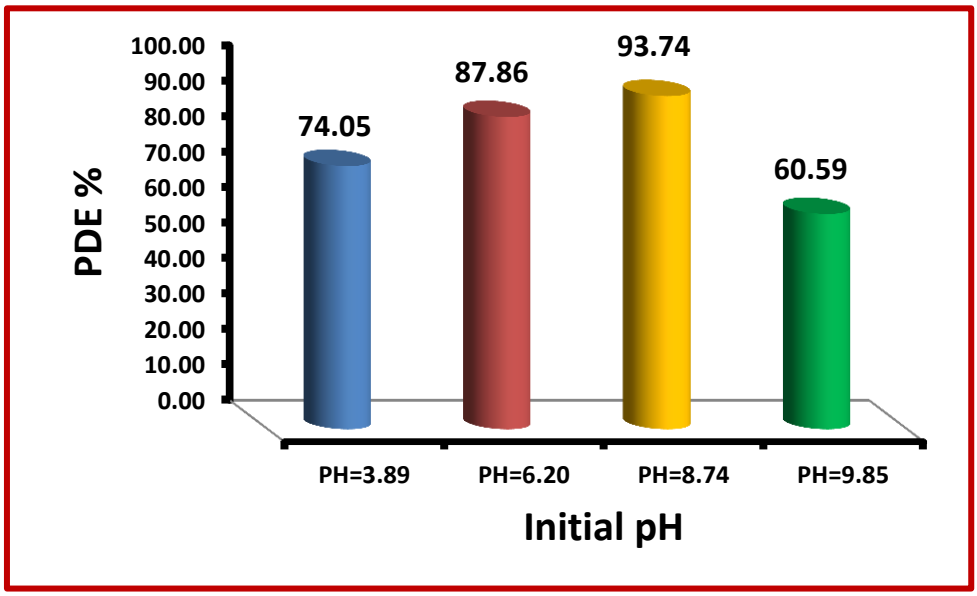

Fig. (3.53): Photocatalytic degradation efficiency using 0.13g / 100 ml ZnO nanoparticle and 10 ppm of AYG dye for different initial pH.

3.6.2.5-Effect of the Hydrogen Peroxide:

Different experiments were carried out to investigate the effect of different initial hydrogen peroxide concentration ranges (0.10 percent, 0.45 percent, 1.50 percent, 2.10 percent) at various pH 7 on the photocatalytic degradation of dye by ZnO nanoparticles , catalyst dosage 0.13 g /100 ml, at various time intervals, and a starting concentration of AYG dye (10 ppm) .The impact of hydrogen peroxide concentration on dye photocatalytic degradation were studied and the obtained resuits are shown in Figure.(3.54), demonstrates that raising the initial hydrogen peroxide concentration increased the degrading efficiency from 71.83 to 96.32 percent from (0.10 %,0.45%,1.50%, 2.10 %,). The greater reactivity between hydrogen peroxide and electron in AYG conduction band explains the enhanced photocatalytic degradation efficiency with the addition of hydrogen peroxide. Hydrogen peroxide, according to, can efficiently reduce electron–hole recombination. Because hydrogen peroxide accepts electrons more efficiently than dissolved oxygen, it might be used in place of oxygen.

The suppression of electron–hole recombination at low hydrogen peroxide concentrations aids the photocatalytic degradation of AYG dye efficiently. However, raising the hydrogen peroxide concentration over 10 mM inhibited the reaction between AYG and electron in the ZnO nanoparticles conduction band, resulting in reduced AYG degradation. Adsorbed H_2O_2 scavenging positive holes on the surface of the ZnO nanoparticle's could potentially account for the inhibitory action[159, 160]

The added H_2O_2 can accelerate the reaction by producing hydroxyl radicals from scavenging the electrons and absorption of UV-light by the following reactions:

$$H_2O_2 + e^- (c.b.) \longrightarrow {}^{\cdot}OH + {}^{-}OH \quad \text{.....(3.6)}$$

$H_2O_2 + O_2^{\cdot -} \longrightarrow {}^{\cdot}OH + {}^{-}OH + O_2$ ……..(3.7)

$H_2O_2 + hv \longrightarrow {}_2{}^{\cdot}OH$ ……..(3.8)

By additing excess H_2O_2, it acts as hydroxyl radical or hole scavenger to form the per hydroxyl radicals ($HO^{\cdot}_2$) which is a much weaker oxidant than hydroxyl radicals :

$H_2O_2 + {}^{\cdot}OH \longrightarrow H_2O + {}^{\cdot}HO_2$ ……(3.9)

$H_2O_2 + {}^{+}h \longrightarrow {}^{+}H + {}^{\cdot}HO_2$ ……(3.10)

Table (3.11): change for A_t/A_0 through irradiation-time on different initial H_2O_2 solution Value .

initial hydrogen Peroxide solution % v/v	0.10	0.45	1.50	2.10
Irradiation Time min	A_t/A_o			
0	1.00	1.00	1.00	1.00
10	0.90	0. 83	0.59	0.96
20	0.74	0.61	0.34	0.86
30	0.62	0.44	0.15	0.71
40	0.64	0.29	0.09	0.62
50	0.36	0. 22	0.08	0.52
60	0.26	0.12	0.06	0.39
70	0.18	0.10	0.05	0.32
80	0.13	0.07	0.04	0.30

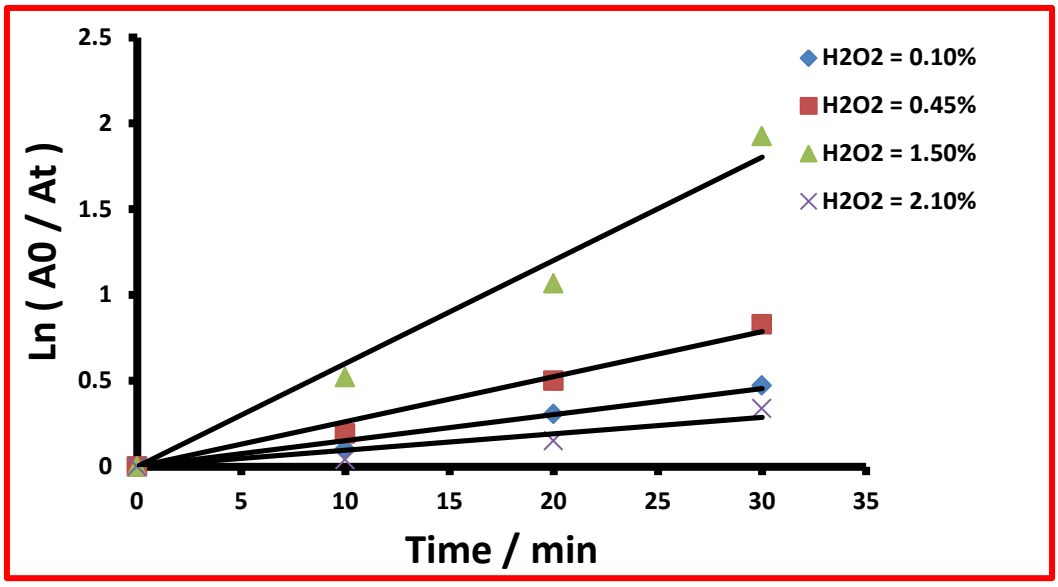

Fig. (3.54): Chang in Ln (A_0 / A_t) through irradiation-time at different-H_2O_2 using UV radiation, initial AYG dye.

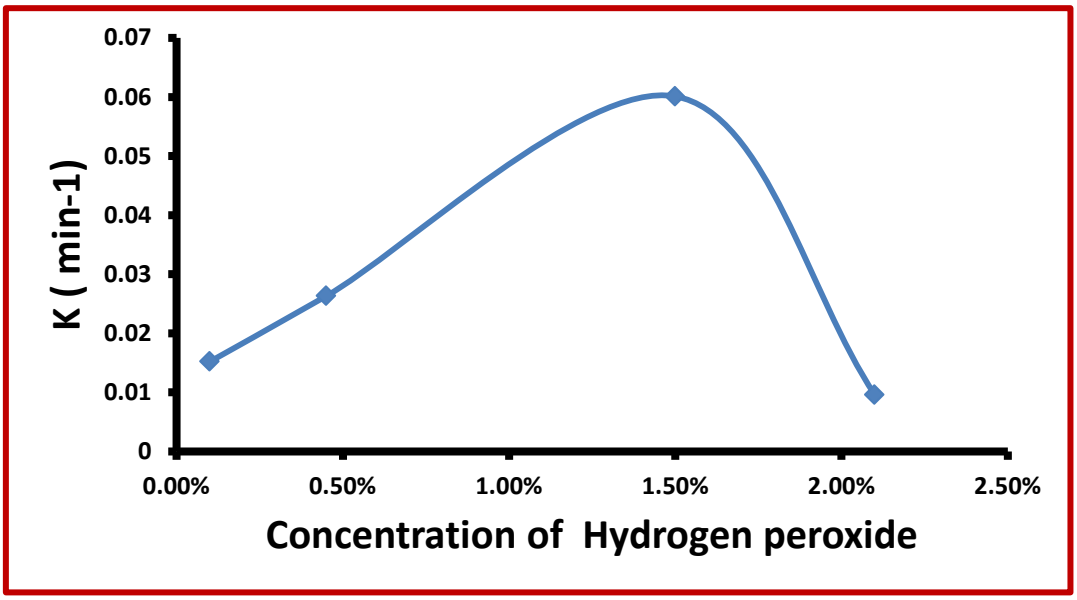

Fig. (3.55): Effect of H_2O_2 on photo degradation rate constants

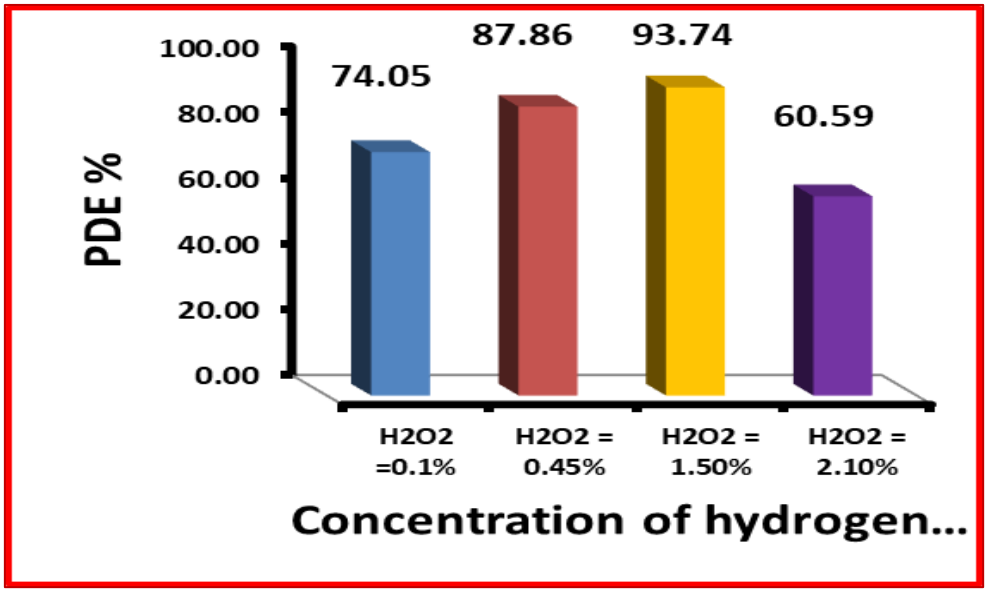

Fig. (3.56): Photocatalytic degradation efficiency using 0.13 g / 100 ml ZnO nanoparticles and 10 ppm of AYG dye for different H_2O_2 concentrations.

3.6.2.6- Temperature effect on photocatalytic-degradation for AYG dye:

A series of experiments were carried out to investigate the effect of temperature on photocatalytic degradation of AYG dye in the temperature range of (281 – 308) K. By conservation other experimental conditions apply constant at initial AYG dye concentration of 10 ppm, prepared ZnO catalyst dosage was 0.13 g /100ml.

Table(3.12) and Figure.(3.57) reveal that, when the temperature rose, the dye degradation process accelerated, possibly due to increased reactive hydroxyl radical formation. The activation energy associated with the photo degradation of dye was calculated according to the Arrhenius equation by plot of In k versus 1/T[161, 162] .

Table (3.12): Change of A_t/A_0 through irradiation-time of different-temperature.

Temperature K	281	298	301	308
Irradiation Time min	A_t/A_0			
0	1.00	1.00	1.00	1.00
10	0.93	0.85	0.84	0.69
20	0.82	0.68	0.61	0.44
30	0.67	0.53	0.42	0.21
40	0.56	0.41	0.25	0.11
50	0.46	0.32	0.21	0.09
60	0.40	0.26	0.17	0.08
70	0.37	0.24	0.15	0.07
80	0.33	0.21	0.13	0.06

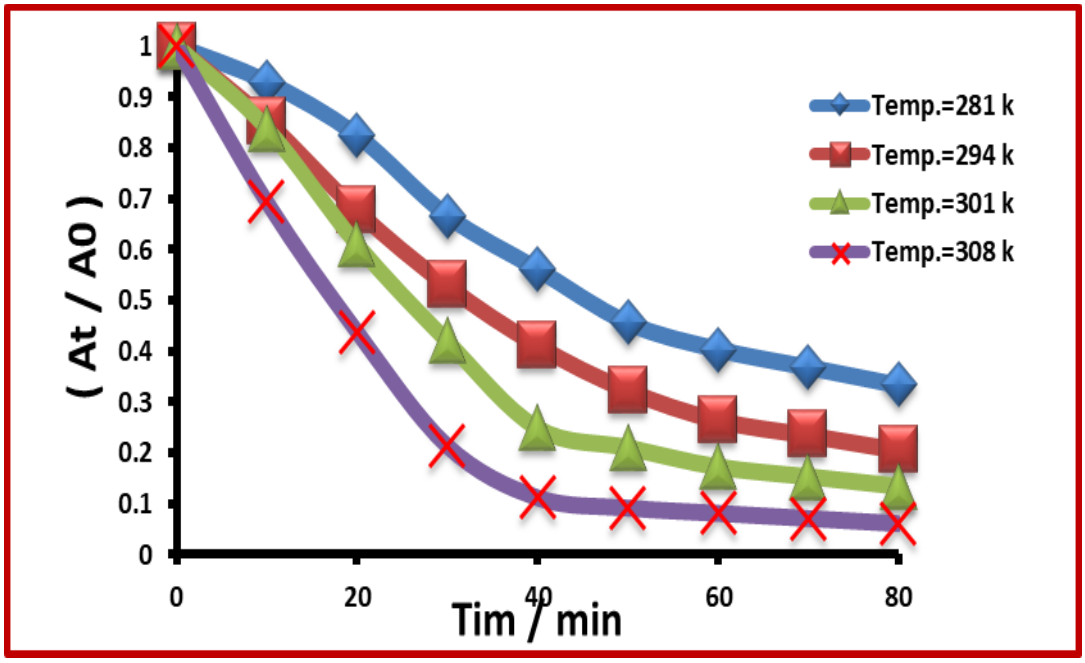

Fig. (3.57): Variation in (At / A0) with irradiation time at different temperature

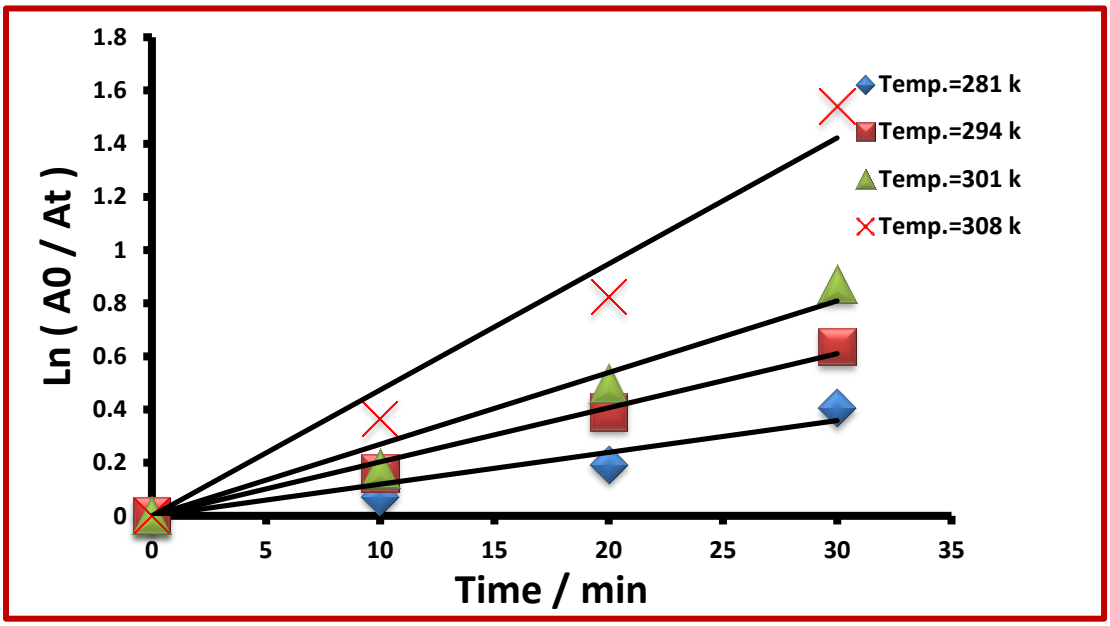

Fig. (3.58): Chang in Ln (A0 / At) through irradiation-time at different-temperature using UV radiation, 10 ppm of AYG dye and (0.13g / 100 ml) ZnO nanoparticle's.

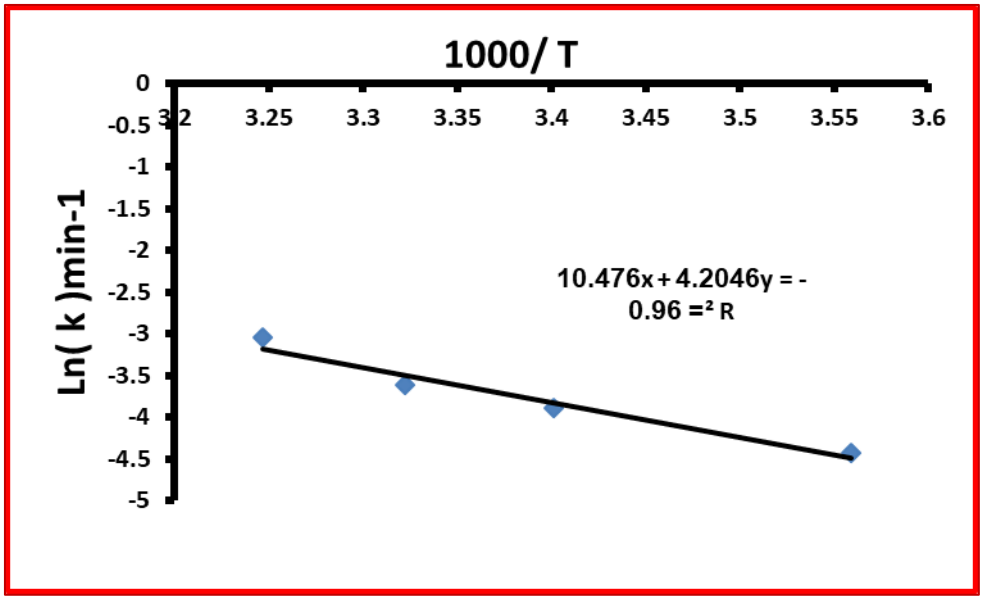

Fig. (3.59): Arrhenius plot of AYG dye.

In order to calculate thermodynamic functions such as ΔH°(Enthalpy of activation) and ΔS°(Entropy of activation), figure (3.60) was shown a linear relationship fitting the graph of Eyring equation (3.11).

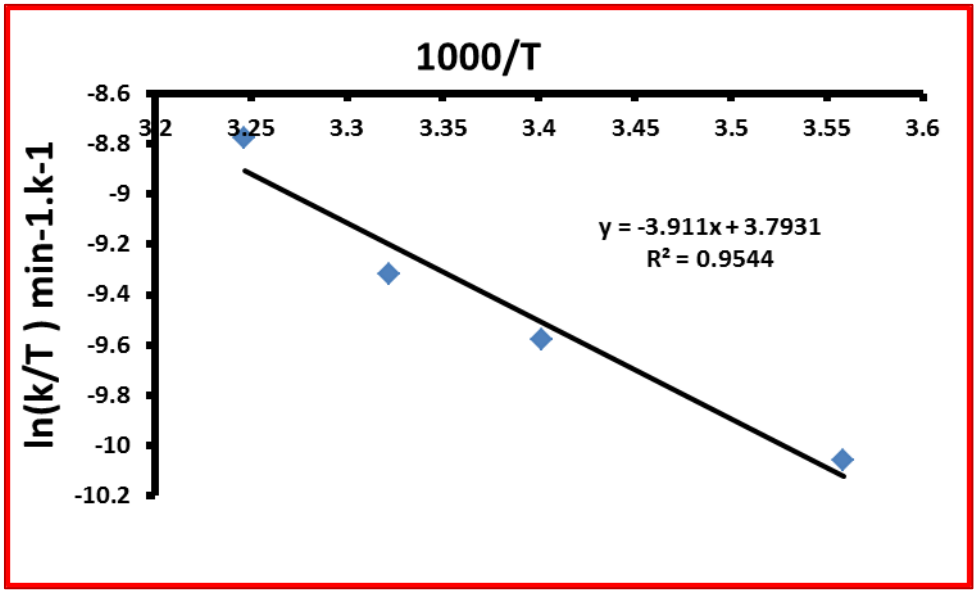

Fig. (3.60): Eyring equation plot ln(k/T) against 1000/T for AYG dye.

A plot of ln(k/T) versus 1/T produces a straight line and the value of Enthalpy of activation can be calculated from the slop of this line (ΔH°= 32.52kJ/mol) . and from the intercept the Entropy of activation value (ΔS°= −0.166k J/ mol.k).

The positive value of Enthalpy of activation refer to endothermic reaction . In the present case the value of Entropy of activation is negative as in Table (3.13), so that the prodect formed is more ordered than the reactants.

The Gibbs' free energy ΔG° can be calculated from the equation and equal 81.98 kJ/mol . The positive values of ΔG° for the reaction indicate the non-spontaneous nature of photocatalytic degradation of AYG dye .

Table (3.13): The thermodynamic parameters of the photocatalytic degradation of dye .

Temperature/ K	Enthalpy of activation/ $KJ.mol^{-1}$	Entropy of activation/ $KJ.mol^{-1}.k^{-1}$	Gibbs' free energy/ $kJ.mol^{-1}$
298	32.52	- 0.166	81.98

3.7- Conclusions:

From the obtained results in this study , the following points are concluded:

The result was found that the (L_1 and L_2) ligands coordinated to the

Zinc ion as a bidentate through the nitrogen atom of azomethane group and oxygen atom in the phenol group to configure of a stable inner hexagonal ring.

1. Ligands plays very important role in the synthesis of ZnO in different Stoichiometric as (1:1) and (1:2) (metal: ligand).The adsorption efficiency for removal of alizarin yellow dye ZnO

Nanoparticles from C_1 andC_3 complexes was found better than prepared ZnO nanoparticles from difference complexes (C_2 and C_4) shows a good photo catalytic activity for removal of AYG dye form aqueous solution while very weak activity in the dark reaction (adsorption)

2. Increase of light intensity caused to increas the rate of photo catalytic degradation and photo degradation efficiency (PDE).
3. Increase of mass amount of catalyst caused to increased of PDE after reached to optimum conditions.
4. Increaseof AYG dye concentration caused to decreas the rate of photo degradation but at the same time reduce the degradation efficiency.
5. Synthesis catalyst show a good and highly response for induced of light (photo catalytic activity), The XRD results show that ZnO nanoparticles had good crystallinity , high purity, and it could be concluded that all ZnO synthesis in hexagonal wurtzite.
6. The SEM and TEM image show that the morphology of ZnO nanoparticles.

7- The EDX analysis showed that synthesized material ws compared of zinc and oxygen without any significant impurity.

8- In this work ZnO nanonanoparticales was prepared using thermal decompastion method. The mean crystallite size for the prepared ZnO nanoparticles were calculated using Scherer equation, and the results showed that the average crystallite size and average particle size of all photo catalysts were ranging from 27.0 to 48.1 nm and 66.72 nm according to XRD.

9- The amount of catalyst dose and the optimal value of 0.13 g /100 ml of ZnO nanoparticles in the photocatalytic degradation of AYG dye were determined. The effect of dye concentration has been studied the optimum value = 10 ppm for AYG dye. Photocatalytic degradation reduces as the dye concentration rises because the concentration of OH adsorbed on the catalyst surface decreases. As the light intensity grows, the photocatalytic destruction of dye speeds up. The photocatalytic degradation of AYG dye was a 92.43% percent efficiency. Using Eyring equation thermodynamic parameters (ΔH°, ΔS°) for AYG dye were calculated (ΔH°＝32.52 kJ/mol and (ΔS°＝－0.166k J/ mol.k) respectively, from the results the reaction is endothermic with low randomness. (ΔG° =81.98 kJ/mol) was calculated and the reaction is non-spontaneous.

3.8 Future work:

1- Conducting more experimental studies by using the adsorbent surface to remove other pollutants such as heavy elements, organic and biological pollutants.

2- The possibility of applying the prepared surface to drug adsorption.

3- Preparation of other oxides such as Titanium dioxide and its composite with ZnO.

4- Improving the properties of synthesized nanoparticals and developing new methods to increase the yields of these materials.

5- Testing the new and modern applications of nanoparticals in various fields .

6- Modification of the prepared surface by using different starting weights of all its components.

7- Conducting further theoretical studies of new compounds.

8- Using these ligands and their complexes in evaluation the iological activity with different microbial organisms.

9- Study the cytotoxic effect of the ligands and their metal complexes on othercancer cell lines. Modification the surface of zinc oxide with Au nanoparticle.

10- Study the biological activity of the prepared nanocomposites.

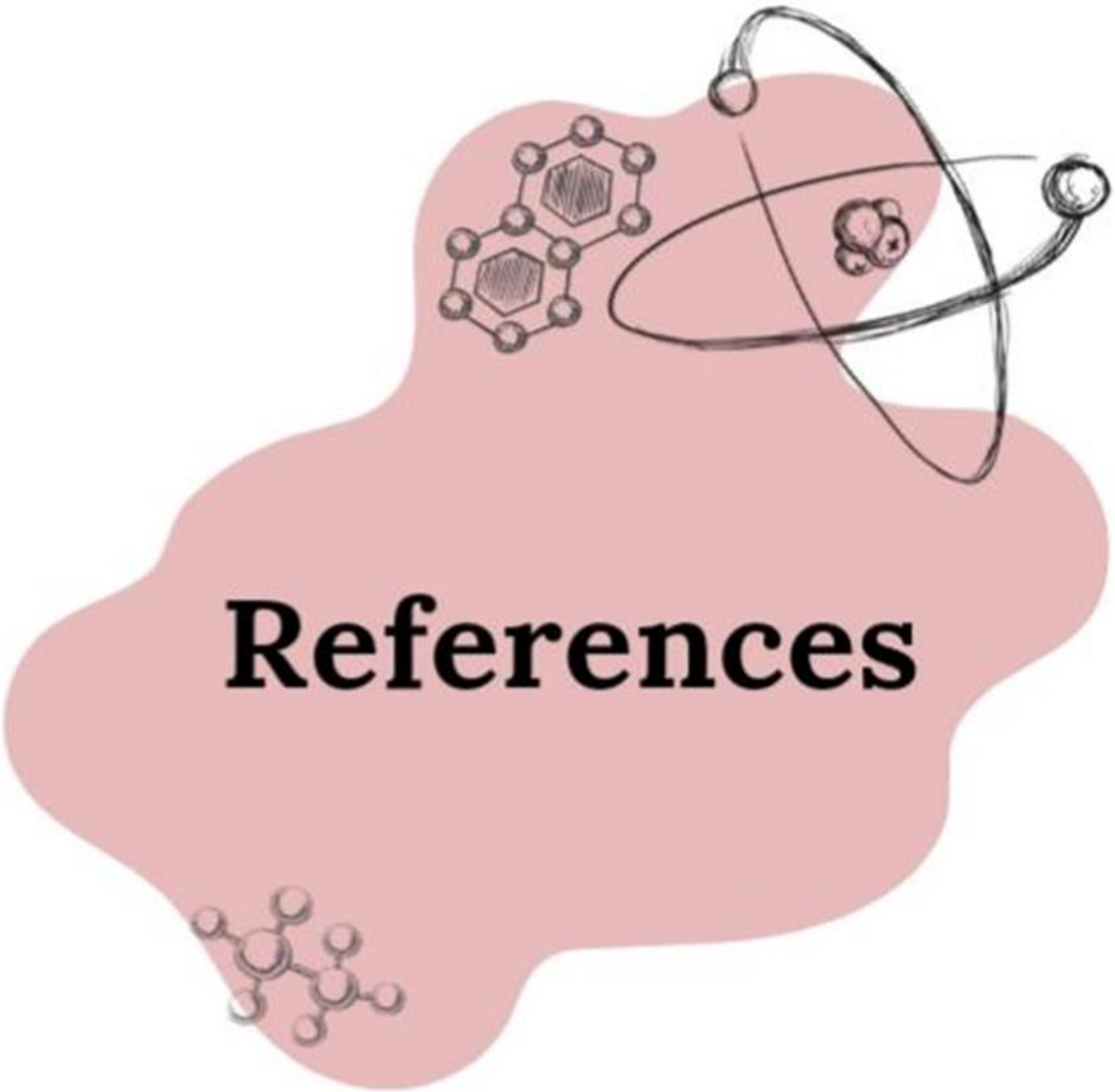

References

References

1. Pillai, G. and M.L. Ceballos-Coronel, *Science and technology of the emerging nanomedicines in cancer therapy: A primer for physicians and pharmacists.* SAGE open medicine, 2013. **1**: p. 2050312113513759.
2. Gopalan, S., S. Kumar, and K.J. Yarema, *Dendrimers in cancer treatment and diagnosis. Nanotechnologies for the Life sciences.* Nanomaterials for Cancer Diagnosis. KGaA, Weinheim. WILEY-VCH Verlag GmbH and Co, 2007: p. 1-33.
3. Rana, Muhammad Z Mehmood, Mazhar Ahmad, Jamil Aslam, Hasanain, Syed K Hameed,and Sohail *Synthesis of nickel nanoparticles in silica by alcogel electrolysis.* Journal of Nanoparticle Research, 2011. **13**(1): p. 375-384.
4. Boverhof, Darrell R Bramante, Christina M Butala, John H Clancy, Shaun F Lafranconi, Mark West, Jay Gordon, and Steve C, *omparative assessment of nanomaterial definitions and safety evaluation considerations.* Regulatory Toxicology and Pharmacology, 2015. **73**(1): p. 137-150.
5. Jeevanandam, Jaison Barhoum, Ahmed Chan, Yen S Dufresne, Alain Danquah, Michael K, *eview on nanoparticles and nanostructured materials: history, sources, toxicity and regulations.* Beilstein journal of nanotechnology, 2018. **9**(1): p. 1050-1074.
6. Koo, J.H., *Fundamentals, properties, and applications of polymer nanocomposites*. 2016: Cambridge University Press.
7. Iravani, S., *Green synthesis of metal nanoparticles using plants.* Green Chemistry, 2011. **13**(10): p. 2638-2650.
8. Cerjak, H., *Book note: introductions to nanoparticles and nanomaterials*. 2014, MANEY PUBLISHING STE 1C, JOSEPHS WELL, HANOVER WALK, LEEDS LS3 1AB, W YORKS ….
9. Gogotsi, Y., *Nanomaterials handbook*. 2006: CRC press.
10. Ealia, S.A.M. and M. Saravanakumar. *A review on the classification, characterisation, synthesis of nanoparticles and their*

application. in *IOP Conference Series: Materials Science and Engineering*. 2017. IOP Publishing.

11. Kumar, S., P. Bhushan, and S. Bhattacharya, *Fabrication of nanostructures with bottom-up approach and their utility in diagnostics, therapeutics, and others*, in *Environmental, chemical and medical sensors*. 2018, Springer. p. 167-198.
12. Gleiter, H., *Nanostructured materials: basic concepts and microstructure.* Acta materialia, 2000. **48**(1): p. 1-29.
13. Tiwari, J.N., R.N. Tiwari, and K.S. Kim, *Zero-dimensional, one-dimensional, two-dimensional and three-dimensional nanostructured materials for advanced electrochemical energy devices.* Progress in Materials Science, 2012. **57**(4): p. 724-803.
14. Pokropivny, V. and V. Skorokhod, *Classification of nanostructures by dimensionality and concept of surface forms engineering in nanomaterial science.* Materials Science and Engineering: C, 2007. **27**(5-8): p. 990-993.
15. Krishnan, J. and S. Shukla, *The behaviour of soil stabilised with nanoparticles: an extensive review of the present status and its applications.* Arabian Journal of Geosciences, 2019. **12**(14): p. 1-25.
16. Zhang, Lei Wang, Lin Jiang, Zhiyuan Xie, and Zhaoxiong, *Synthesis of size-controlled monodisperse Pd nanoparticles via a non-aqueous seed-mediated growth.* Nanoscale research letters, 2012. 7(1): p. 1-6. 17. Li, C., J. Adamcik, and R. Mezzenga, *Biodegradable nanocomposites of amyloid fibrils and graphene with shape-memory and enzyme-sensing properties.* Nature Nanotechnology, 2012. **7**(7): p. 421-427.

18. Zhang, J., M.R. Langille, and C.A. Mirkin, *Synthesis of silver nanorods by low energy excitation of spherical plasmonic seeds.* Nano letters, 2011. **11**(6): p. 2495-2498.

19. Badrossamay, M. and H. McIlwee, *J. Goss A. and KK Parker.* Nano Lett, 2010. **10**: p. 2257-2261.

20. Zhou, Jun Ding, Yong Deng, Shao Z Gong, Li Xu, Ning S and Wang, Zhong L., *Three‐dimensional tungsten oxide nanowire networks.* Advanced Materials, 2005. **17**(17): p. 2107-2110.

21. Pal, Sovan Lal Jana, Utpal Manna, Prabal Kumar Mohanta, Guru Prasad and Manavalan, R., *Nanoparticle: An overview of preparation and characterization.* Journal of applied pharmaceutical science, 2011(Issue): p. 228-234.

22. Amna Sirelkhatim, Shahrom Mahmud , Azman Seeni, Noor Haida Mohamad Kaus, Ling Chuo Ann, Siti Khadijah Mohd Bakhori ,Habsah Hasan ,and Dasmawati Mohamad, *"Review on zinc oxide nanoparticles: antibacterial activity and toxicity mechanism"*. Nano-Micro Letters, 2015. **7**(3): p. 219-242.

23. Noor Alhuda Rasool Makki, A.F.A., *A comparative studying of morphological and photocatalytic activity of synthesized ZnO nanoparticles under different amount of oxalic acid*. 2021, Babylon university

24. Z. Song, T.A. Kelf, W.H. Sanchez, M.S. Roberts, J. Ricˇka, M. Frenz, A.V. Zvyagin, *"Characterization of optical properties of ZnO nanoparticles for quantitative imaging of transdermal transport"*. Biomedical optics express, 2011. **2**(12): p. 3321-3333.

25. Svetozar Music´ ,Đurdica Dragcevi,and Stanko Popovic, *"Influence of synthesis route on the formation of ZnO particles and their morphologies"*. Journal of Alloys and Compounds, 2007. **429**(1): p. 242-249.

26. N. Yahya, H. Daud, N.A. Tajuddin, H.M. Daud, A. Shafie,and P. Puspitasari. *"Application of ZnO nanoparticles EM wave detector prepared by sol-gel and self-combustion techniques"*. in *Journal of Nano Research*. 2010. Trans Tech Publ.

27. G. Amin, M. H. Asif, A. Zainelabdin, S. Zaman, O. Nur, and M.Willander, *"Influence of pH, precursor concentration, growth time, and temperature on the morphology of ZnO nanostructures grown by the hydrothermal method"*. Journal of Nanomaterials, 2011. **2011**: p. 5.

28. A. B. M. A. Ashrafi, A. Ueta, A. Avramescu, H. Kumano, I. Suemune, Y. W. Ok, and T. Y. Seong, *"Growth and characterization of hypothetical zinc-blende ZnO films on GaAs (001) substrates with ZnS buffer layers"*. Applied Physics Letters, 2000. **76**(5): p. 550-552.

29. N. Rajeswari Yogamalar, and A. Chandra Bose, *"Synthesis, Dopant study and device fabrication of zinc oxide nanostructures: mini review"*. Prog Nanotechnol Nanomater, 2013. **2**(1): p. 1-20.

30. Archana Tiwari, *"Growth of ZnO Nanowire and Its Application as UV Photodetector"*. 2014 Astronomy National Institute of Technology

31. Aggarwal, Nupur Vasishth, Ajay Singh, Bikramjit Singh, and Bhupinderpal, *Investigation of room temperature ferromagnetic behaviour in dilute magnetic oxides.* 2018. **186**(1): p. 10-16.

32. Ü. Özgür, Y.I.A., C. Liu, A. Teke, M. A. Reshchikov, S. Doğan, V. Avrutin, S.-J. Cho, and H. Morkoç, *"A comprehensive review of ZnO materials and devices"*. Journal of applied physics, 2005. **98**(4): p. 041301.

33. C. Jagadish, and S. J. Pearton, , *"Zinc Oxide Bulk, Thin Films and Nanostructures Processing, Properties and Application"*. 2011: Edition Elsevier.

34. Gautam Sheel Thool, Ajaya Kumar Singh, R.S. Singh, Ashish Gupta,Md. Abu Bin Hasan Susan, *"Facile synthesis of flat crystal ZnO thin films by solution growth method: A micro-structural investigation"*. Journal of Saudi Chemical Society, 2014. **18**(5): p. 712-721.

35. G.Y.Mustafa, *photocatalytic degradation of organic contaminants in the presence of Graphite-Supported and Unsupported ZnO Modified with CdS particles.* 2009(17-19).

36. T.P. De Graaf, E.G., K.E. Butcher, *Use of an antimicrobial agent,*. European Patent EP1079799, 1999.

37. Yadav. A, P.V., Kathe. A.A, Raj. S, Yadav. D, Sundaramoorthy. C, Vigneshwaran. N, *Functional finishing in cotton fabrics using zinc oxide nanoparticles.* Bulletin of Materials Science, 2006. **29**: p. 641-645.

38. Bakin. A, E.-S.A., Mofor. A Che, Al-Suleiman. M, Schlenker. E, and Waag. A,, *"ZnMgO-ZnO quantum wells embedded in ZnO nanopillars: Towards realisation of nano-LEDs"*. physica status solidi (c), 2007. **4**(1): p. 158-161.

39. A.A. Khodja, T.S., J.F. Pilichowski, P. Boule,, *Photocatalytic degradation of 2-phenylphenol on TiO2 and ZnO in aqueous suspensions.* J. Photochem. Photobiol. A: Chem., 2001. **141**(231-239).

40. S. Sakthivel, B.N., M.V. Shankar, B. Arabindoo, M. Palanichamy, V. Murugesan,, *Solar photocatalytic degradation of azo dye: comparison of photocatalytic efficiency of ZnO and TiO2.* Sol. Energ. Mater. Sol. Cells, 2003. **77**(65-82).

41. S. Sharma, A.T., O. Nalamasu, P. Dutta, J. Electron, *Mater. 35.* 2006.
42. N.E. Danjushevskaya, O.V.A., B.G. Pogostkina, V.M. Kovalenko, Z.A. Mironova, Process for producing zinc phosphate, U.S. Patent 4207301 (1980).
43. Sillanpää, K.P.a.M., *Heterogeneous water phase catalysis as an environmental application: a review.* Chemosphere, 2002. **48**(1047-60).
44. Bhatkhande, D.S., V.G. Pangarkar, and A.A.C.M. Beenackers, *Photocatalytic degradation for environmental applications–a review.* Journal of Chemical Technology & Biotechnology: International Research in Process, Environmental & Clean Technology, 2002. **77**(1): p. 102-116.
45. Barelko, Y.M.-M.a.V., *Cloth catalysts for water denitrification: II. Removal of nitrates using Pd–Cu supported on glass fibers.* Applied Catalysis B: Environmental, 2001. **31**: p. 233-240.
46. Y. Peter, and Y. Cardona, *"Fundamentals of Semiconductors: Physics and Materials Properties"*. 2010: Springer Science & Business Media.
47. M. A. Fox, and M. T. Dulay *"Heterogeneous Photocatalysis"*. Chem. Rev, 1993. **93**(1): p. 341-357.
48. P. W. Atkins, *"Physical chemistry"*. 2002, Oxford University presses Oxford.
49. Kumar, D., P. Kuchhal, and K.S. Parmar, *Optimization of photovoltaic conversion performance of a TiO2 based dye sensitized solar cells (DSSCs).* Engineering Research Express, 2021. **3**(4): p. 045021.
50. Keith Leaver *"Energy Bands and Carrier Statistics"*, in *Microelectronic Devices*. 1997, World Scientific. p. 32-59.

51. Leaver, K., *Microelectronic devices*. 1997: World Scientific.
52. Nigam, P., et al., *Microbial process for the decolorization of textile effluent containing azo, diazo and reactive dyes.* Process biochemistry, 1996. **31**(5): p. 435-442.
53. Morkoç, H. and Ü. Özgür, *Zinc oxide: fundamentals, materials and device technology*. 2008: John Wiley & Sons.
54. Fox, M.A. and M.T. Dulay, *Heterogeneous photocatalysis.* Chemical reviews, 1993. **93**(1): p. 341-357.
55. Al-Nour, G., *Photocatalytic degradation of organic contaminants in the presence of graphite-supported and unsupported ZnO modified with CdS particles*. 2009, National University San Diego.
56. Olatunde, O.C., A.T. Kuvarega, and D.C. Onwudiwe, *Photo enhanced degradation of contaminants of emerging concern in waste water.* Emerging Contaminants, 2020. **6**: p. 283-302.
57. Oh, W.-D., Z. Dong, and T.-T. Lim, *Generation of sulfate radical through heterogeneous catalysis for organic contaminants removal: current development, challenges and prospects.* Applied Catalysis B: Environmental, 2016. **194**: p. 169-201.
58. Bartolomeu, Maria Neves, MGPMS Faustino and , MAF Almeida, A., *Wastewater chemical contaminants: Remediation by advanced oxidation processes.* Photochemical & Photobiological Sciences, 2018. **17**(11): p. 1573-1598.
59. Saravanan, R., F. Gracia, and A. Stephen, *Basic principles, mechanism, and challenges of photocatalysis*, in *Nanocomposites for visible light-induced photocatalysis*. 2017, Springer. p. 19-40.
60. Qi, K., et al., *Review on the improvement of the photocatalytic and antibacterial activities of ZnO.* Journal of Alloys and Compounds, 2017. **727**: p. 792-820.
61. Karthikeyan, C Arunachalam, Prabhakarn Ramachandran,

Kaliappan Al-Mayouf, Abdullah M and Karuppuchamy, S, *Recent advances in semiconductor metal oxides with enhanced methods for solar photocatalytic applications.* Journal of Alloys and Compounds, 2020. **828**: p. 154281.

62. Rajamanickam, D. and M. Shanthi, *Photocatalytic degradation of an organic pollutant by zinc oxide–solar process.* Arabian Journal of Chemistry, 2016. **9**: p. S1858-S1868.
63. Noorimotlagh, Zahra Kazeminezhad, Iraj Jaafarzadeh, Neemat Ahmadi, Mehdi Ramezani, Zahra Martinez, and Susana Silva, *The visible-light photodegradation of nonylphenol in the presence of carbon-doped TiO2 with rutile/anatase ratio coated on GAC: Effect of parameters and degradation mechanism.* Journal of hazardous materials, 2018. **350**: p. 108-120.
64. Anjali, R. and S. Shanthakumar, *Insights on the current status of occurrence and removal of antibiotics in wastewater by advanced oxidation processes.* Journal of environmental management, 2019. **246**: p. 51-62.
65. Deng, Y. and R. Zhao, *Advanced oxidation processes (AOPs) in wastewater treatment.* Current Pollution Reports, 2015. **1**(3): p. 167-176.
66. Vogelpohl, A. and S.-M. Kim, *Advanced oxidation processes (AOPs) in wastewater treatment.* Journal of Industrial and Engineering Chemistry, 2004. **10**(1): p. 33-40.
67. Zahoor, Mehvish Arshad, Amara Khan, Yaqoob Iqbal, Mazhar Bajwa, Sadia Zafar Soomro, Razium Ali Ahmad, Ishaq Butt, Faheem K Iqbal, M Zubair Wu, and Aiguo., *Enhanced photocatalytic performance of CeO2–TiO2 nanocomposite for degradation of crystal violet dye and industrial waste effluent.* Applied Nanoscience, 2018. **8**(5): p. 1091-1099.

68. Amor, Carlos Marchão, Leonilde Lucas, Marco S Peres, and José A, *Application of advanced oxidation processes for the treatment of recalcitrant agro-industrial wastewater: A review*. Water, 2019. **11**(2): p. 205.

69. Xin, Z. and L. Rehmann, *Application of Advanced Oxidation Process in the Food Industry*. Advanced Oxidation Processes, 2020: p. 101.

70. Jirat, Jiri Cech, Petr Znamenacek, Jiri Simek, Miroslav Skuta,Ctibor Vanek, Tomas Dibuszová, Eva Nic, Miloslav Svozil, and Daniel, *Developing and Implementing a Combined Chemistry and Informatics Curriculum for Undergraduate and Graduate Students in the Czech Republic*. Journal of Chemical Education, 2013. **90**(3): p. 315-319.

71. Naumov, Roman N Itazaki, Masumi Kamitani, Masahiro Nakazawa, and Hiroshi., *Selective Dehydrogenative Silylation–hydrogenation reaction of Divinyldisiloxane with Hydrosilane catalyzed by an Iron complex*. Journal of the American Chemical Society, 2012 . **134**(2): p. 804-807.

72. Pfennig, B.W., *Principles of inorganic chemistry*. 2021: John Wiley & Sons.

73. Crichton, R. and R. Louro, *Practical approaches to biological inorganic chemistry*. 2019: Elsevier.

74. Huheey, James E Keiter, Ellen A Keiter, Richard L Medhi, and Okhil K., *Inorganic chemistry: principles of structure and reactivity*. 2006: Pearson Education India.

75. Chao, JC Hong, A Okey, RW and Peters, RW. *Selection of chelating agents for remediation of radionuclide-contaminated soil*. in *Proceedings of the 1998 conference on hazardous waste research*. 1998.

76. Atkins, P. and T. Overton, *Shriver and Atkins' Inorganic Chemistry*. 2010: OUP Oxford.

77. Atkinson, G. and J. Bauman Jr, *The Chelate Effect Studied by Calorimetry, Potentiometry, and Electron Spin Resonance.* Inorganic Chemistry, 1963. **2**(1): p. 64-67.

78. DeStefano, N., D. Johnson, and L. Venanzi, *Square Planar Transition Metal Complexes with a Bidentate Ligand Spanning trans- Positions.* Angewandte Chemie International Edition in English, 1974. **13**(2): p. 133-134.

79. Dinku, Worku Megersa, Negussie Raju, VJT Solomon, Theodros Jönsson, and Jan Åke Retta, Negussie., *Studies of transition metal complexes of herbicidal compounds. I: Transition metal complexes of 2- methylthio-4-azido-6-isopropylamino-s-triazine (aziprotryn).* Bulletin of the Chemical Society of Ethiopia, 2001. **15**(1).

80. Catalano, Alessia Sinicropi, Maria Stefania Iacopetta, Domenico Ceramella, Jessica Mariconda, Annaluisa Rosano, Camillo Scali, Elisabetta Saturnino, Carmela Longo , and Pasquale., *A Review on the Advancements in the Field of Metal Complexes with Schiff Bases as Antiproliferative Agents.* Applied Sciences, 2021. **11**(13): p. 6027.

81. Shi, Mengyu Xu, Chen Yang, Zhihong Wang, Lei Tan, Shujuan Xu ,and Guoyue., *Tuning of reversible thermochromic properties of salicylaldehyde Schiff bases through the substitution of methoxy and nitro groups.* Journal of Molecular Structure, 2019. **1182**: p. 72-78.

82. Yamada, S., *Advancement in stereochemical aspects of Schiff base metal complexes.* Coordination Chemistry Reviews, 1999. **190**: p. 537-555.

83. Schiff, H., *Mittheilungen aus dem Universitätslaboratorium in Pisa: Untersuchungen ü das Chinolin.* Justus Liebigs Annalen der Chemie, 1864. **131**(1): p. 112-117.

84. Schiff, H., *Mittheilungen aus dem Universitätslaboratorium in Pisa: eine neue Reihe organischer Basen.* Justus Liebigs Annalen der Chemie, 1864. **131**(1): p. 118-119.

85. Karmakar, M. and S. Chattopadhyay, *A comprehensive overview of the orientation of tetradentate N2O2 donor Schiff base ligands in octahedral complexes of trivalent 3d metals.* Journal of Molecular Structure, 2019. **1186**: p. 155-186.

86. Alaghaz, ANMA Alturiqi, S Ammar, RA Zayed, and ME, *Synthesis, spectral characterization, docking analysis, DNA binding/cleavage, antimicrobial and cytotoxic activity of new dimeric antipyrine-Schiff base metal complexes.* Asian J. Chem, 2019. **31**: p. 199- 212.

87. Pratihar, Jahar Lal Mandal, Paritosh Lai, Chung Kung Chattopadhyay, and Surajit, *Tetradentate amido azo Schiff base Cu (II), Ni (II) and Pd (II) complexes: Synthesis, characterization, spectral properties, and applications to catalysis in C–C coupling and oxidation reaction.* Polyhedron, 2019. **161**: p. 317-324.

88. Mohamed, GG Mahmoud, WH Diab, MA El-Sonbati, AZ and Abbas, SY., *Synthesis, characterization, theoretical study and biological activity of Schiff base nanomaterial analogues.* Journal of Molecular Structure, 2019. **1181**: p. 645-659.

89. Ayaz, Furkan Gonul, Ilyas Demirbag, Burcu Ocakoglu and , Kasim., *Novel copper bearing schiff bases with photodynamic anti-inflammatory and anti-microbial activities.* Applied Biochemistry and Biotechnology, 2020. **191**(2): p. 716-727.

90. Chen, Shujiao Liu, Xicheng Ge, Xingxing Wang, Qinghui Xie, Yaoqi Hao, Yingying Zhang, Ying Zhang, Lei Shang, Wenjing Liu, and Zhe, *Lysosome-targeted iridium (III) compounds with pyridine- triphenylamine Schiff base ligands: Syntheses, antitumor applications and mechanisms.* Inorganic Chemistry Frontiers, 2020. **7**(1): p. 91-100.

91. Maryam, Maqsood Tan, Sang Loon Crouse, Karen Ann Tahir, Mohamed Ibrahim Mohamed CHEE, and HUI YEE, *Synthesis, characterization and evaluation of antidengue activity of enantiomeric Schiff bases derived from S-substituted dithiocarbazate.* Turkish Journal of Chemistry, 2020. **44**(5): p. 1395-1409.

92. Ashassi-Sorkhabi, H., A. Kazempour, and Z. Frouzat, *Superior potentials of hydrazone Schiff bases for efficient corrosion protection of mild steel in 1.0 M HCl.* Journal of Adhesion Science and Technology, 2021. **35**(2): p. 164-184.

93. Dharmaraj, N., P. Viswanathamurthi, and K. Natarajan, *Ruthenium (II) complexes containing bidentate Schiff bases and their antifungal activity.* Transition Metal Chemistry, 2001. **26**(1): p. 105-109.

94. Spinu, C. and A. Kriza, *Co (II), Ni (II) and Cu (II) complexes of bidentate Schiff bases.* Acta Chimica Slovenica, 2000. **47**(2): p. 179-186.

95. Lalehzari, A., J. Desper, and C.J. Levy, *Double-stranded monohelical complexes from an unsymmetrical chiral Schiff-base ligand.* Inorganic chemistry, 2008. **47**(3): p. 1120-1126.

96. Dehghani-Firouzabadi, A.A. and S. Firouzmandi, *Synthesis and characterization of a new unsymmetrical potentially pentadentate Schiff base ligand and related complexes with manganese (II),*

nickel (II), copper (II), zinc (II) and cadmium (II). Journal of the Brazilian Chemical Society, 2017. **28**: p. 768-774.

97. Tang, A.Y., C.K. Lo, and C.w.J.C.T. Kan, *Textile dyes and human health: A systematic and citation network analysis review.* 2018. **134**(4): p. 245-257.
98. Benkhaya, S., S. M'rabet, and A.J.H. El Harfi, *Classifications, properties, recent synthesis and applications of azo dyes.* 2020. **6**(1): p. e03271.
99. Yazdani, M.R., *Engineered adsorptive materials for water remediation-Development, characterization, and application.* 2018.
100. Masoud, M.S., R.M. Elsamra, and S.S. Hemdan, *Solvent, substituents and pH effects towards the spectral shifts of some highly colored indicators*. Journal of the Serbian Chemical Society, 2017. **82**(7-8): p. 851-864.
101. Ebenso, EE Alemu, Hailemichael Umoren, SA and Obot, IB., *Inhibition of mild steel corrosion in sulphuric acid using alizarin yellow GG dye and synergistic iodide additive.* Int. J. Electrochem. Sci, 2008. **3**(12): p. 1325-1339.
102. Krithiga, Thangavelu Salla, Sunitha Jayabalan, Karthikeyan Kumar, and Jagadeesan A, *One-pot Synthesis of β-acetamido-β-(phenyl) Propiophenone using ZnO/Carbon Nanocomposites.* Combinatorial Chemistry & High Throughput Screening, 2021. **24**(2): p. 213-219.
103. Ramamoorthy, S Das, S Balan, R and Lekshmi, IC, *TiO2-ZrO2 nanocomposite with tetragonal zirconia phase and photocatalytic degradation of Alizarin Yellow GG azo dye under natural sunlight.* Materials Today: Proceedings, 2021. **47**: p. 4641-4646.
104. Tiwari, Diwakar Lalhriatpuia, C Lee, Seung-Mok Kong, and Sung-Ho, *Efficient application of nano-TiO2 thin films in the photocatalytic removal of Alizarin Yellow from aqueous solutions.*

Applied Surface Science, 2015. **353**: p. 275-283.

105. Islam, Muhammad Amirul Siddiquey, Iqbal Ahmed Khan, Md Azizur Rahman Alam, Md ahbubul Islam, Saiful SM Hasnat, and Mohammad A, *Adsorption and UV-visible light induced degradation of methylene blue over ZnO nano-particles.* International Journal of Chemical Reactor Engineering, 2011. **9**(1).

106. Joshi, K. and V. Shrivastava, *Removal of methylene blue dye aqueous solution using photo catalysis.* 2012.

107. Saravanan, R Thirumal, E Gupta, VK Narayanan, V Stephen, and AJJOML., *The photocatalytic activity of ZnO prepared by simple thermal decomposition method at various temperatures.* Journal of Molecular Liquids, 2013. **177**: p. 394-401.

108. Miao, Jing Jia, Zhe Lu, Hai-Bo Habibi, Daryoush Zhang, and Lai-Chang, *Heterogeneous photocatalytic degradation of mordant black 11 with ZnO nanoparticles under UV–Vis light.* Journal of the Taiwan Institute of Chemical Engineers, 2014. **45**(4): p. 1636-1641.

109. Bijanzad, K., A. Tadjarodi, and O. Akhavan, *Photocatalytic activity of mesoporous microbricks of ZnO nanoparticles prepared by the thermal decomposition of bis (2-aminonicotinato) zinc (II).* Chinese Journal of Catalysis, 2015. **36**(5): p. 742-749.

110. Sood, S., A. Kumar, and N. Sharma, *Photocatalytic and antibacterial activity studies of ZnO nanoparticles synthesized by thermal decomposition of mechanochemically processed oxalate precursor*. ChemistrySelect, 2016. **1**(21): p. 6925-6932.

111. Barfeie, Hamide Grivani, Gholamhossein Eigner, Vaclav Dusek, Michal Khalaji, and Aliakbar Dehno, *Copper(II), nickel(II),zinc(II) and vanadium(IV) Schiff base complexes: Synthesis, characterization, crystal structure determination, and thermal studies.* Polyhedron, 2018. **146**: p. 19-25.

112. Kanagamani, Krishnaswamy Muthukrishnan, Pitchaipillai Saravanakumar, Karunamoorthy Shankar, Karikalan Kathiresan , and Ayyasami, *Photocatalytic degradation of environmental perilous gentian violet dye using leucaena-mediated zinc oxide nanoparticle and its anticancer activity.* Rare metals, 2019. **38**(4): p. 277-286.

113. Abass, Suhad Kareem Al-Hilfi, Jassim Abbas Abbas, Sawsan Khudhair Ahmed, and Luma Majeed, *reparation, Characterization and Study of the Photodecolorization of Mixed-Ligand Binuclear Co (II) Complex of Schiff Base by ZnO.* Indonesian Journal of Chemistry, 2020. **20**(2): p. 404-412.

114. Katouah, H.A., *Facile synthesis of Co3O4 and ZnO nanoparticles by thermal decomposition of novel Co (II) and Zn (II) Schiff base complexes for studying their biological properties and photocatalytic degradation of crystal violet dye.* Journal of Molecular Structure, 2021. **1241**: p. 130676.

115. Al-Wasidi, Asma S AlZahrani, Ibtisam IS Thawibaraka, Hotoun I Naglah, and Ahmed M., *Facile synthesis of ZnO and Co3O4 nanoparticles by thermal decomposition of novel Schiff base complexes: Studying biological and catalytic properties.* Arabian Journal of Chemistry, 2022. **15**(2): p. 103628.

116. Vaz, Patricia AAM Rocha, Joao Silva, Artur MS Guieu, and Samuel., *Aggregation-induced emission enhancement of chiral boranils.* New Journal of Chemistry, 2018. **42**(22): p. 18166-18171.

117. Alothman, A.A. and M.D. Albaqami, *Nano- sized Cu (II) and Zn (II) complexes and their use as a precursor for synthesis of CuO and ZnO nanoparticles: A study on their sonochemical synthesis, characterization, and DNA- binding/cleavage, anticancer, and*

antimicrobial activities. Applied Organometallic Chemistry, 2020. **34**(10): p. e5827.

118. Anacona, and J.R, *Synthesis and characterization of transition metal complexes with a Schiff base derived from cephalexin and 1,2–diaminobenzene. antibacterial activity.* Inorganic and Nano-Metal Chemistry, 2018. **48**(8): p. 404-411.
119. Takahashi, Yusuke Kubuki, Shiro Akiyama, Kazuhiko Sinkó, Katalin Kuzmann, Ernő Homonnay, Zoltán Ristić, Mira Nishida, and Tetsuaki., *Visible light activated photo-catalytic effect and local structure of iron silicate glass prepared by sol-gel method.* Hyperfine Interactions, 2014. **226**(1): p. 747-753.
120. Cai, Fan Yang, Lefu Shan, Shiyao Mott, Derrick Chen, Bing H Luo, Jin Zhong, and Chuan-Jian, *Preparation of PdCu alloy nanocatalysts for nitrate hydrogenation and carbon monoxide oxidation.* Catalysts, 2016. **6**(7): p. 96.
121. Kausar, Abida Iqbal, Munawar Javed, Anum Aftab, Kiran Bhatti, Haq Nawaz Nouren, and Shazia, *Dyes adsorption using clay and modified clay: a review.* Journal of Molecular Liquids, 2018. **256**: p. 395- 407.
122. Olajire, A. and A. Olajide, *Kinetic study of decolorization of methylene blue with sodium sulphite in aqueous media: influence of transition metal ions.* 2014.
123. Maderova, Z Baldikova, E Pospiskova, K Safarik, I and Safarikova, M, *Removal of dyes by adsorption on magnetically modified activated sludge.* International journal of Environmental science and technology, 2016. **13**(7): p. 1653-1664.
124. Fu, Jianwei Chen, Zhonghui Wang, Minghuan Liu, Shujun Zhang, Jinghui Zhang, Jianan Han, Runping Xu, and Qun, *Adsorption of*

methylene blue by a high-efficiency adsorbent (polydopamine microspheres): kinetics, isotherm, thermodynamics and mechanism analysis. Chemical Engineering Journal, 2015. **259**: p. 53-61.

125. Abdallah, Sayed M Mohamed, Gehad G Zayed, MA Abou El-Ela , and Mohsen S, *Spectroscopic study of molecular structures of novel Schiff base derived from o-phthaldehyde and 2-aminophenol and its coordination compounds together with their biological activity*. Spectrochimica Acta Part A: Molecular and Biomolecular Spectroscopy, 2009. **73**(5): p. 833-840.
126. Pavia, Donald L Lampman, Gary M Kriz, George S Vyvyan, and James A, *Introduction to spectroscopy*. 2014: Cengage learning.
127. Abdallah, Sayed M Mohamed, Gehad G Zayed, MA Abou El-Ela, and Mohsen S, *Spectroscopic study of molecular structures of novel Schiff base derived from o-phthaldehyde and 2-aminophenol and its coordination compounds together with their biological activity*. 2009. **73**(5): p. 833-840.
128. Khosravi, Iman Hosseini, Farnaz Khorshidifard, Mahsa Sahihi, Mehdi Rudbari, and Hadi Amiri, *ynthesis, characterization, crystal structure and HSA binding of two new N, O, O-donor Schiff-base ligands derived from dihydroxybenzaldehyde and tert-butylamine*. 2016. **1119**: p. 373-384.
129. González-García, Cristina Mata, Alejandro Zani, Franca Mendiola, M Antonia López-Torres, and lena, *Synthesis and antimicrobial activity of tetradentate ligands bearing hydrazone and/or thiosemicarbazone motifs and their diorganotin (IV) complexes.* Journal of inorganic biochemistry, 2016. **163**: p. 118-130.
130. Abdulghani, A.J., A.M.N.J.B.c. Khaleel, and applications, *Preparation and characterization of Di-, Tri-, and tetranuclear*

Schiff base complexes derived from diamines and 3, 4-dihydroxybenzaldehyde. 2013. **2013**.

131. Nakamoto, K., *Infrared and Raman spectra of inorganic and coordination compounds, part B: applications in coordination, organometallic, and bioinorganic chemistry*. 2009: John Wiley & Sons.
132. Silverstein, R.M. and G.C. Bassler, *Spectrometric identification of organic compounds.* Journal of Chemical Education, 1962. **39**(11): p. 546.
133. Ferahtia, A., *See discussions, stats, and author profiles for this publication. researchgate. net/publication/350567414 SURFACE WATER QUALITY ASSESSMENT IN SEMI-ARID REGION (EL HODNA WATERSHED, ALGERIA) BASED ON WATER QUALITY INDEX (WQI).* 2021.
134. Yin, C.-M.L., Zi-Ru Kong, Yang-Hui Wu, Cheng-Yun Ren, De-Hou Lü, Yu-Gang Xue, Hong-Fu, *Studies on the thermal behaviour and decomposition mechanism of complexes of rare earth (III) nitrates with 18-crown-6.* Thermochimica acta, 1992. **204**(2): p. 251-260.
135. Abdel-Latif, S., H. Hassib, and Y. Issa, *Studies on some salicylaldehyde Schiff base derivatives and their complexes with Cr (III), Mn (II), Fe (III), Ni (II) and Cu (II).* Spectrochimica Acta Part A: Molecular and Biomolecular Spectroscopy, 2007. **67**(3-4): p. 950-957.
136. Macdonald, A. and P. Sirichanya, *The determination of metals in organic compounds by oxygen-flask combustion or wet combustion.* Microchemical Journal, 1969. **14**(2): p. 199-206.
137. Nath, M. and P. Arora, *Spectral and thermal studies of cobalt (II), nickel (II) and copper (II) complexes of Schiff bases obtained from*

o-hydroxyacetophenone and amino acids. Synthesis and Reactivity in Inorganic and Metal-Organic Chemistry, 1993. **23**(9): p. 1523-1546.

138. Bragg, W.H. and W.L. Bragg, *The reflection of X-rays by crystals.* Proceedings of the Royal Society of London. Series A, Containing Papers of a Mathematical and Physical Character, 1913. **88**(605): p. 428-438.
139. Kang, Jihye Yun, Jaeyong Oh, Yoo-Young Kim, Sung-Jin Kamiko, Masao Kim, Nam-Hoon Koh,and Jung-Hyuk, *Defects controlled stress engineering in Al-doped ZnO transparent multilayered thin films.* Journal of the Korean Ceramic Society, 2022.
140. Zhou, Jianguo Zhao, Fengying Wang, Yingling Zhang, Yan Yang, and Lin, *Size-controlled synthesis of ZnO nanoparticles and their photoluminescence properties.* Journal of luminescence, 2007. **122**: p. 195-197.
141. Khoshhesab, Z.M., M. Sarfaraz, and M.A. Asadabad, *Preparation of ZnO nanostructures by chemical precipitation method.* Synthesis and Reactivity in Inorganic, Metal-Organic, and Nano-Metal Chemistry, 2011. **41**(7): p. 814-819.
142. JCPDS, P.D.F., *Alphabetical Index.* Inorganic Compounds, International Centre for Diffraction Data, Newtown Square, Pa, USA, 1977.
143. Cullity, B., *Elements of X-ray Diffraction, Adison–Wesley Publ.* Co., London, 1967.
144. Geetha, MS Nagabhushana, H and Shivananjaiah, HN, *Green mediated synthesis and characterization of ZnO nanoparticles using Euphorbia Jatropa latex as reducing agent.* 2016. **1**(3): p. 301-310.

145. Talam, S., S.R. Karumuri, and N. Gunnam, *Synthesis, characterization, and spectroscopic properties of ZnO nanoparticles.* International Scholarly Research Notices, 2012. **2012**.

146. Sales Amalraj, A., S. Christina Joycee, and G. Natarajan, *Investigation of the properties of tungsten doped ZnO thin films synthesised by SILAR method.* Materials Research Innovations, 2021: p. 1-7.

147. Ismail, MA Taha, KK Modwi, A and Khezami, L, *ZnO nanoparticles: Surface and X-ray profile analysis.* 2018. **14**: p. 381-393.

148. Varadavenkatesan, T., et al., *Photocatalytic degradation of Rhodamine B by zinc oxide nanoparticles synthesized using the leaf extract of Cyanometra ramiflora.* 2019. **199**: p. 111621.

149. Rahman, R.O.A., A.M. El-Kamash, and Y.-T. Hung, *Applications of Nano-Zeolite in Wastewater Treatment: An Overview.* Water, 2022. **14**(2): p. 137.

150. Siong, Valerie Ling Er Lee, Kian Mun Juan, Joon Ching Lai, Chin Wei Tai, Xin Hong Khe, and Cheng Seong, *Removal of methylene blue dye by solvothermally reduced graphene oxide: a metal-free adsorption and photodegradation method.* RSC advances, 2019. **9**(64): p. 37686- 37695.

151. Kansal, Sushil Kumar Lamba, Randeep Mehta, SK Umar, and Ahmad., *Photocatalytic degradation of Alizarin Red S using simply synthesized ZnO nanoparticles.* Materials letters, 2013. **106**: p. 385-389.

152. Hu, Q. and B. Liu, *Zhang z, Song M, Zhao X. Temperature effect on the photocatalytic degradation of methyl orange under UV-vis light*

irradiation. Journal of Wuhan University of Technology-Mater Sci Ed, 2010. **25**(2): p. 210-3.

153. Al-Mamun, Md Rashid Islam, Md Shofikul Hossain, Md Rasel Kader, Shahina Islam, Md hahinoor Khan, and Md Zaved Hossain, *A novel and highly efficient Ag and GO co-synthesized ZnO nano photocatalyst for methylene blue dye degradation under UV irradiation.*Environmental Nanotechnology, Monitoring & Management, 2021. **16**: p. 100495.
154. Kurniawan, Tonni Agustiono Mengting, Zhu Fu, Dun Yeap, Swee Keong Othman, Mohd Hafiz Dzarfan Avtar, Ram Ouyang, and Tong, *Functionalizing TiO2 with graphene oxide for enhancing photocatalytic degradation of methylene blue (MB) in contaminated wastewater*. Journal of environmental management, 2020. **270**: p. 110871.
155. Hayat, Khizar Gondal, Mohammed A Khaled, Mazen M Ahmed, and Shakeel., *Kinetic study of laser-induced photocatalytic degradationof dye (alizarin yellow) from wastewater using nanostructured ZnO*. Journal of Environmental Science and Health Part A, 2010. **45**(11): p. 1413-1420.
156. Meetani, MA Rauf, MA Hisaindee, S Khaleel, A AlZamly, A and Ahmad, A, *Mechanistic studies of photoinduced degradation of Orange G using LC/MS*. Rsc Advances, 2011. **1**(3): p. 490-497.
157. Madhavan, J., F. Grieser, and M. Ashokkumar, *Degradation of orange-G by advanced oxidation processes*. Ultrasonics sonochemistry, 2010. **17**(2): p. 338-343.
158. Aliouche, S., K. Djebbar, and T. Sehili, *Removal of an azo dye (Alizarin yellow) in homogeneous medium using direct photolysis, acetone/UV, H2O2/UV,/UV, H2O2//UV, and/heat*. Desalination and water treatment, 2016. **57**(39): p. 18182-18193.

159. Behnajady, M., N. Modirshahla, and R. Hamzavi, *Kinetic study on photocatalytic degradation of CI Acid Yellow 23 by ZnO photocatalyst.* Journal of hazardous materials, 2006. **133**(1-3): p. 226-232.

160. Daneshvar, N Rasoulifard, MH Khataee, AR and Hosseinzadeh, F, *Removal of CI Acid Orange 7 from aqueous solution by UV irradiation in the presence of ZnO nanopowder*. Journal of Hazardous Materials, 2007. **143**(1-2): p. 95-101.

161. Mohammad, Eman J Lafta, Abbas J Kahdem, Salih H and Alkaim, Ayad F, *Enhancement the photocatalytic activity of zinc oxide surface by combination with functionalized and non-functionalized activated carbon.* Int J ChemTech Res, 2016. **9**(12): p. 656.

162. Hu, X., X. Meng, and Z. Zhang, *Synthesis and characterization of graphene oxide-modified Bi2WO6 and its use as photocatalyst.* International Journal of Photoenergy, 2014. **2016**.

ISSN : 1411-9420 (print) / 2460-1578 (online)

Indonesian Journal of Chemistry

Accredited by RISTEK-BRIN No. 85/M/KPT/2020

Yogyakarta, July 10, 2022

To.
Ali Taleb Bader
Department of Chemistry, College of Sciences for Women, University of Babylon, Iraq.

ACCEPTANCE LETTER

We are glad to inform you that your article,
Entitle:

Synthesis and Characterization of ZnO Nanoparticles Via thermal decompation for Zn(II) Schiff base complex

written by:

Hadeer Mohammed Subhi, Ali Taleb Bader* and Hazim Yahya Al-Gubury,

has been reviewed and accepted in the Indonesian Journal of Chemistry (*Indones. J. Chem.*); and will be published in Vol. 22(5), the end of October 2022.

We highly appreciate your kind cooperation and contribution to the journal, and we are also looking forward to receiving your next qualified manuscript.

Best regards,

ISSN 1411 - 9420
Indones. J. Chem.
INDONESIAN JOURNAL OF CHEMISTRY

Prof. Dr. Nuryono, MS
Editor in Chief

الخلاصة :

يتضمن هذا العمل ثلاث اجزاء

الجزء الاول :

الليكاندان (بنزو امنيومثيل بنزين) الليكاند الاول والليكاند الثاني بنزو امنيو مثيل بنزين 1-4 ثنائي الهيدروكسيل حضرتا بواسطة تكاثف بنزيل امين مع الديهايد اروماتي : 2-هيدروكسي بنزلديهايد و 2-هديدروكسي 3-ميثوكسي بنزلديهايد على التوالي .اليكاندان المحضرة تم تشخيصها بواسطة استخدام تقنيات مختلفه مثل درجة الانصهار و تقنية الاشعة تحت الحمراء وطيف الاشعة فوق البنفسجية وطيف الرنين المغناطسي و التحليل الوزني الحراري.تم تحضير بعض المعقدات لهذه اليكاندات المحضرة بواسطة مفاعلتها خلات الخارصين ثنائية الماء مع اليكاندان بنسب مولية مختلفة (1:1) او (1:2) (فلز :ايكاند).تم تشخيص المعقدات الفلزية مثل مثل درجة الانصهار و تقنية الاشعة تحت الحمراء وطيف الاشعة فوق البنفسجية و التوصيلية المولارية و التحليل الوزني الحراري.

الجزء الثاني :

اوكسيد االزنك النانوي تم تحضيره بواسطة طريقة التكسير الحراري للمعقدات المحضرة من خلال حرقها بدرج حرارها 700 درجة مؤية . تم دراسة الخصائص لاوكسيد الخارصين النانوي للعينات المحضرة مثل بحيود الأشعة السينية (XRD) ، مجهر إلكتروني ماسح ومجهرية النفاذ الإلكتروني و مطيافية تشتت الطاقة بالأشعة السينية والتحليل الطيفي ومطيافية الانعكاس المنتشر.

من خلال النتائج المتحصلة من التقنيات المختلفه تم اقتراح اشكال المعقدات المحضرة فوجود انها جميعها رباعية السطوح .

الجزء الثالث:

تم فحص النشاط التحفيزي للهيكل النانوي لأكسيد الزنك (ZnO) باستخدام صبغة الأليزارين الصفراء كصبغة اختبار في محلول مائي تحت إشعاع الأشعة فوق البنفسجية.

كانت العوامل المدروسة هي التركيز الأولي لصبغة الإليزارين الصفراء ، وكمية المحفز ، ودرجة الحموضة الأولية للمحلول ، وشدة الضوء ، وبيروكسيد الهيدروجين ، ودرجة حرارة محلول الصبغة.

تمت دراسة تأثير التركيز الأولي لمحلول الصبغة وأظهرت النتائج أن معدل التفاعل ينخفض مع زيادة تركيز الصبغة وأن التفاعل هو تفاعل زائف من الدرجة الأولى. تم العثور على الجرعة المثلى للمحفز لتكون (0.13 جم / 100 مل) لهياكل نانوية أكسيد الزنك ((ZnOالمحضرة.

كشف التحقيق في تأثير الأس الهيدروجيني الأولي للصبغة أن الأس الهيدروجيني الأمثل للمحلول هو (8.75). أدت الزيادة في شدة الضوء إلى زيادة معدل التحلل التحفيزي الضوئي.

تم دراسة تأثير درجة الحرارة باستخدام معادلة أرهينيوس ، وأظهرت النتائج أن الزيادة في درجة الحرارة تترافق مع زيادة في معدل التفاعل. يشير إلى أن التحلل الضوئي لصبغة Light Green هو تفاعل ماص للحرارة.

تم حساب قيم الانتروبيا والمحتوى الحراري باستخدام معادلة .Eyring تم العثور على قيم الانتروبيا لتكون (0.166-) $kJ.mol^{-1}$ ، وأظهرت هذه النتائج انخفاض العشوائية. تم العثور على قيم المحتوى الحراري لتكون (32.52) kJ.mol-1 وهي القيمة الموجبة التي تشير إلى أن التحلل الضوئي للصبغة هو تفاعل ماص للحرارة.

جمهورية العراق

وزارة التعليم العالي والبحث العلمي

جامعة بابل

كلية العلوم للبنات

قسم الكيمياء

تخليق جسيمات ZnO النانوية عن طريق التكسير الحراري لمعقدات قاعدة زنك شيف و استخدامها للتحلل الضوئي لصبغة الاليزارين الصفراء G

رسالة

مقدمة الى مجلس كلية العلوم للبنات في جامعة بابل

كجزء من متطلبات نيل درجة الماجستير في العلوم الكيمياء

تقدمت بها الطالبة

هدير محمد صبحي

بإشراف

أ.م.د (حازم يحيى الجبوري) **أ . م .د (علي طالب بدر)**

هـ ١٤٤٤ **م ٢٠٢٢**